12-2015

Estimating the water quality condition of river and lake water in the Midwestern United States from its spectral characteristics

Jing Tan
Purdue University

PURDUE UNIVERSITY
GRADUATE SCHOOL
Thesis/Dissertation Acceptance

This is to certify that the thesis/dissertation prepared

By Jing Tan

Entitled

ESTIMATING THE WATER QUALITY CONDITION OF RIVER AND LAKE WATER IN THE MIDWESTERN UNITED STATES FROM ITS SPECTRAL CHARACTERISTICS

For the degree of Doctor of Philosophy

Is approved by the final examining committee:

Keith Cherkauer
Chair

Indrajeet Chaubey

Cary Troy

Melba Crawford

To the best of my knowledge and as understood by the student in the Thesis/Dissertation Agreement, Publication Delay, and Certification Disclaimer (Graduate School Form 32), this thesis/dissertation adheres to the provisions of Purdue University's "Policy of Integrity in Research" and the use of copyright material.

Approved by Major Professor(s): Keith Cherkauer

Approved by: Bernard Engel 12/18/2015

Head of the Departmental Graduate Program Date

ESTIMATING THE WATER QUALITY CONDITON OF RIVER AND LAKE WATER IN THE MIDWESTERN UNITED STATES FROM ITS SPECTRAL CHARACTERISTICS

A Dissertation

Submitted to the Faculty

of

Purdue University

by

Jing Tan

In Partial Fulfillment of the

Requirements for the Degree

of

Doctor of Philosophy

May 2016

Purdue University

West Lafayette, Indiana

THIS IS FOR YOU, SHUO AND IAN. THANKS FOR BRINING SO MUCH JOY TO MY LIFE.

ACKNOWLEDGEMENTS

I would like to express deepest gratitude to my advisor Dr. Keith A. Cherkauer for his guidance and support during my study and research. Without his encouragement and trust, I would not have learned how to conduct research independently. In addition, I express my appreciation to Dr. Indrajeet Chaubey for providing a wonderful lab in which I enjoyed my lab analyses, to Dr. Melba Crawford for lending me the GER 1500 spectrometer and helping request satellite imagery acquisition for my research, and to Dr. Cary D. Troy for facilitating the boat sampling of the St Joseph River plume on April 21, 2014 and providing valuable suggestions and comments on my manuscript. And thank all of them for having served on my committee.

I would also like to thank Dr. Ruben Goforth and Dr. Tomas Höök for the use of their boats for field sampling of the Wabash River and Lake Michigan respectively.

Special thanks to all the people who have helped me with field work and lab analyses: Margaret McCahon Kalcic, Rebecca Logsdon, Andi Hodaj, Natalie Chinn, Wei-Chih Chen, Sarah Rutkowski, Rebecca Essig, Emily Grimm, Sarah Stein, Jayson Beugly, Mandy Montgomery, Megan Heller Haas, Megan Gunn, Alison Coulter, Irma Remigio, Courtney M. Cripe, Austin Prechtel, Conner, and Ali.

Thank you, Dr. Curt Mobley, for recommending the ocean optics summer class at Darling Marine Center, University of Maine. Thanks to this class, I learned a lot and met wonderful faculty and colleagues there.

Finally, I would like to thank NASA for providing financial support during the last two years of my PhD, which allows me to collect valuable data to complete my research.

TABLE OF CONTENTS

Page

LIST OF TABLES viii

LIST OF FIGURES ix

LIST OF SYMBOLS xiv

ABSTRACT xv

CHAPTER 1. INTRODUCTION 1

1.1 Background 1

1.2 Research Questions 7

1.3 Organization 8

CHAPTER 2. USING HYPERSPECTRAL DATA TO QUANTIFY WATER QUALITY PARAMETERS IN THE WABASH RIVER AND ITS TRIBUTARIES 10

2.1 Abstract 10

2.2 Introduction 11

2.3 Study Area 15

2.4 Data Sources 16

2.4.1 Field Spectrometer Measurements and Sampling 16

2.4.2 Laboratory Analyses 17

2.5 Methods 18

2.5.1 Glint Removal for Field Measurements 18

2.5.2 Empirical Model Calibration and Validation 22

2.6 Results and Discussion 23

2.6.1 Glint Removal of Field Spectrometer Data 23

2.6.2 Spectral Characteristics of the Wabash River 29

2.6.3 Water Quality Models 33

Page

2.7 Conclusions 39
2.8 Acknowledgements 41
CHAPTER 3. WATER QUALITY ESTIMATION OF RIVER PLUMES IN SOUTHERN LAKE MICHIGAN USING HYPERION 42
3.1 Abstract 42
3.2 Introduction 43
3.3 Study Area 47
3.4 Data Sources and Methods 50
3.4.1 Satellite Imagery 50
3.4.2 Field Sampling 51
3.4.3 Lab Analyses 51
3.4.4 Field and Lab Data Processing 52
3.4.5 Image Processing 53
3.4.6 Algorithm Description 55
3.4.6.1 Bio-geo-optical Model 55
3.4.6.2 Look-up Table Method 57
3.5 Results and Discussion 59
3.5.1 Lab Measurements of IOPs 59
3.5.2 Bio-geo-optical Model vs Hydrolight Physical Radiative Transfer Model 62
3.5.3 Sensitivity Analysis 63
3.5.4 Model Results 66
3.5.4.1 Spectrometer Measurements 66
3.5.4.2 Hyperion Imagery 71
3.6 Conclusions 79
3.7 Acknowledgements 81

Page

CHAPTER 4. DEVELOPING A COMPREHENSIVE SPECTRAL-BIOGEOCHEMICAL DATABASE OF MIDWESTERN RIVERS FOR WATER QUALITY RETRIEVAL USING REMOTE SENSING DATA: A CASE STUDY OF THE WABASH RIVER AND ITS TRIBUTARY, INDIANA 82
4.1 Abstract 82
4.2 Introduction 83
4.3 Background 88
4.4 Materials and Methods 89
4.4.1 Study Area 89
4.4.2 Field Work Activities 92
4.4.3 Laboratory Analyses 92
4.4.4 Data Preprocessing and Analysis 94
4.4.5 Water Quality Retrieval 95
4.5 Results and Discussion 97
4.5.1 Water Quality Observations 97
4.5.2 Inherent Optical Properties 107
4.5.3 Bottom Properties 114
4.5.4 Spectral Characteristics 117
4.5.5 Water Quality Retrieval 117
4.6 Conclusions 124
4.7 Acknowledgements 127
CHAPTER 5. SUMMARY AND CONCLUSIONS 128
REFERENCES 135
VITA 153

LIST OF TABLES

Table Page

Table 2.1 Statistics (mean and standard deviation (SD)) showing that the Wabash River typically has higher chl and TSS concentrations than the Tippecanoe River based on the data collected in the summer of 2013. 30

Table 3.1 Retrieved concentrations of NAP, CDOM and chl through finding the closest match of field measured R_{rs} spectra and finding the spectra with RMSD <=0.00035 sr^{-1}. Mean, median and std (standard deviation) of the retrieved values are listed. 70

Table 3.2 Hyperion derived concentrations of NAP and chl as compared to field measurements. Both the closest match spectrum and spectra showing RMSD <=0.0009 sr^{-1} are used for retrieval. Median, mean and std (standard deviation) of the retrieved values are listed. Sampled sites are determined as in or out of plume based on the image. 76

Table 4.1 Summary of water quality observations of the Wabash River and the Tippecanoe Rive in summer 2014 98

Table 4.2 Pearson's correlations between concentrations and streamflow of the Wabash River and the Tippecanoe River. The values in bold text represent those correlations that were significant (p<0.05). 102

Table 4.3 Spectral values for phytoplankton absorption in summer 2014. 111

LIST OF FIGURES

Figure Page

Figure 1.1 Diagrams showing the contributions to the total upwelling radiance above the water surface, L_u. Yellow is the downwelling solar irradiance E_d, red is the surface reflected radiance, L_r, purple is the atmospheric path radiance, L_a, and green is the water leaving radiance, L_w. 3

Figure 2.1 Main study area includes two reaches of the Wabash River, including the confluence with the Tippecanoe River. Field spectrometer measurements and water samples (marked as black star) were collected through the summer of 2013. 16

Figure 2.2 (a) Above-water reflectance spectra and (b) corrected water-leaving reflectance spectra for nine sample sites on the Wabash River (seven sites, red solid line) and the Tippecanoe River (two sites, blue dashed line) using the method of Mobley (1999). 24

Figure 2.3 Comparisons of glint removal methods for a single site on the Wabash River. 27

Figure 2.4 Results of Hydrolight simulations carried out for representative turbid inland waters with different IOPs. Definitions of L_u, L_w, and E_d are given in the main text. L_u / E_d is the simulated above-water reflectance and L_w / E_d the simulated water-leaving reflectance. Calculated values of the index E (Equation 2.11) are 0.33% and 0.88%, respectively. 28

Figure Page

Figure 2.5 (a) Characteristic reflectance spectra from 2013 field measurements. See Section 2.5.2 for a description of areas D, L, and A. (b) Corrected water-leaving reflectance of all field data in the summer of 2013 using Tan's method. Red solid lines represent the Wabash River and the blue dashed lines represent the Tippecanoe River.. 32

Figure 2.6 (a) Empirical model for estimating [chl] using the band ratio $R_{rs}(704)/R_{rs}(677)$ for the field data collected in the summer of 2013 and (b) comparison between measured [chl] and modeled [chl] for the Wabash River and the Tippecanoe River. Dashed line represents the 1:1 line. 35

Figure 2.7 Empirical model for estimating [TSS] using $R_{rs}(704)$ for the field data in the summer of 2013. 37

Figure 2.8 Correlation between reflectance at the near-infrared wavelengths and TSS concentrations. 37

Figure 2.9 (a) Empirical model for estimating [TSS] musing $R_{rs}(752)$ for the field data collected in the summer of 2013 and (b) comparison between measured [TSS] and modeled [TSS] for the Wabash River and the Tippecanoe River. Dashed line represents the 1:1 line..... 38

Figure 3.1 Major study area focuses on the St Joseph River tributary in southern Lake Michigan. River plumes occurred at the river mouth and the near shore region. The Hyperion image was collected on August 7, 2012. 49

Figure Page

Figure 3.2 Specific absorption coefficients of CDOM – a^*_{cdom} (grey) are measured using 23 water samples collected at the near shore region of St Joseph when the plume occurred on April 21, 2014. The ensemble mean (black) is used to represent the a^*_{cdom} of our study area. The fitted exponential line (red) has a spectral slope S_{cdom} =0.0176 nm^{-1}. 60

Figure 3.3 (a) Lab measured total particulate absorption; and (b) specific absorption coefficients of chl (solid line) and NAP (dashed line)..... 61

Figure 3.4 Simulated remote sensing reflectance R_{rs} using the bio-optical model used in this study (dashed line) and Hydrolight (solid line)..... 63

Figure 3.5 (a) MSE of R_{rs} with percent change of one parameter at one time; and (b) R_{rs} change with change of a parameter at one time ([NAP] – increase 1 g m^{-3}, $a_{cdom}(440)$ – increase 0.2 m^{-1}, [chl] – increase 5 mg m^{-3}, γ – increase 0.1, $b^*_{b,p}(550)$ – increase 0.01 m^2 g^{-1}). The initial R_{rs} is simulated using the bio-optical model with inputs: [NAP] =6 g m^{-3}, $a_{cdom}(440)$ =1.2 m^{-1}, [chl] = 20 mg m^{-3}, γ =1, and $b^*_{b,p}(550)$ =0.02 m^2 g^{-1}. 65

Figure 3.6 Comparison between field measured R_{rs} spectrum (dash line) and 20 randomly selected matching spectra (solid red line) when RMSD <= 0.00035 sr^{-1} for a single sampled site..... 67

Figure 3.7 Comparison of the (a) NAP, (b) chl, and (c) CDOM concentrations obtained from field measurements and from model retrieval using field spectrometer data for the St Joseph River plume observed on April 21, 2014. Circles and diamonds represent the model retrieved mean and field measured values, respectively, and lines extending from the mean indicate one standard deviation. 68

Figure Page

Figure 3.8 Comparison of the (a) NAP and (b) chl concentrations obtained from field measurements and from model retrieval using Hyperion imagery for the St Joseph River plume observed on August 7, 2012. Circles and diamonds represent the model retrieved mean and field measured values, respectively, and lines extending from the mean show standard deviation. 73

Figure 3.9 Hyperion retrieved concentrations of (a) chl and (b) NAP of all sampled sites on August 7, 2012. Site numbers are placed at the bottom center of each site..... 74

Figure 3.10 Maps show (a) the Hyperion image and the spatial distribution of the modeled mean (b) [NAP] (g m^{-3}), (c) [chl] (mg m^{-3}), and (d) $a_{cdom}(440)$ (m^{-1}) concentrations on August 7, 2012..... 78

Figure 4.1 Main study area includes two reaches of the Wabash River, including the confluence with the Tippecanoe River. Field spectrometer measurements and water samples (marked as red stars) were collected through the summer of 2014. 91

Figure 4.2 Scatterplots of measured (a) [TSS] and (b) $a_{cdom}(440)$ versus [chl] for samples in the Wabash River (circles) and the Tippecanoe River (triangles) in summer 2014. 99

Figure 4.3 Time series of measured concentrations of water quality parameters and nutrients (circles) versus streamflow (solid line) of the Wabash River (left panel) and the Tippecanoe River (right panel). (a) and (b) - [TSS], (c) and (d) - [chl], (e) and (f) - $a_{cdom}(440)$, (g) and (h) - [DOC], (i) and (j) - [TN], and (k) and (l) - [TP]. 104

Figure 4.4 Scatterplot showing measured [DOC] versus $a_{cdom}(440)$ for samples collected for the Wabash River (circles) and the Tippecanoe River (triangles) in summer 2014. 105

Figure Page

Figure 4.5 Boxplots of measured [chl] for samples collected in the Wabash River during the summer of 2014. Boxes filled with yellow indicate that there is a statistically significant difference (p<0.05) between observations on the highlighted day and the previous day. 106

Figure 4.6 Scatterplots of measured IOPs (circles) versus water quality parameters (filled squares) of the Wabash River (left panel) and the Tippecanoe River (right panel). (a) and (b) – $a_{ph}(676)$ vs [chl], (c) and (d) – $a_{nap}(440)$ vs [TSS]. 108

Figure 4.7 Specific inherent optical properties for the Wabash River and the Tippecanoe River: (a) absorptions, and (b) backscattering. 113

Figure 4.8 Variability of the retrieved $b_{b,p}(550)$ (circles) with measured (a) [TSS] (filled squares) and (b) [chl] (filled squares) in the Wabash River and the Tippecanoe River. 114

Figure 4.9 Bottom types identified for the Wabash River and the Tippecanoe River. (a) fines, (b) sand, (c) gravel, and (d) cobble. 115

Figure 4.10 Albedo measured for different bottom types of the Wabash River and the Tippecanoe River. 116

Figure 4.11 (a) All R_{rs} spectra collected in summer 2014 and (b) examples showing phytoplankton dominated (solid lines) and sediment dominated (dotted line) spectra. . 119

Figure 4.12 Randomly chosen selection of the 550,054 spectra in the LUT database. .. 121

Figure 4.13 Comparison between measured (a) [chl], (b) [TSS], and (c) $a_{cdom}(440)$, and the LUT estimates for the Wabash River and the Tippecanoe River. 122

Figure 4.14 Relative error versus (a) [chl] and (b) [NAP] for the Wabash River and the Tippecanoe River. 123

LIST OF SYMBOLS

a	Absorption coefficients of the total ($=a_w+a_{nap}+a_{chl}+a_{cdom}$)
a_w	Absorption coefficient of pure water
a_p	Total absorption coefficients of particles
a_{chl}	Absorption coefficient of chlorophyll (chl)
a^*_{chl}	Specific absorption coefficient of chlorophyll
a_{cdom}	Absorption coefficient of colored dissolved organic matter (CDOM)
$a_{cdom}(440)$	Absorption coefficient of CDOM at 440 nm
a_{nap}	Absorption coefficient of non-algal particles (NAP)
a^*_{nap}	Specific absorption coefficient of non-algal particles
b_b	Backscattering coefficients of the total ($=b_{b,w}+b_{b,p}$)
$b_{b,w}$	Backscattering coefficients of pure water
$b_{b,\,p}$	Backscattering coefficients of particles (including chl and NAP)
$b^*_{b,p}(550)$	Specific backscattering coefficient of particles at 550 nm
S_{cdom}	Spectral slope of CDOM
S_{nap}	Spectral slope and NAP
γ	Power-law exponent of particle scattering
[chl]	Concentration of chlorophyll
[NAP]	Concentration of non-algal particles (NAP)
[TSS]	Concentration of total suspended solids (TSS)
[DOC]	Concentration of dissolved organic carbon (DOC)
[TN]	Concentration of total nitrogen (TN)
[TP]	Concentration of total phosphorous (TP)
[p]	Concentration of suspended particles including both chl and NAP
G	Sun and sky glint
R_{rs}	Above-water remote sensing reflectance
r_{rs}	Radiance reflectance just below the water surface
L_w	Water-leaving radiance
L_u	Total upwelling radiance of water
L_s	Sky radiance
E_d	Downwelling solar radiation
ρ	Water surface reflection coefficient
λ	Wavelength

ABSTRACT

Tan, Jing. Ph.D., Purdue University, May 2016. Estimating the Water Quality Condition of River and Lake Water in the Midwestern United States from Its Spectral Characteristics. Major Professor: Keith Cherkauer.

Water quality impairment due to excessive concentrations of nutrients and sediments has been a concern in the Midwestern United States. Alternatives to traditional in situ water quality sampling methods, which are limited in frequency or to a small number of locations, are needed for regional monitoring and assessment. Remote sensing has the potential to provide a synoptic view of water quality condition at multiple temporal scales. This study focuses on developing/calibrating remote sensing algorithms for water quality retrieval in Midwestern rivers and lakes. In the first part of this study, the spectral measurements collected using a hand-held spectrometer as well as water quality observations for the Wabash River and its tributary the Tippecanoe River in Indiana were used to develop empirical models for the retrieval of chlorophyll (chl) and total suspended solids (TSS). A method for removing sky and sun glint from field spectra for turbid inland waters was developed and tested. Empirical models were then developed using a subset of the field measurements with the rest for model validation. Spectral characteristics indicative of waters dominated by different inherent optical properties (IOPs) were identified and used as the basis of selecting bands for empirical model development. The second part of this study focuses on the calibration of an existing bio-

geo-optical model for studying the spatial variability of chl, non-algal particles (NAP), and colored dissolved organic matter (CDOM) in episodic St. Joseph River plumes in southern Lake Michigan. One set of EO-1 Hyperion imagery and one set of boat-based spectrometer measurements were successfully acquired to capture episodic plume events. Coincident water quality measurements were also collected during these plume events. A database of inherent optical properties (IOPs) measurements and spectral signatures was generated and used to calibrate a bio-geo-optical model. Finally, a comprehensive spectral-biogeochemical database was developed for the Wabash River and its tributaries in Indiana by conducting field sampling of the rivers using a boat platform over different hydrologic conditions during summer 2014. In addition to the various spectral measurements taken by a handheld field spectrometer, this database includes corresponding in situ measurements of water quality parameters (chl, NAP, and CDOM), nutrients (TN, TP, dissolved organic carbon (DOC)), water-column IOPs, water depths, substrate types and bottom reflectance spectra. The temporal variability of water quality parameters and nutrients in the rivers was analyzed and studied. A look-up table (LUT) based spectrum matching methodology was applied to the collected observations in the database to simplify the retrieval of water quality parameters and make the data accessible to a wider range of end users.

It was found that the ratio of the reflectance peak at the red edge (704 nm) with the local minimum caused by chlorophyll absorption at 677 nm was a strong predictor of chl concentrations (coefficient of determination (R^2) = 0.95). The reflectance peak at 704 nm was also a good predictor for TSS estimation (R^2 = 0.75). In addition, we also found that reflectance within the NIR wavelengths (700 - 890 nm) all showed strong correlation (0.85-0.91) with TSS

concentrations and generated robust models. Results suggest that hyperspectral information provided by field spectrometer can be used to distinguish and quantify water quality parameters under complex IOP conditions.

Field measured concentrations of NAP and CDOM at 67% of the sampled sites in the St Joseph River plume fall within one standard deviation of the retrieved means using the spectrometer measurements and the calibrated bio-geo-optical model. The percentage of sites within one standard deviation (88%) is higher for the estimation of chl concentrations. Despite the dynamic nature of the observed plume and the time lag during field sampling, 77% of the sampled sites were found to have field measured chl and NAP concentrations falling within one standard deviation of the Hyperion derived values. The spatial maps of water quality parameters generated from the Hyperion image provided a synoptic view of water quality conditions. Analysis highlights that concentrations of NAP, chl, and CDOM were more than three times higher in conjunction with river outflow and inside the river plumes than in ambient water. It is concluded that the storm-initiated plume is a significant source of sediments, carbon and chl to Lake Michigan.

The temporal variability of water quality parameters and nutrients in the Wabash River was closely associated with hydrologic conditions, while no significant correlations existed between these parameters and streamflow for the Tippecanoe River, probably due to the two upstream reservoirs. The poor relationship between CDOM and DOC indicates that most DOC in the rivers was from human sources such as wastewater. It was also found that the source of water (surface runoff or combined sewer overflows (CSO)) to a river, water temperature, and nutrients are important factors controlling instream concentrations of phytoplankton. The LUT retrieved chl and NAP concentrations were in

good agreement with field measurements with slopes close to 1.0. The average estimation errors for NAP and chl were within 4.1% and 37.7%, respectively, of independently obtained lab measurements. The CDOM levels were not well estimated and the LUT retrievals for CDOM showed large variability, probably due to the small data range collected in this study and the insensitivity of remote sensing reflectance, R_{rs}, to CDOM change.

This study demonstrates the ability of remote sensing in monitoring water quality retrieval in inland rivers and lakes. In addition, the datasets collected in this study provide useful ground truth data for remote sensing of water quality in inland waters and valuable sources for further investigation of the relationship between optical and biogeochemical properties.

CHAPTER 1. INTRODUCTION

1.1 Background

Inland waters provide water resources for a variety of human uses including transportation, recreation, commerce, water supply, and human health. In addition to that, they support important and diverse habitats that are essential for aquatic plant and animal communities (Bronmark and Hansson, 2002; Duker and Bore, 2001). Other ecosystem services provided by inland waters and that are vital to human development include climate regulation (Thiery et al., 2015; Notaro et al., 2013), flood mitigation (Fu et al., 2013; Potter, 1994), and carbon and nutrient recycling (Bastviken et al., 2011). However, like many other ecosystems, inland waters are under pressure from human activities as well as climate change (Allan et al., 2013). The United Stated Environmental Protection Agency (USEPA) has been monitoring and investigating long-term water quality across the nation since the passage of Clean Water Act in 1972. Nonpoint source pollution has been identified as the dominant source of water quality impairment in the rivers and lakes of the United States (United States Environmental Protection Agency, 2011a; Brown and Froemke, 2012). This is especially true in the Midwest where agricultural activities are intense (Alexander et al., 2008). Moreover, the Midwestern rivers, including those in Indiana, are also major contributors to downstream problems in water quality, especially

the hypoxic zone in the Gulf of Mexico, of which the year 2008 measurement has been reported as one of the two largest since 1985 (Louisiana Universities Marine Consortium, http://www.gulfhypoxia.net/Overview/). With an increasing desire for biomass for biofuel production (Cibin et al., 2011) and more frequent and intense precipitation events projected in the future (Kling et al., 2003), the delivery of nutrients and sediments to Midwestern rivers and lakes have the potential to be enhanced, which will exacerbate the water quality problems in this area. Therefore, the assessment and monitoring of water quality and developing an improved understanding of how environmental pressures affect the ecological and biogeochemical properties of these water bodies are very important.

Traditional water quality monitoring relies on in situ measurements and collection of water samples for laboratory analyses. While such measurements are accurate for a point in time and space, they are not done frequently or at sufficiently large numbers of locations to capture temporal or spatial variability in water quality conditions. This handicap is the driving force behind the development other methods which can increase the coverage and frequency of water quality monitoring. Remote sensing has long been recognized as having the potential to provide an instantaneous synoptic overview of water quality (Olmanson et al., 2013; Shuchman et al., 2013a; O'Reilly et al., 1998; Ritchie et al., 1994). Previous studies have demonstrated that optically active water quality parameters such as clarity and chlorophyll (chl) concentrations can be retrieved by analyzing the spectral signals backscattered from water and received by remote spectral imagers (Horion et al., 2010; Shafique et al., 2003). Remote sensing, when coupled with in situ measurements, provides a cost-effective way for water quality monitoring.

The spectral signal of interest in this study is remote sensing reflectance, R_{rs}, which is defined as the ratio of water leaving radiance, L_w, over downwelling solar irradiance, E_d. Most of the remote sensing sensors measure total upwelling radiance L_u, which contains both L_w and surface reflected radiance L_r if measured in field, or contains L_w, L_r, and atmospheric path radiance L_a if measured by satellite (Figure 1.1). The atmospheric path radiance L_a is caused by the absorption and backscattering of particles in the atmosphere. Therefore, in order to obtain R_{rs}, L_a and L_r need to be removed from L_u. The process of removing L_a is atmospheric correction and the process of removing L_r is glint removal.

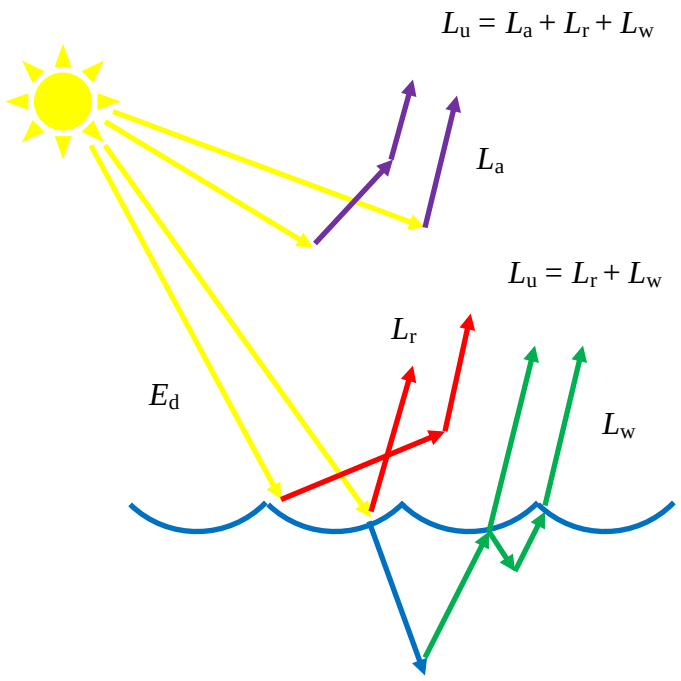

Figure 1.1 Diagrams showing the contributions to the total upwelling radiance above the water surface, L_u. Yellow is the downwelling solar irradiance E_d, red is the surface reflected radiance, L_r, purple is the atmospheric path radiance, L_a, and green is the water leaving radiance, L_w.

While remote sensing of oceanic systems has been undertaken and made progress for decades (Blondeau-Patissier et al., 2014), the use of remotely sensed data on an operational basis for monitoring water quality in lakes and rivers has faced many challenges. First of all, remote sensing of inland waters has been limited by either the spatial or temporal resolution of current satellite products. For example, the spatial resolution of the Sea-viewing Wide Field-of-View Sensor (SeaWiFS), Advanced Very-High Resolution Radiometer (AVHRR), and MODerate resolution Imaging Spectroradiometer (MODIS), which are at least 1 km, is too coarse for rivers and most lakes. Satellite sensors with higher spatial resolution such as the various Landsat Thematic Mapper missions (TM, ETM, ETM+) and the Advanced Spaceborne Thermal Emission and Reflection Radiometer (ASTER) are capable of resolving finer scale features, but their temporal resolutions are approximately 16 days, which limits the access of cloud-free images. It should also be noted that both systems are designed primarily for observing terrestrial systems and therefore are not optimal for rivers and lakes (Handcock et al., 2006). The second problem is that inland waters are often optically complex and considered as Case II waters (Morel and Prieur, 1977). Since the optical properties of rivers and lakes are not solely influenced by phytoplankton (Case I waters), current satellite algorithms for oceanic systems do not apply (O'Reilly et al., 1998). Moreover, bottom reflectance from optically shallow riverine and lake systems can contribute to the total backscattered signals from water (Lee et al., 1998; Lee et al., 1994), which makes algorithm development more difficult. Although band ratio type algorithms and more sophisticated neural network method have been developed by many authors for estimating various inland water characteristics ranging from chl, colored

dissolved organic matter (CDOM) and water turbidity/clarity (Chebud et al., 2012; Matthews, 2011; Shafique et al., 2003), these algorithms rely heavily on the in situ data and sampling location and therefore are often not repeatable. To develop reliable and transferrable models for retrieving water quality information in inland waters, it is important to understand the underlying absorption and backscattering properties of water column and in-water optically active constituents (OACs) and how these properties affect the apparent optical properties (AOPs) measured by remote sensing instruments. This brings the third challenge for remote sensing of inland water bodies: while much attention has been paid to collecting coincident measurements of inherent optical properties (IOPs) and AOPs for oceanic systems (e.g., NASA SeaWiFS Bio-optical Archive and Storage System, http://seabass.gsfc.nasa.gov/), inland waters, especially river systems, have been poorly observed, even though what happens in ocean and coastal waters is highly dependent on these systems. The IOPs are the properties of the medium itself and are not affected by the ambient light field. The AOPs are radiometric quantities that display enough stability and can be used for approximately describing the optical properties of the water body, e.g., the remote sensing reflectance, R_{rs}, in this study.

Many efforts have been made to mitigate the challenges mentioned above and to improve remote sensing of inland waters. In order to collect images of sufficiently high spatial resolution from which rivers and lakes can be appropriately resolved, airborne systems are often used and the application of such systems has proven to be capable of measuring water quality conditions in optically complex water bodies (Olmanson et al., 2013). The major drawback of airborne platforms is that they cannot be used on a regular basis due to the high organization and realization cost. The use of handheld spectrometers

provides a way to collect spectral signals in a realistic and cost-effective fashion. Although limited in spatial coverage, field spectrometers are designed to have high spectral resolution and can be used to capture measurements at a temporal frequency better than daily. The high spectral resolution enables the identification of key spectral regions for water quality retrieval, while such regions may not be effectively captured by current satellite sensors. Indeed, field spectroscopy can be used as a potential investigative technique for inland water quality retrieval, to complement satellite and airborne remote sensing (Hadjimitsis and Clayton, 2011).

There is growing consensus that physical models, which focus on the water column and bottom properties and quantify the relationship between IOPs and AOPs, are preferred for water quality assessment (IOCCG, 2000). It has been demonstrated that physical models produce good estimates that agree quite favorably with field measurements, and improve the retrieval accuracy of chl concentration in the Great Lakes as compared to the empirical band ratio approach (Shuchman et al., 2006, 2013a). There are two approaches to develop physical models: the analytical modeling and the radiative transfer modeling approach. Whatever approach is used, the success of physical models depends much on the accuracy of measured IOPs and AOPs. Therefore, in situ observations of biogeochemical properties, IOPs, and radiometric parameters are always collected using standard protocol, not only for algorithm development but also for satellite validation. Open community databases with all in situ observations and relevant data are also recommended for future inland water remote sensing (Mouw et al., 2015).

1.2 Research Questions

This research focuses on the development/calibration of remote sensing algorithms to retrieve water quality parameters in Midwestern rivers and lakes. Two study areas are selected: (1) the Wabash River and its tributary, the Tippecanoe River, both in Indiana and (2) St Joseph River plumes in southern Lake Michigan. This research makes use of the extensive datasets developed for the study areas, including in situ water quality, IOPs, bottom properties, and radiometric measurements collected for the Wabash River under various hydrologic conditions, as well as satellite and ground based data collected for the episodic river plumes in southern Lake Michigan. Using those datasets, this research addresses the following science hypotheses:

1. Field spectroscopy provides a potential way to capture spectral characteristics that are indicative of the absorption and backscattering properties of each OAC. Therefore, key spectral regions can be identified to improve the development of empirical models for inland waters, as well as to provide useful suggestions for future satellite remote sensing missions.
2. In situ observations of water quality parameters are spatially limited, but this spatial limitation can be addressed in part through the use of remote sensing imagery. Physical models which are based on the water column and bottom properties are reliable and transferrable in quantifying water quality parameters from the spectral signatures.
3. Concentrations of water quality parameters including chl, non-algal particles (NAP) and CDOM are indicative of the health of riverine and lake aquatic systems and the spatial and temporal variability of these parameters are closely

related to concurrent hydrologic conditions and land use patterns.

In order to address these hypotheses, I (1) collected in situ measurements of water quality, bottom properties, and radiometric measurements of the Wabash River and its tributaries over different hydrologic conditions; (2) developed empirical models by identifying key spectral regions indicative of IOPs of each OAC for retrieving water quality parameters in the Wabash River and its tributaries; (3) calibrated a transferrable remote sensing algorithm for the river plumes study in Southern Lake Michigan and evaluated the spatial variability of water quality parameters in episodic river plume events using remote sensing imagery; and (4) developed a comprehensive spectral-biogeochemical database with in situ measurements and spectral look-up tables for retrieving water quality parameters in the Wabash River.

1.3 Organization

These hypotheses are addressed in the next three chapters. In the second chapter, the in situ water quality and radiometric measurements collected in summer 2013 are used to develop semi-empirical models for retrieve water quality parameters in the Wabash River. Instead of selecting bands that show best-fit correction with measured remote sensing data, these semi-empirical models are developed by identifying the key spectral characteristics indicative of waters dominated by different IOPs. In the third Chapter, a transferrable bio-optical model is calibrated using field measurements for the river plumes in southern Lake Michigan. This bio-optical model is then applied to Hyperion imagery collected on August 10, 2012 to evaluate the spatial variability of water quality conditions. In Chapter 4, in situ measurements of water quality, IOPs, and bottom properties, as well as radiometric measurements of the Wabash River are

conducted in summer 2014 under various hydrologic conditions. The temporal variability of water quality observations is analyzed and possible factors affecting the temporal variability are identified. A look-up table (LUT) based spectrum matching methodology is applied to the collected dataset to retrieve water quality parameters. The final chapter provides overall conclusions to this research.

Chapter 2 has been published in the International Journal of Remote Sensing, while Chapter 3 has been revised and resubmitted to the Journal of Great Lakes Research.

CHAPTER 2. USING HYPERSPECTRAL DATA TO QUANTIFY WATER QUALITY PARAMETERS IN THE WABASH RIVER AND ITS TRIBUTARIES

2.1 Abstract

A hand-held spectrometer was used to collect above water spectral measurements for measuring optically active water quality characteristics of the Wabash River and its tributaries in Indiana. Water sampling was undertaken concurrent with spectral measurements to estimate concentrations of chlorophyll (chl) and total suspended solids (TSS). A method for removing sky and sun glint from field spectra for turbid inland waters was developed and tested. Empirical models were then developed using the corrected field spectra and in situ chl and TSS data. A subset of the field measurements was used for model development and the rest for model validation. Spectral characteristics indicative of waters dominated by different inherent optical properties (IOPs) were identified and used as the basis of selecting bands for empirical model development. It was found that the ratio of the reflectance peak at the red edge (704 nm) with the local minimum caused by chl absorption at 677 nm was a strong predictor of chl concentrations (coefficient of determination (R^2) = 0.95). The reflectance peak at 704 nm was also a good predictor for TSS estimation (R^2 = 0.75). In addition, we also found that reflectance within the NIR wavelengths (700 - 890 nm) all showed strong correlation (0.85-0.91) with TSS concentrations and generated robust models. Results suggest that

hyperspectral information provided by field spectrometer can be used to distinguish and quantify water quality parameters under complex IOP conditions.

Tan, J., K. A. Cherkauer, and I. Chaubey, 2015. Using hyperspectral data to quantify water quality parameters in the Wabash River and its tributaries, Indiana. International Journal of Remote Sensing 36(21), 5466-5484.

2.2 Introduction

Excessive concentrations of sediment and nutrients originating from agricultural activities are two primary sources of water quality impairment in the rivers of the Midwestern United States (Committee on the Mississippi River, the Clean Water Act, and National Research Council, 2008; Brown and Froemke, 2012). Midwestern rivers, especially in Indiana, are major contributors to downstream problems in water quality, especially the hypoxic zone in the Gulf of Mexico (Burkart and James, 1999). The Wabash River system is one of the biggest river systems in Indiana and water quality has been reported as impaired due to excessive nutrients, according to the Indiana and Illinois 2010, 2012, and 2014 Clean Water Act (CWA) Section 303(d) listings. Also, the Wabash River has been identified as one of the largest contributors of nutrient loadings to the Mississippi River and the Gulf of Mexico via the Ohio River Basin (Ohio River Valley Water Sanitation Commission, http://www.orsanco.org/wabash-river-project). According to analysis of simulations using the United States Geological Survey (USGS) SPAtially Referenced Regressions On Watershed attributes (SPARROW) model, the Wabash River watershed contributes approximately 10.0×10^6 kg of total phosphorus and 139.3×10^6 kg of total nitrogen to the Gulf of Mexico each year (United States Environmental Protection Agency, 2011b).

The optical properties, or spectral signature backscattered from water, can be captured by remote sensing instruments and used to quantify the water quality parameters by empirical or analytical modelling. Multiple remote sensing platforms and sensors exist, and theoretically remote sensing can provide ways to quickly capture a synoptic view of water quality conditions spatially. While multi-spectral sensors such as MODerate resolution Imaging Spectroradiometer (MODIS) and Medium Resolution Imaging Spectrometer (MERIS) provide spectral bands that have been successfully used to measure chlorophyll (chl) level in inland and coastal waters (Gilerson et al., 2010; Olmanson et al., 2013; Shuchman et al., 2013a), most rivers and streams are not able to be appropriately resolved due to the coarse resolution of these satellite products (Handcock et al., 2006). Landsat imagery, which has a finer spatial resolution of 30 m, may still be too coarse for small rivers. Although aircraft platforms provide a way to collect images of high spatial resolutions from which river systems can be appropriately resolved, they are limited to the number of events they can capture due to their higher organization and realization cost. Although limited in spatial coverage, in situ sampling using a handheld spectrometer provides a realistic, convenient, and accurate approach for measuring spectral signatures of rivers and streams.

The ability of remote sensing for rivers and streams monitoring has also been hampered by more fundamental problems. First, rivers and streams are often optically complex and the optical properties are not solely influenced by phytoplankton (Morel and Prieur, 1977). Secondly, some rivers and streams are so shallow that river bottoms can contribute to the total backscattered signals from water. Therefore, existing algorithms for estimating water quality parameters of oceanic systems (O'Reilly et al., 1998) do not

apply to river systems. In theory, to adequately retrieve water quality parameters in rivers and streams, it is important to understand the underlying absorbing and backscattering properties of the water column and optically active constituents and how these properties affect the spectral signature measured by remote sensing instruments. This brings the third challenge for remote sensing of rivers and streams: few optical characterization studies of rivers and streams have been conducted and presented. In addition, rivers and streams are closely associated with terrestrial surroundings and therefore usually display regional optical conditions. The success of analytical models depends largely on the accurate measurements of inherent optical properties. Unless the analytical models are validated and widely available for rivers and streams, we believe that the empirical approach will provide the primary practical means of estimating water quality parameters in rivers and streams. Through identifying key spectral characteristics that are indicative of waters dominated by different inherent optical properties (IOPs), water quality parameters including chl and total suspended solids (TSS) can be successfully quantified using empirical models (Olmanson et al., 2013).

One of the problems in interpreting the data collected above the water surfaces is removing sun and sky glint. One common approach to removing the effects of sun and sky glint is to use the optimal measuring angles suggested by Mobley (1999) and then correct the reflectance spectra using the sky radiance measurements. This method suggests a viewing direction of 40° from the nadir and 135° from the Sun, requires simultaneous measurements of water radiance, sky radiance, and downwelling irradiance, and assumes wind speed less than 5 m s^{-1} for the use of sea-surface reflectance $\rho \approx 0.028$. However, natural water surfaces are almost never flat and the air-sea interface reflection

coefficient ρ is expected to vary strongly with wind speed (Ruddick et al., 2006). There are other types of glint removal procedures such as those utilizing the brightness in a near-infrared band (Hedley et al., 2005) or the oxygen absorption feature near 760 nm (Kutser et al. 2009), or applying a bio-optical model and a spectral optimization approach (Lee et al., 2010a), to estimate the amount of glint in measured reflectance spectra. The methods described above either depend on certain viewing geometry or are image-based, or require extra information such as wind speed, water depth, and optical properties of bottom. Kutser et al. (2013) suggested a simple method that does not need any auxiliary parameters and fits power functions using reflectance values at the ultraviolet (350-380 nm) and near-infrared (890-900 nm) wavelengths to represent glint. But this method assumes the water-leaving reflectance at 890-900 nm to be zero, which is usually not true for turbid rivers and streams.

In this study, a hand-held spectrometer was used to collect above water spectral measurements for measuring optically active water quality characteristics of the Wabash River and the Tippecanoe River in the summer (May to August) 2013. Water sampling was undertaken concurrent with spectral measurements to estimate concentrations of chl and TSS. A method of removing sky and sun glint from field spectra for turbid inland water was developed and tested. Spectral characteristics indicative of waters dominated by different IOPs were then identified and used to develop empirical models for estimating chl and TSS. The accuracy and usefulness of the empirical models was also evaluated.

2.3 Study Area

The primary study site includes the Wabash River and one of its tributaries, the Tippecanoe River. The Tippecanoe River flows through two reservoirs and the Norway Dam and the Oakdale Dam before joining the Wabash River. The two dams are located 48 km and 29 km, respectively upstream above the confluence (Figure 2.1). There are several tributaries along this reach, however, the Tippecanoe River is the most significant, most accessible and exhibits the largest variance in water quality relative to the main river. Within the study area the Wabash River flows about 90 km from French Post Park (about halfway between Delphi, Indiana, and Logansport, Indiana) to Attica, Indiana, and ranges in width from 100 m to over 150 m. The Wabash River originates from west-central Ohio and runs through Indiana State draining an area of over 85,000 km^2. Water depth of the Wabash River in the summer typically ranges from 0.6 m to 4.5 m while the Tippecanoe River is shallower with the typical depth of 0.6 m to 2.7 m.

The land use in the Wabash River basin is dominated by agricultural management, primarily corn and soybean rotations (Bukaveckas et al., 2005). The water flows a distance of over 650 km from the Indiana/Ohio State boundary before entering the Ohio River and eventually reaching the Mississippi River. Due to agricultural activities such as intensive farming and significant fertilizer use, as well as runoff events during the planting season in the upland areas, nitrogen and phosphorus loads in the Wabash River are highest in the Spring months when flows are typically greatest. Despite the heavy agricultural use also occurring in the Tippecanoe River watershed, water in the river carries significantly lower sediment loads than the Wabash River, likely due to the presence of the two upstream reservoirs.

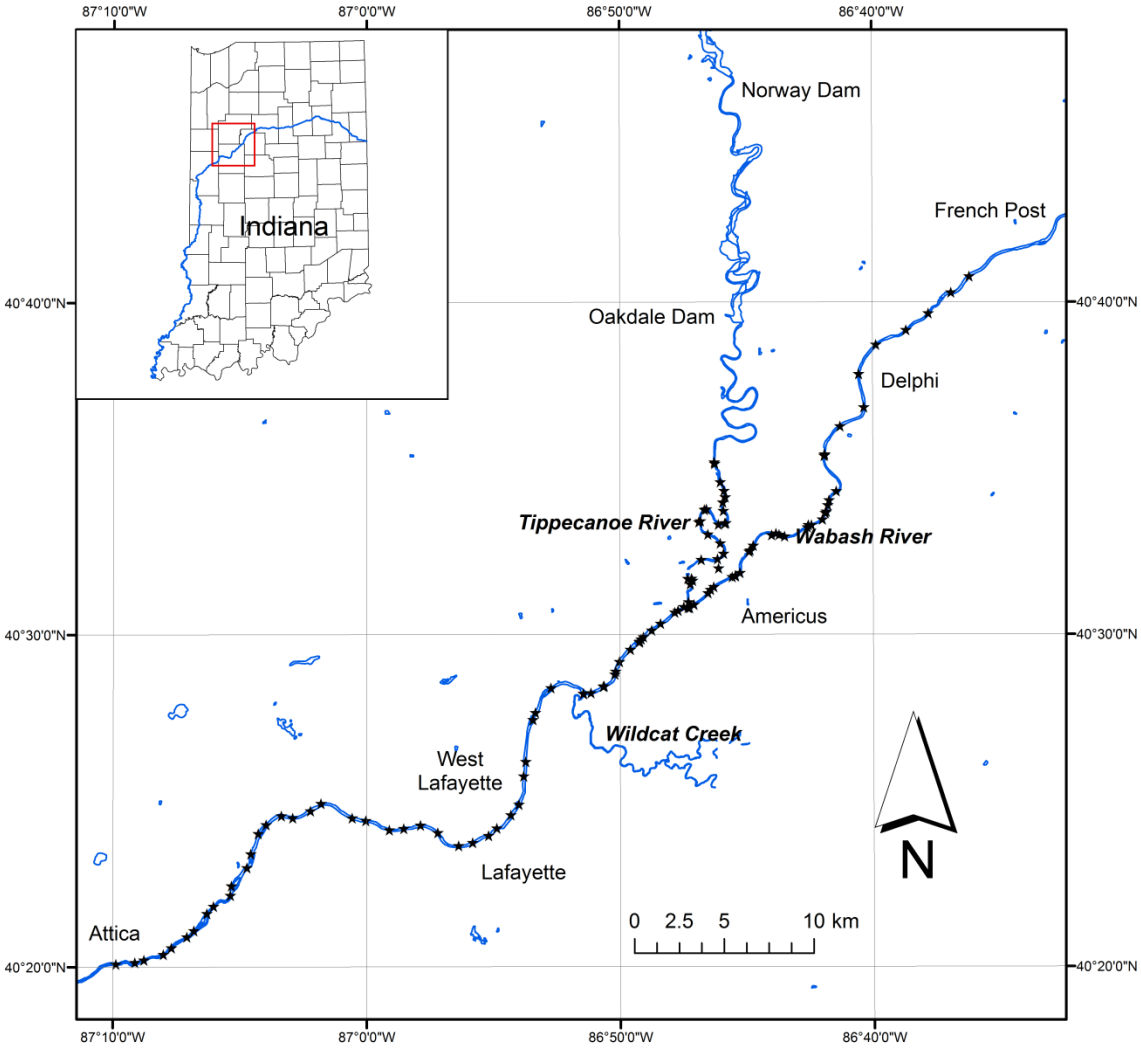

Figure 2.1 Main study area includes two reaches of the Wabash River, including the confluence with the Tippecanoe River. Field spectrometer measurements and water samples (marked as black star) were collected through the summer of 2013.

2.4 Data Sources

2.4.1 Field Spectrometer Measurements and Sampling

In the summer of 2013 (May to August), in situ water quality and spectral measurements were taken over the Wabash River (from French Post to Attica) and the

Tippecanoe River using a boat platform (Figure 2.1). Field samples were collected every 2-3 kilometers along the river through the summer to capture various water quality conditions. Above-water spectral measurements were collected using a GER 1500 spectrometer (Spectral Vista Corporation) and a Spectralon panel. At each site, upwelling water surface radiance, L_u, and downwelling solar irradiance, E_d, were measured. The spectrometer was pointed off nadir at the water target and the Spectralon panel respectively within a very short time period with the intent of avoiding significant changes in illumination conditions. For 15 August 2013, nine spectral measurements were completed using the recommended viewing direction of 135° from the sun and 40° from the nadir for the measurements of sky radiance, L_s, and L_u (Mobley, 1999). The GPS locations of each sampled site were recorded. In addition, water depths of each site were measured using an ultrasonic device and sky conditions were also recorded. Water samples of each site were collected and stored in brown polyethylene bottles until returned to the laboratory for further analysis.

2.4.2 Laboratory Analyses

All water samples were stored in the dark and on ice until returned to the laboratory for water quality analysis. Water quality indicators that were quantified were chl and TSS. Standard methods of analysis were applied (Eaton et al., 1998). For chl estimation, a sub-sample was filtered onto Whatman GF/F 25 mm filters, then macerated in 10 ml 90% acetone solution and analyzed spectrophotometrically. TSS concentration was determined by filtering a sub-sample using Whatman GF/F 47 mm filters and then oven drying the pre-weighted filter at 105°C for at least one hour to calculate the weight difference.

2.5 Methods

2.5.1 Glint Removal for Field Measurements

For water targets, it should be noted that the upwelling signal measured by remote sensing sensors, L_u, includes both water leaving signal, L_w, and surface reflected signal, L_r. The data of interest is the remote sensing reflectance R_{rs}, which is defined as the ratio of water leaving radiance to downwelling irradiance (E_d), i.e., L_w/E_d. The surface reflectance component L_r must be removed from L_u in order to calculate the R_{rs} of water targets. As L_r is directly related to the sky radiance, L_s, most spectrometers for field measurements are composed of one sensor measuring L_u, one measuring E_d and the third measuring L_s. Then, L_w can be calculated as

$$L_w = L_u - \rho L_s \qquad (2.1)$$

where ρ is the water surface reflection coefficient. For the field spectrometer measurements on 15 August 2013, L_w was calculated using $\rho \approx 0.028$ (Mobley, 1999). Glint in other spectrometer measurements collected in the summer of 2013, however, cannot be removed using this method since neither the recommended viewing geometry was followed nor appropriate L_s data collected.

In the work of Kutser et al. (2013), the field measured L_u data at 350-380 nm and 890-900 nm were fitted to power functions to represent the glint spectra, which can then be removed from the L_u spectra. This method, which is referred as Kutser's correction in this paper, does not require L_s measurements and is appropriate for spectral measurements collected with the radiance sensor looking into nadir. The major assumption of Kutser's correction is that the water-leaving reflectance is close to zero at

the ultraviolet (UV) range as well as at 890-900 nm; therefore, the non-zero values at these wavelengths are simply the results of sun and sky glint. But this is often not the case for optically shallow or turbid inland waters, of which water reflectance at these wavelengths is usually not zero due to bottom signals or high concentration of suspended solids (Moore et al., 1999). As we analyzed our measurements (based on the inherent optical properties and bottom albedo measurements collected in 2014), no significant effect from the bottom (within 5% percent of the total signal) was found when water depths in the Wabash River and the Tippecanoe River exceeded 1 m. Only site measurements where water depths were more than 1 m are used, therefore bottom contribution is not an issue in this study.

In the near infrared (NIR) wavelengths, due to the increased absorption of pure water and the fact that absorption by phytoplankton and colored dissolved organic matter (CDOM) are negligible, water reflectance in this spectral region is closely associated with the backscattering coefficients and the spectral properties can be used in glint correction (Gould et al., 2001). As Ruddick et al. (2006) found in their study of seaborne measurements, the shape of remote sensing reflectance spectra in the NIR range (700-900 nm) is largely determined by pure water absorption and almost invariant for turbid waters. They normalized the NIR reflectance spectra using the reflectance at 780 nm and defined it as the “similarity spectrum”. In this study, we developed a new correction method, which combines Kutser’s correction, Gould’s glint removal algorithm, and Ruddick’s similarity spectrum, to remove the sun and sky glint effects for the Wabash River and the Tippecanoe River. This method is referred as Tan’s correction in this paper and the detailed procedure is shown below.

Based on Kutser's correction, an estimate of the amount of glint in the measured reflectance spectra can be expressed as

$$G(\lambda) = m \times \lambda^{n} \qquad (2.2)$$

where $G(\lambda)$ is the estimated amount of glint and λ is the wavelength. The values of m and n need to be determined and the detailed procedure is described below.

The amount of glint can also be quantified using measured above-water reflectance at two NIR wavelengths.

$$G(\lambda_1) = \frac{\frac{L_u(\lambda_1)}{E_d(\lambda_1)} a_w(\lambda_1) - \frac{L_u(\lambda_2)}{E_d(\lambda_2)} a_w(\lambda_2)}{a_w(\lambda_1) - a_w(\lambda_2)} \qquad (2.3)$$

where $L_u(\lambda_1)$ and $L_u(\lambda_2)$ are the total upwelling radiance at wavelength λ_1 and λ_2, $E_d(\lambda_1)$ and $E_d(\lambda_2)$ are the downwelling solar irradiance at wavelength λ_1 and λ_2, and $a_w(\lambda_1)$ and $a_w(\lambda_2)$ are the absorption coefficients of pure water at these two wavelengths. See Gould et al. (2001) for the derivation of Equation (2.3). The assumptions here are that the amount of glint and values of backscattering coefficients are nearly constant within 5 nm in NIR wavelength ranges. A total of 4 wavelength pairs (745 nm, 750 nm), (805 nm, 810 nm), (845 nm, 850 nm), and (895 nm, 900 nm) spanning the NIR wavelength range were selected. Combining Equation (2.2) and Equation (2.3),

$$m \times 750^{n} = \frac{\frac{L_u(750)}{E_d(750)} a_w(750) - \frac{L_u(745)}{E_d(745)} a_w(745)}{a_w(750) - a_w(745)} \qquad (2.4)$$

$$m \times 810^{n} = \frac{\frac{L_u(810)}{E_d(810)} a_w(810) - \frac{L_u(805)}{E_d(805)} a_w(805)}{a_w(810) - a_w(805)} \qquad (2.5)$$

$$m \times 850^{n} = \frac{\frac{L_u(850)}{E_d(850)} a_w(850) - \frac{L_u(845)}{E_d(845)} a_w(845)}{a_w(850) - a_w(845)} \qquad (2.6)$$

$$m \times 900^{n} = \frac{\frac{L_u(900)}{E_d(900)} a_w(900) - \frac{L_u(895)}{E_d(895)} a_w(895)}{a_w(900) - a_w(895)} \qquad (2.7)$$

Absorption coefficients of pure water at these wavelengths are: $a_w(745)$ =2.4590 m^{-1}, $a_w(750)$ =2.4700 m^{-1}, $a_w(805)$ =2.0494 m^{-1}, $a_w(810)$ =2.0916 m^{-1}, $a_w(845)$ =3.9835 m^{-1}, $a_w(850)$ =4.3758 m^{-1}, $a_w(895)$ =6.4708 m^{-1}, and $a_w(900)$ =6.8198 m^{-1}, which can be found from the work of Smith and Baker (1981) and Segelstein (1981).

The water-leaving reflectance $R_{rs}(\lambda)$ is calculated as

$$R_{rs}(\lambda) = \frac{L_u(\lambda)}{E_d(\lambda)} - G(\lambda) \qquad (2.8)$$

According to the Ruddick similarity spectrum, in the NIR wavelengths,

$$\frac{R_{rs}(\lambda_1)}{R_{rs}(\lambda_2)} = \frac{R_{rs\_n}(\lambda_1)}{R_{rs\_n}(\lambda_2)} = \frac{a_w(\lambda_2)}{a_w(\lambda_1)} \left(\frac{\lambda_1}{\lambda_2} \right)^{-\gamma} \qquad (2.9)$$

where R_{rs_n} represents the normalized remote sensing reflectance and γ is the spectral exponent of particle scattering. The absorption coefficients of pure water are $a_w(780)$ =2.3600 m^{-1} and $a_w(870)$ =5.3659 m^{-1}, respectively (Segelstein, 1981; Smith and Baker, 1981). For highly scattering waters dominated by non-algal particles, the value of γ mostly lies in the range of 0-1 (Gould et al. 1999; Babin et al., 2003). In this study, γ was set to be 1 and the wavelength pair (780 nm, 870 nm) suggested by Ruddick et al. (2005) was used. Therefore, combining Equations (2.8) and (2.9),

$$\frac{\frac{L_u(870)}{E_d(870)} - m \times 870^n}{\frac{L_u(780)}{E_d(780)} - m \times 780^n} = \frac{a_w(780)}{a_w(870)} \left(\frac{870}{780} \right)^{-1} \qquad (2.10)$$

Based on Equations (2.4)-(2.7) and Equation (2.10), model fits were applied by using the least-squares approach. The values of *m* and *n* were then retrieved, and the sky and sun glint was quantified. Initial values of *m* and *n* were both set to 0. The range of *m* and *n* were (0, +∞) and (-∞, 0), respectively.

2.5.2 Empirical Model Calibration and Validation

The corrected in situ spectrometer data, combined with in situ TSS and chl concentrations ([TSS] and [chl], respectively), were used to develop empirical relationships. Only subsets of the sampled sites were randomly selected for model development. The basis for selection of the bands is described in the Results and Discussion section. Single linear regressions were performed using the in situ TSS and chl values as the dependent variables and the selected single band, band ratios, and band differences as the independent variables. Log transforms of the dependent variables were also considered. Two independent variables that contributed most to the single regression fit were analyzed further using multiple linear regression techniques. In situ measurements of the sampled sites that were not selected for model development were used to evaluate the performance of models. Statistics including coefficient of determination (R^2), percentage root mean square error (RMSE), and number of data points (*n*) were listed.

2.6 Results and Discussion

2.6.1 Glint Removal of Field Spectrometer Data

Although no actual L_w measurements were collected in the field, we applied the method of Mobley (1999) as it is commonly used and accepted for sky and sun glint removal. Here we assume that the L_s correction results from using a constant water surface reflection coefficient ρ are close to the actual L_w values collected in the field. For the water-leaving reflectance spectra of the field measurements after L_s correction (Figure 2.2), the reflectance values at 350-380 nm and 890-900 nm are not zero. In particular, one reflectance spectrum of the Tippecanoe River is overcorrected and shows negative values. This could be due to the fact that L_s and L_u were not measured simultaneously, though the measurements were made within as short a time as possible.

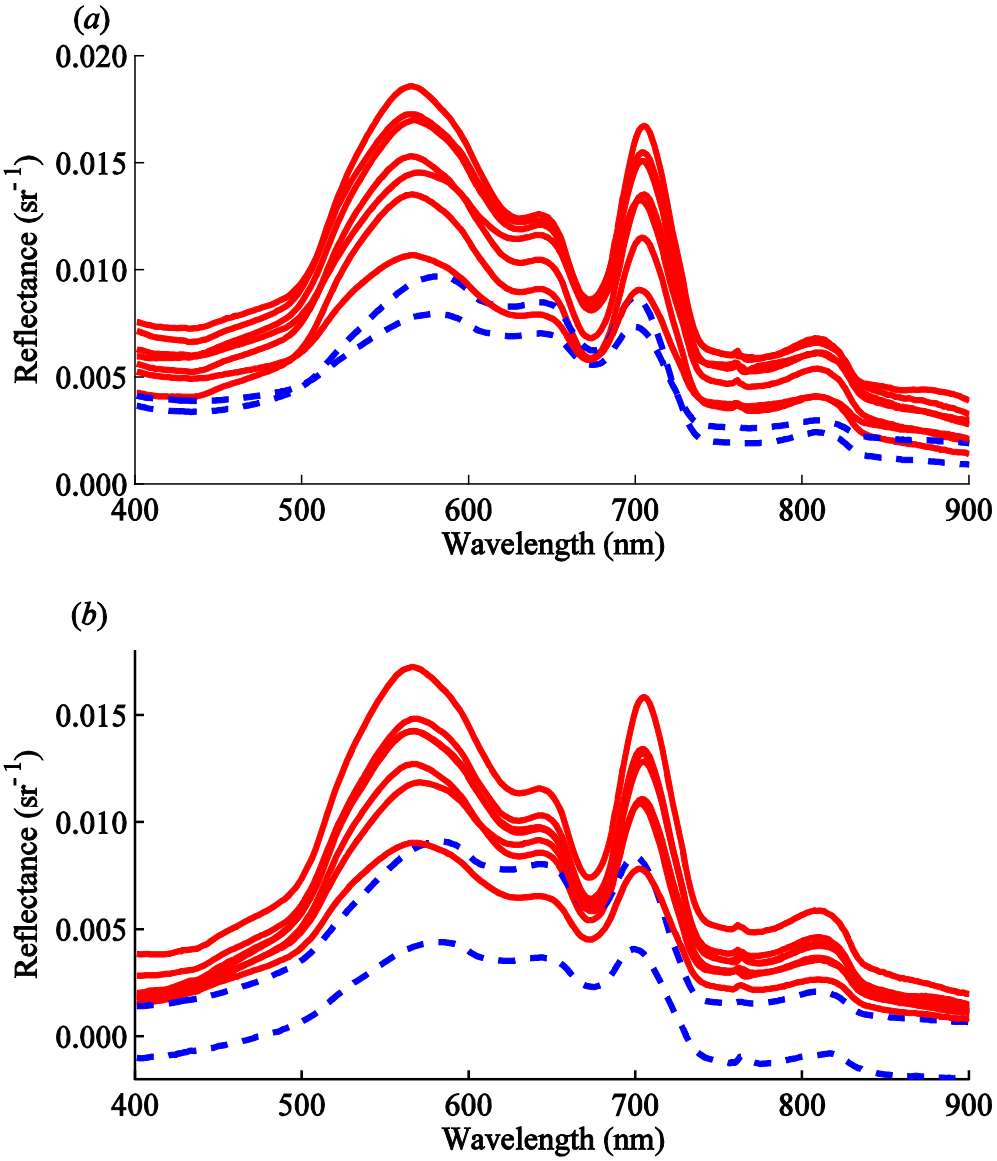

Figure 2.2 (a) Above-water reflectance spectra and (b) corrected water-leaving reflectance spectra for nine sample sites on the Wabash River (seven sites, red solid line) and the Tippecanoe River (two sites, blue dashed line) using the method of Mobley (1999).

The field spectral measurements were also analyzed using Kutser's correction and Tan's correction and the corrected reflectance spectra using these two methods were then compared to the results using Mobley's L_s correction (Figure 2.3). We only show the corrected spectra for a single site here since results at other sites are similar. As seen from the figure, Kutser's correction forces L_w to be zero in UV and NIR wavelengths, and therefore is not appropriate for our case; however, the reflectance spectra using Tan's correction are fairly close to the corrected results of using Mobley's correction.

To validate the robustness of Tan's method, we also ran the Hydrolight 5.2 radiative transfer model (Mobley and Sundman, 2013) to simulate total surface reflectance L_u/E_d and the remote sensing reflectance L_w/E_d in representative inland waters. The simulated L_u/E_d was processed using Kutser's correction as well as Tan's correction and the results were compared with the simulated L_w/E_d. A total of 500 simulations were run using the Case 2 IOP model from 350 nm to 900 nm with a 5 nm interval and assumed cloud free condition. The IOP characteristics were set to the typical values of inland waters and included a variety of absorption and backscattering spectra. Details can be found in the work of Gilerson et al. (2007). Optically deep water was assumed so that the bottom contribution was zero. Fluorescence of chl and CDOM were included. The solar zenith angle was 30^o and the wind speed was 5 m s^{-1}. The difference between corrected and Hydrolight-simulated reflectance spectra is measured using the index E,

$$E = \frac{\sqrt{\sum_{j=1}^{J} [\tilde{R}_{rs}(\lambda_j) - R_{rs}(\lambda_j)]^2}}{\sum_{j=1}^{J} R_{rs}(\lambda_j)} \qquad (2.11)$$

where $\tilde{R}_{rs}(\lambda_j)$ and $R_{rs}(\lambda_j)$ are the corrected and Hydrolight-measured remote sensing reflectance at wavelength λ_j, respectively, and J is the total number of bands. As calculated, the value of E for the 500 random simulations ranges from 0.03% to 0.88%. Since results are similar, Figure 2.4 only shows two examples for inland waters with different IOPs. As seen from the figure, the corrected spectrum using Tan's correction is almost identical to the remote sensing reflectance, which greatly improves on the results from the original Kutser's correction for application in turbid inland waters. We also tested simulations under different zenith angles (60° and 90°) and cloud cover conditions (30%, 60%, and 90%). Results are similar and E are within 1%. Therefore, the improved glint removal procedure was then used for all additional glint removal for the Wabash River and Tippecanoe River in this study.

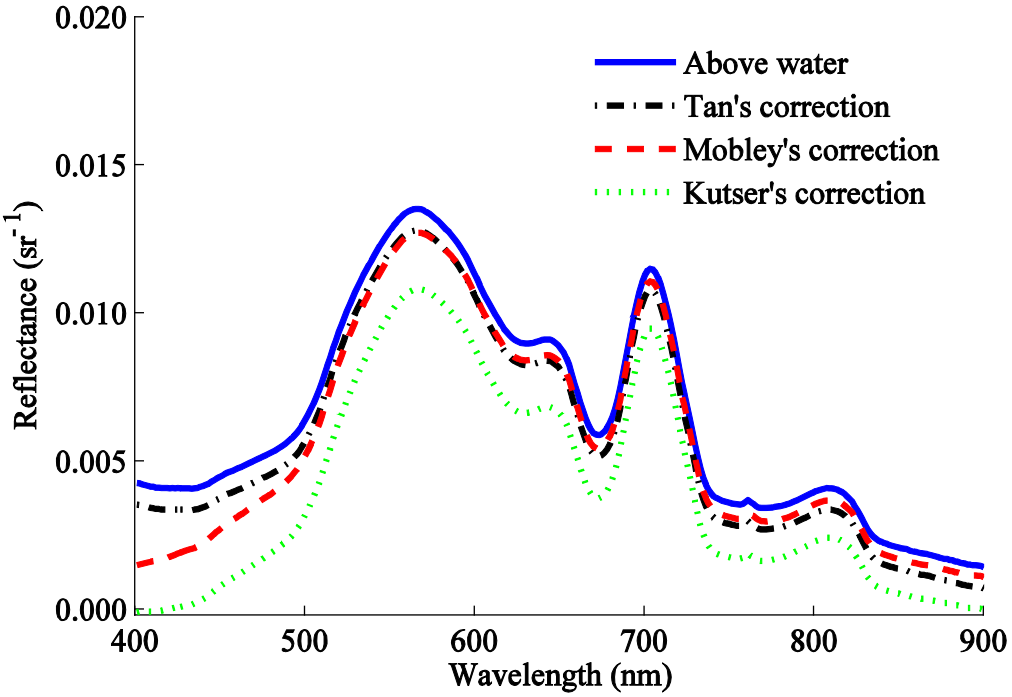

Figure 2.3 Comparisons of glint removal methods for a single site on the Wabash River.

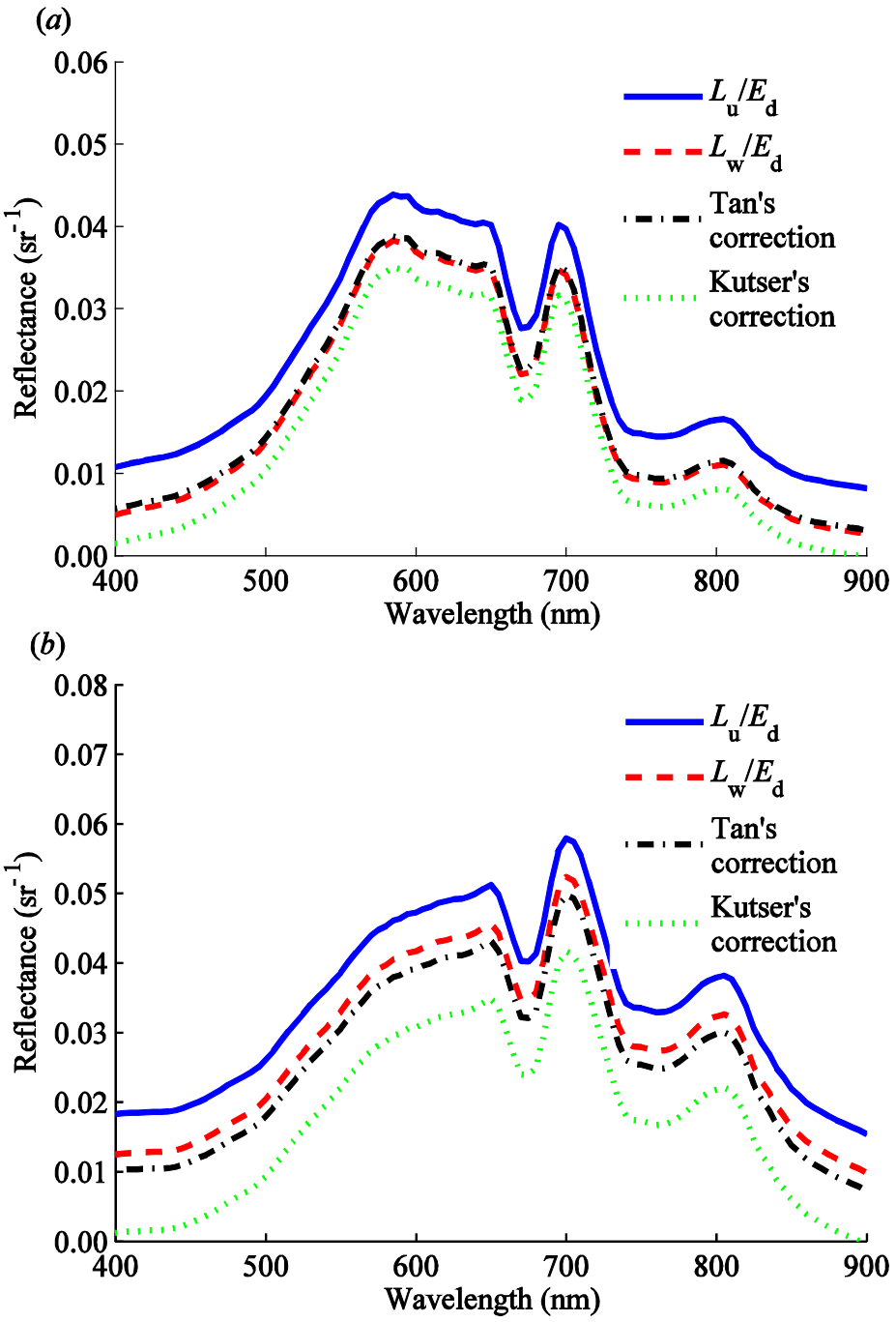

Figure 2.4 Results of Hydrolight simulations carried out for representative turbid inland waters with different IOPs. Definitions of L_u, L_w, and E_d are given in the main text. L_u / E_d is the simulated above-water reflectance and L_w / E_d the simulated water-leaving reflectance. Calculated values of the index E (Equation 2.11) are 0.33% and 0.88%, respectively.

2.6.2 Spectral Characteristics of the Wabash River

The hyperspectral information provided by field spectrometer enable the reconstruction of spectral characteristics of water bodies in the visible and near infrared wavelengths which can be used to distinguish waters dominated by different optical features. The Wabash River typically experiences two different types of IOPs during summer: (1) phytoplankton dominated and (2) sediment dominated. The IOP features of the Wabash River are closely associated with summer storm events. High concentrations of TSS were typically observed in the Wabash River following storm events, which deliver large amounts of sediment from terrestrial lands. The sediments also carry significant nutrients to the river, which results in phytoplankton development and turns the river water visibly green. Low concentrations of chl and TSS were found in the Wabash River after periods of time when few precipitation events occurred. Although no quantitative information was available on CDOM, the river water was never visibly stained brown during the summer, which indicates that the river water was not CDOM dominated. Despite the heavy agricultural use in the Tippecanoe River watershed, concentrations of both chl and TSS are lower in the Tippecanoe River (Table 2.1), likely due to the presence of two reservoirs upstream.

Table 2.1 Statistics (mean and standard deviation (SD)) showing that the Wabash River typically has higher chl and TSS concentrations than the Tippecanoe River based on the data collected in the summer of 2013.

	[TSS] (g m^{-3})		**[chl] (mg m^{-3})**	
	mean	**SD**	**mean**	**SD**
Tippecanoe River	9.6	4.2	15.7	6.2
Wabash River	65.8	55.3	29.9	20.0

To identify and differentiate IOPs that are indicative of different water quality variables, locations representing phytoplankton dominated and sediment-dominated waters were selected and analyzed (Figure 2.5(a)). For better description, “D” was used to represent the Wabash River stretch from Delphi to Americus, “A” to represent the stretch from Lafayette to Attica, and “L” to represent the stretch from Americus to Lafayette. Spectra from three dates represent phytoplankton dominated water: (1) D (24 May) ([chl]=70 mg m^{-3}, [TSS]=25 g m^{-3}), (2) D (24 June) ([chl]=43 mg m^{-3}, [TSS]=22 g m^{-3}), and (3) L (25 June) ([chl]=39 mg m^{-3}, [TSS]=16 g m^{-3}). The absorption by chlorophyll and other pigments results in low reflectance in blue (400-500 nm) and red (600-700 nm) wavelengths. In particular, the local minimum at 677 nm and peak at 704 nm are caused by the decreasing absorption of chlorophyll and increasing absorption of water as well as the fluorescence of chlorophyll. High TSS concentrations (48 g m^{-3}, 62 g m^{-3}, and 27 g m^{-3}) were found in dates (1) L (19 June), (2) D (20 June), and (3) A (21 June) following storm events. While the chl levels (13 mg m^{-3}, 11 mg m^{-3}, and 9 mg m^{-3}) were low, these waters represent sediment-dominated waters. This is also supported by the fact that the reflectance values of these waters are relatively high in the green and

red wavelengths, especially from 560 to 700 nm, so they lack the reflectance trough and peak in the red region caused by the absorption characteristics of chl.

The corrected water leaving reflectance spectra of all sampling sites with depth of more than 1 m are shown in Figure 2.5(b). Generally the reflectance values of the Wabash River are higher than those of the Tippecanoe River. The differences between R_{rs} (677) and R_{rs} (704) for the Tippecanoe River are not as obvious as those of the Wabash River. This is indicative of the lower chl concentrations in the Tippecanoe River. Another noticeable characteristic of the reflectance spectra is the relatively high reflectance values of the Wabash River at near infrared region (750-900 nm). As Gould et al. (2001) and Ruddick et al. (2006) suggest, in the NIR wavelengths the backscattering coefficient (b_b) can be viewed as negligible in comparison with the total absorption coefficient (a) and a can be further simplified as equal to the absorption coefficient of pure water (a_w) due to strong water absorption. Therefore, remote sensing reflectance can be expressed as

$$R_{rs} \propto b_b/a_w \qquad \text{when } b_b << a,\ a \approx a_w \qquad (2.12)$$

Since a_w can be treated as a constant for the Wabash River and Tippecanoe River where differences caused by variability in salinity and temperature are negligible, R_{rs} in the NIR wavelength range is determined by b_b. Therefore, it is quite likely that the relatively high reflectance values of the Wabash River from 750 to 900 nm are caused by high TSS concentrations in the Wabash River.

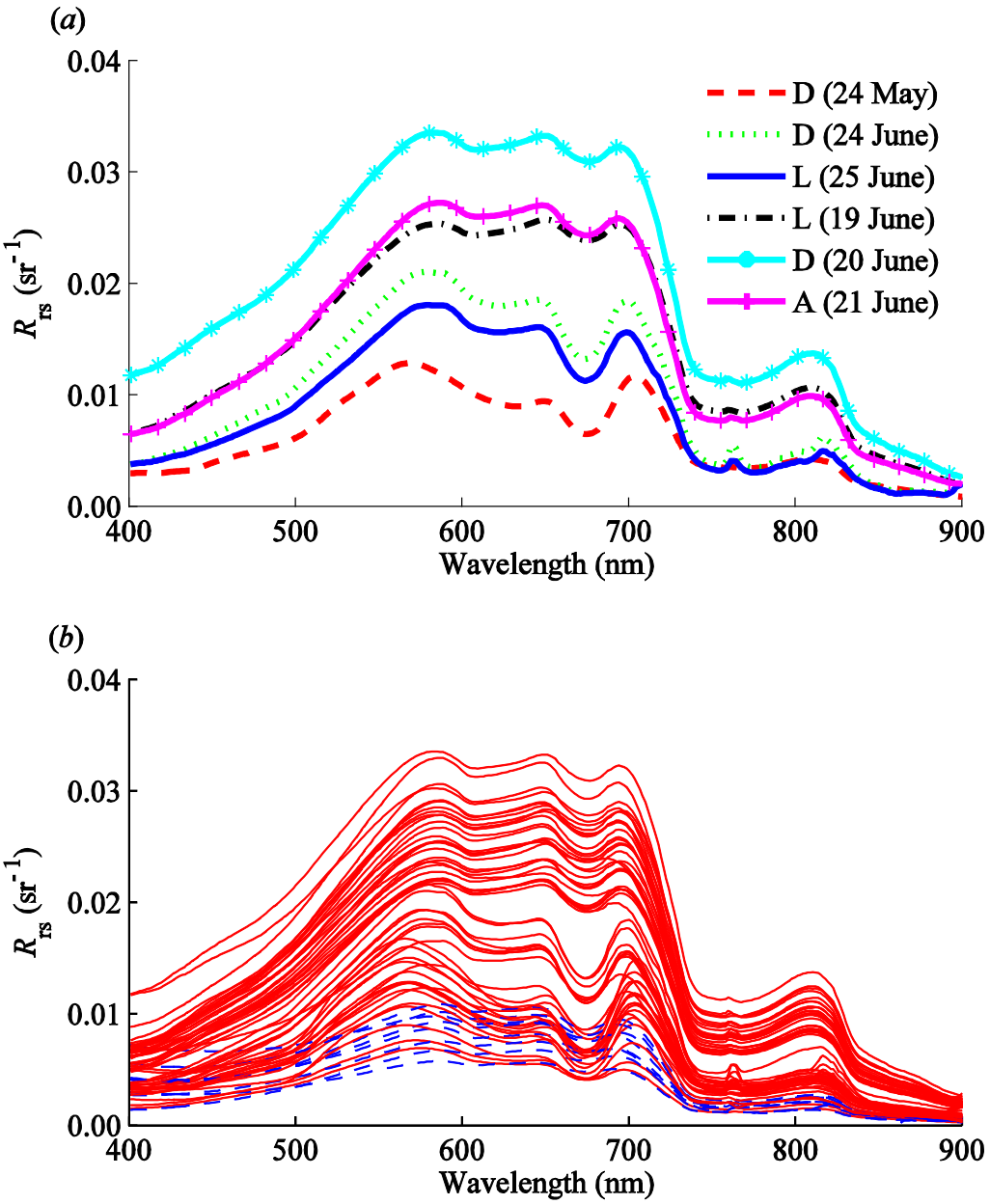

Figure 2.5 (a) Characteristic reflectance spectra from 2013 field measurements. See Section 2.5.2 for a description of areas D, L, and A. (b) Corrected water-leaving reflectance of all field data in the summer of 2013 using Tan's method. Red solid lines represent the Wabash River and the blue dashed lines represent the Tippecanoe River.

Empirical models are often based on developing best-fit correlational models between measured spectral characteristics and concentrations of OACs – often individually. To develop successful empirical models for inland waters, which are viewed as optically complex due to the suspended solids and CDOM delivered from terrestrial sources, it is important to use wavelengths that reflect the physical characteristics of water quality variables and are free of interference from competing optical features. For example, instead of using the blue and green wavelengths for [chl] estimation, which are common for Case I waters (Morel and Prieur, 1977; O'Reilly et al., 1998), most models for inland waters are focused on the red wavelengths, of which the reflectance trough around 670 nm and peak around 700 nm are closely related to the absorption and fluorescence of chl and the influence from CDOM and suspended solids is minimal (Moses et al., 2012; Olmanson et al., 2013). Models that use the reflectance ratio for wavelengths of ~670 nm in place of that for ~700 nm have been reported effective for estimating chl concentrations in inland waters (Moses et al., 2009; Gitelson et al., 2010; Matthews, 2011). Similarly, successful models for [TSS] in inland waters would avoid the blue and red wavelengths where the absorption by CDOM and chl are not negligible. Therefore, most algorithms utilize the scattering peak at the red edge, i.e., ~700 nm (Kallio et al., 2001; Olmanson et al., 2013) or the NIR wavelengths, such as the reflectance difference $R_{rs}(710) - R_{rs}(740)$ (Shafique et al., 2003).

2.6.3 Water Quality Models

A strong relationship was found between the ratio of $R_{rs}(704) / R_{rs}(677)$ and measured chl concentration, with R^2 values up to 0.95 (Figure 2.6(a)). Similar relationships have also been found in several previous studies (Moses et al., 2009;

Gitelson et al., 2010; Matthews, 2011; Olmanson et al., 2013). As discussed earlier, the local minimum at 677 nm and peak at 704 nm are caused by the decreasing absorption of chl and increasing absorption of water as well as the fluorescence of chl. Theoretically, the increase of chl concentration should be closely associated with the decrease of reflectance at 677 nm and the increase of reflectance at 704 nm. Therefore it is not surprising to find the high R^2 values for modeled [chl]. Scatter plots are generated using the modelled [chl] and measured [chl] of the remaining 20 samples (Figure 2.6 (b)). The resulting points fall close to the 1:1 line, which means that the model estimates provide a strong match to the field measurements. Furthermore, modelled and measured values show significant linear relationships with slopes close to 1.0. The RMSE value indicates that [chl] can be estimated with an accuracy of 18%. The uncertainty in [chl] estimation is likely to be related to the uncertainties in the [chl] analyses and/or field spectral measurements.

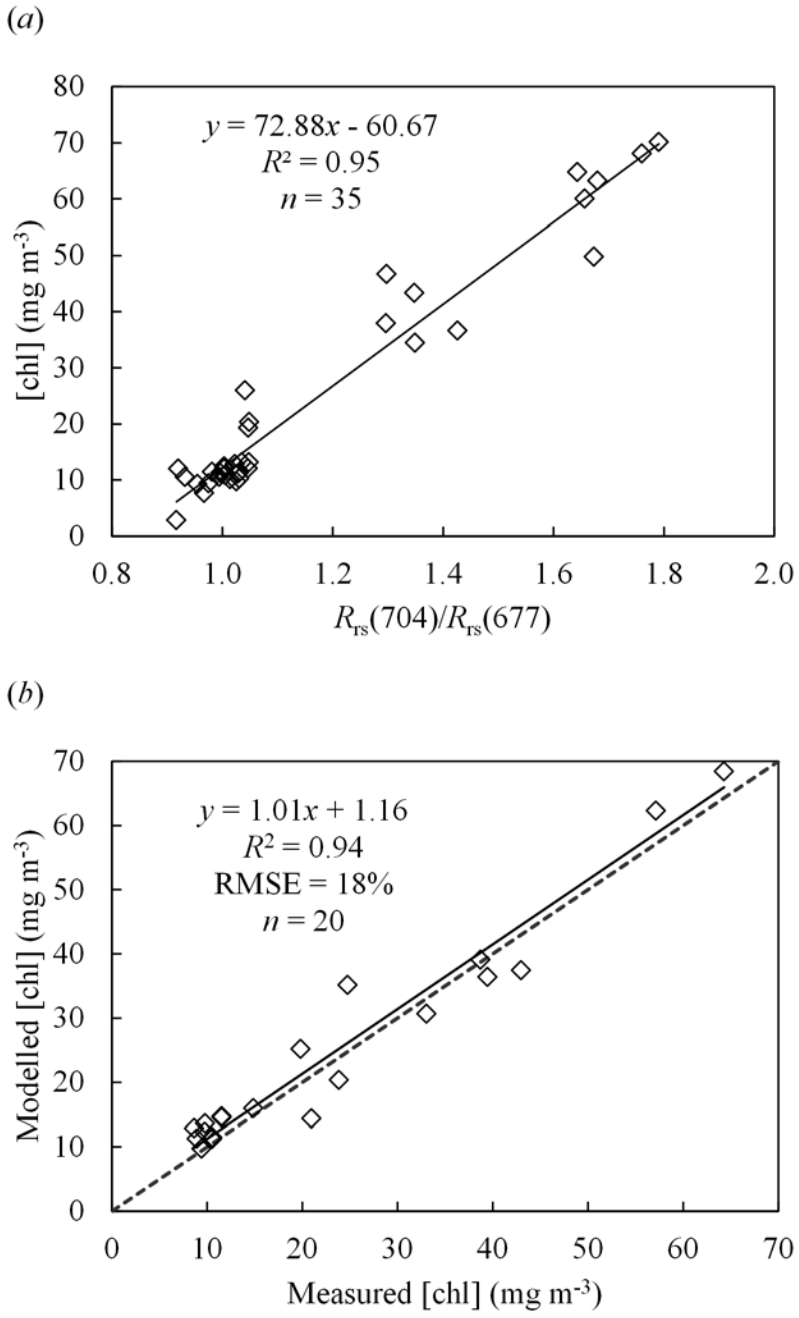

Figure 2.6 (a) Empirical model for estimating [chl] using the band ratio $R_{rs}(704)/R_{rs}(677)$ for the field data collected in the summer of 2013 and (b) comparison between measured [chl] and modeled [chl] for the Wabash River and the Tippecanoe River. Dashed line represents the 1:1 line.

TSS is composed of both chl and non-algal particles and therefore its IOP feature is complex and dependent on the specific water quality condition. For our dataset, a robust model was found between [TSS] and R_{rs} (704) with R^2 equal to 0.75 (Figure 2.7). This model avoids the absorption characteristics of chl and CDOM but uses the reflectance peak at 704 nm, which has been found to work well for TSS estimation in previous literature (Kallio et al., 2001; Olmanson et al., 2013). As discussed earlier, the reflectance values at NIR wavelengths are closely associated with TSS concentrations. Therefore, we also tested all bands from 700 nm to 900 nm and found that they showed strong correlation with [TSS] (Figure 2.8). As seen from Figure 2.8, correlation increases as wavelengths increase from 700 nm to 750 nm. The highest correlation (0.91) occurs at 752 nm and then correlation drops at ~765 nm, which is most possibly associated with the small peak of remote sensing reflectance at ~765 nm for some site measurements (Figure 2.5). The relatively low correlation around 890 - 900 nm is caused by the instrument noises and therefore the wavelengths from 890 nm to 900 nm were not included in the analysis. The reflectance at 752 nm generated a better model for [TSS] estimation with R^2 value up to 0.83 (Figure 2.9). Measured and modelled [TSS] show significant linear relationship with the regression slope close to 1.0 and The RMSE of TSS model is 29%. The estimates of [TSS] are in good agreement with measured values when [TSS] are less than 25 g m^{-3}, but show higher variance (up to 16 g m^{-3}) as [TSS] increases, which is expected since the predictive equation is ln([TSS]). Hence we conclude that the reflectance values at the red edge (704 nm) as well at the NIR wavelengths are valid in estimating the concentrations of TSS for the Wabash River.

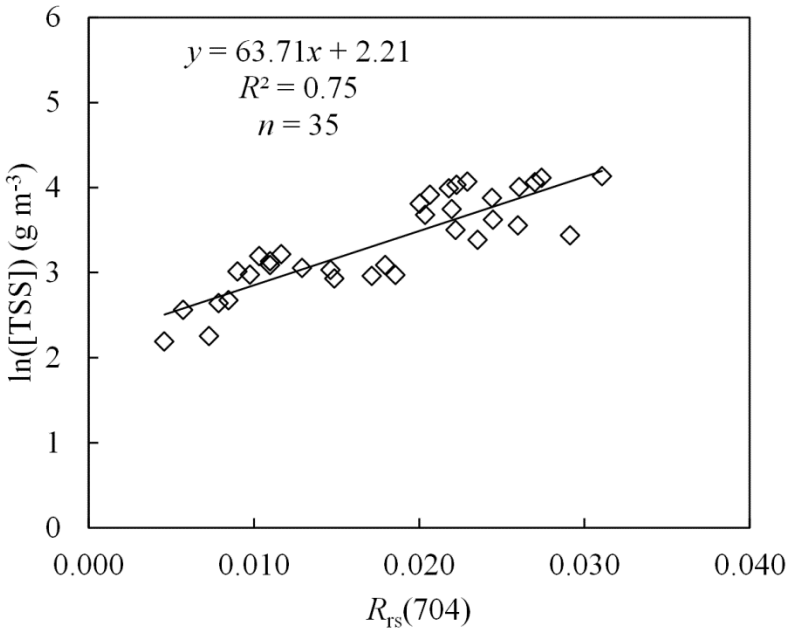

Figure 2.7 Empirical model for estimating [TSS] using $R_{rs}(704)$ for the field data in the summer of 2013.

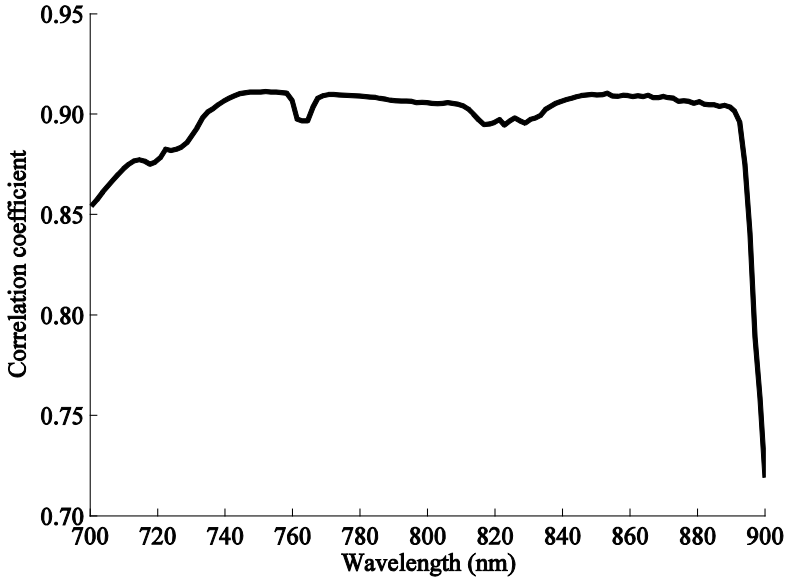

Figure 2.8 Correlation between reflectance at the near-infrared wavelengths and TSS concentrations.

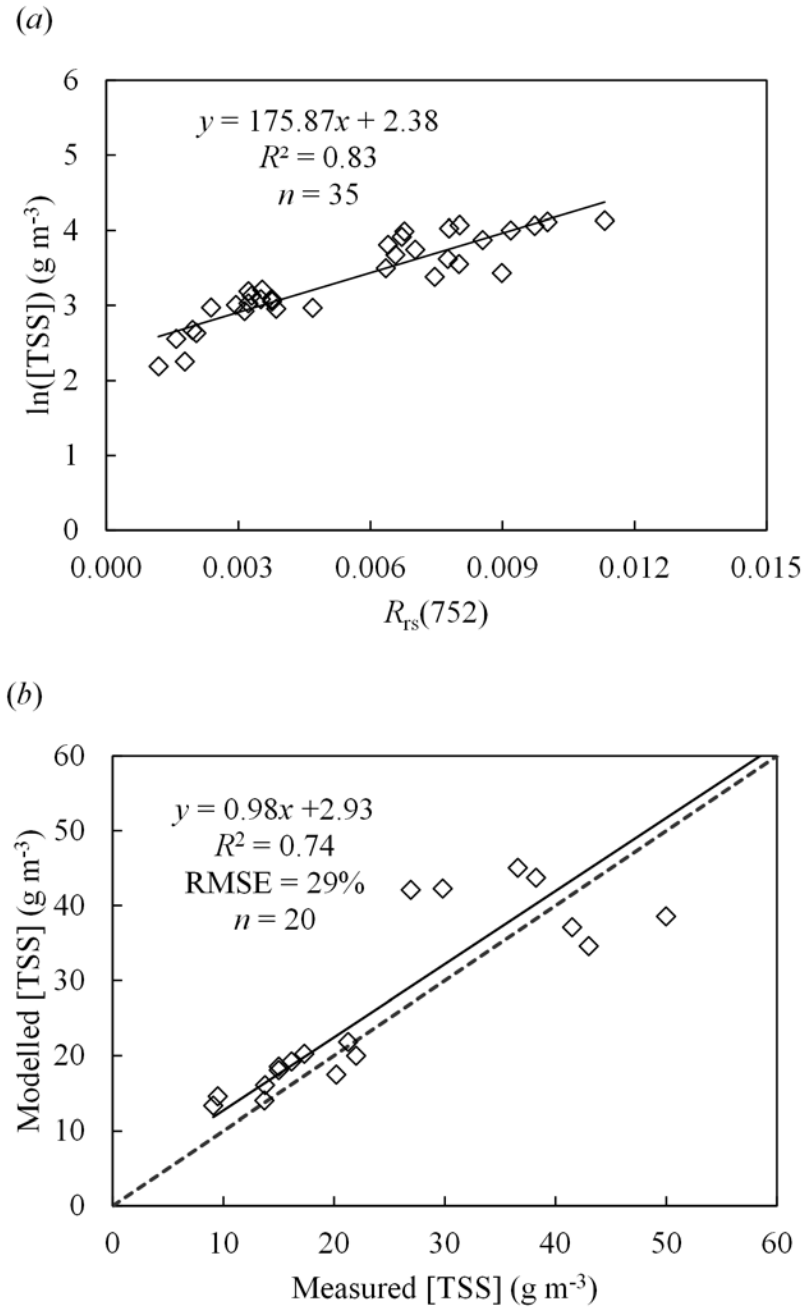

Figure 2.9 (a) Empirical model for estimating [TSS] musing $R_{rs}(752)$ for the field data collected in the summer of 2013 and (b) comparison between measured [TSS] and modeled [TSS] for the Wabash River and the Tippecanoe River. Dashed line represents the 1:1 line.

2.7 Conclusions

In this study, a method of removing sky and sun glint from above water reflectance spectra for turbid inland waters was developed. Since the assumption that water-leaving reflectance at UV and NIR wavelength region can be viewed as zero does not hold for turbid inland waters, Kutser's correction by fitting a power function using reflectance at 350-380 nm and 890-900 nm to represent the amount of glint does not apply. The method in this study combines Kutser's correction, Gould's glint removal algorithm, and Ruddick's similarity spectrum and is shown to successfully estimate the surface reflected component in water reflectance spectra with collected field data and radiative transfer modelling. In addition, this method does not require auxiliary measurements such as sky radiance, L_s, and wind speed.

Empirical models were developed to estimate [chl] and [TSS] for the Wabash River and the Tippecanoe River. Most empirical models are based on developing best-fit correlational models between measured reflectance/radiance and concentrations of OACs, and are not necessarily based on any physical insight to why the correlation exists and are highly dependent on the data and often not repeatable. The empirical models in this study are developed by identifying the key spectral characteristics indicative of waters dominated by various IOPs, while wavelengths that experience interference through competing optical features are avoided. For example, the concentration of chl is closely associated with the light absorption in the red wavelengths where the influences from CDOM and suspended solids are minimal. The ratio of the reflectance peak at 704 nm to the reflectance trough at 677 nm is a strong predictor of [chl]. Similarly, for estimation of TSS concentration, a robust model avoids the absorption characteristics of chl and

CDOM and utilized the reflectance peak at 704 nm. As analyzed, reflectance values at the NIR wavelengths are closely related to the amount of TSS and are also good predictors of TSS concentrations. The empirical models for [chl] and [TSS] estimation are validated by our field measurements. It has to be noted that the spectral reflectance and reflectance ratios that used for model development in this study also worked well for other researchers under different water quality regimes (Kallio et al., 2001; Kallio et al., 2003; Koponen et al., 2007; Olmanson et al., 2013). Therefore we conclude that these wavelengths and reflectance ratios are generally robust for the retrieval of water quality parameters.

While remote sensing has the advantage of quickly capturing a synoptic view of water quality condition, satellite remote sensing for monitoring water quality of rivers and streams are limited by resolutions that are too coarse to appropriately resolve the headwater rivers and streams contributing most significantly to the overall water quality. Meanwhile airborne platforms can collect highly resolved imagery for river systems, but they are not likely to be operated for regular monitoring due to the high operational cost and requirement of clear atmospheric conditions. Therefore, until the technical problems in satellites or unmanned aerial systems are solved, hand-held spectrometers provide a realistic and convenient way to collect spectral signatures of river waters.

Field spectrometer measurements have been widely used to obtain radiance, irradiance and reflectance of water targets. Spectral data collected by field spectrometers are considered to be accurate and are hence mostly used for the validation of atmospheric correction algorithms used to process remote sensing imagery. However, it is often overlooked that field spectrometers are designed to have high spectral resolutions and

provide continuous spectral signatures that can be used to identify the optimal or key spectral regions for water quality retrieval. These spectral regions, however, may not be effectively captured by some current multi-spectral sensors. Our results for the Wabash River show the key spectral bands needed for the estimation of water quality parameters and therefore provide useful suggestions for future satellite remote sensing. It is recommended that field spectroscopy should be used as a potential investigative technique of water quality, especially for rivers and streams, to complement satellite/airborne remote sensing which is limited by spatial resolution or high operating cost.

2.8 Acknowledgements

This project was financially supported by Indiana Water Resources Research Centre (IWRRC) and Purdue Water Community (PWC). The IOPs and bottom albedo measurements in the summer of 2014, as well as the data analysis and manuscript writing, were conducted in the frame of the author's PhD research work, funded by NASA Earth and Space Science Fellowship under Grant NNX14AL31H. We thank Dr. Reuben Goforth and his research group in the department of Forestry and Natural Resources at Purdue University for scheduling our boat sampling trips into their field work timeline. We also greatly appreciate comments and suggestions by three anonymous reviewers.

CHAPTER 3. WATER QUALITY ESTIMATION OF RIVER PLUMES IN SOUTHERN LAKE MICHIGAN USING HYPERION

3.1 Abstract

This study focuses on the calibration of an existing bio-geo-optical model for studying the spatial variability of water quality parameters including chlorophyll (chl), non-algal particles (NAP), and colored dissolved organic matter (CDOM) in episodic river plumes. The geographic focus is the St. Joseph River plume in southern Lake Michigan. One set of EO-1 Hyperion imagery and one set of boat-based spectrometer measurements were successfully acquired to capture episodic plume events. Coincident water quality measurements were also collected during these plume events. In this study, a database of inherent optical properties (IOPs) measurements and spectral signatures was generated and used to calibrate the bio-geo-optical model. Field measured concentrations of NAP and CDOM at 67% of the sampled sites fall within one standard deviation of the retrieved means using the spectrometer measurements. The percentage of sites is higher for the estimation of chl concentrations, which is 88%. Despite the dynamic nature of the observed plume and the time lag during field sampling, 77% of the sampled sites show field measured chl and NAP concentrations falling within one standard deviation of the Hyperion derived values. The spatial maps of water quality parameters generated from the Hyperion image provided a synoptic view of water quality conditions. Results show that concentrations of NAP, chl, and CDOM were more than

three times higher in conjunction with river outflow and inside the river plumes than in ambient water. It is concluded that the storm-initiated plume is a significant source of sediments, carbon and chl to Lake Michigan.

3.2 Introduction

As the second largest of the five Laurentian Great Lakes, Lake Michigan is an important resource of the Earth's surface fresh water, supports a variety of fish species and supplies drinking water for much of the population around the basin. In recent years, Lake Michigan has suffered water quality and ecological problems such as the decrease of primary productivity and fish populations (Fahnenstiel et al., 2010a, b). The Episodic Events Great Lake Experiment (EEGLE, 1998-2000) showed that river plumes in southern Lake Michigan have a significant and complex effect on water quality and the lake ecosystem (Lohrenz et al., 2004). These river plumes enhance the amount of nutrients and sediments delivered from terrestrial resources, diminish light that can penetrate through water, and in turn can regulate nutrient cycling and affect the rate and amount of primary production in the lake. As the observed river plumes are closely associated with episodic storm events, it is important to monitor and understand the water quality condition of Lake Michigan during these storm events for better protection and management of the lake, especially since such precipitation events are projected to be more intense and frequent in the future (Kling et al., 2003).

Conventional water sampling programs are often not adequate to report changes in nutrient levels, phytoplankton biomass and sediment loadings given that river plumes can vary rapidly in time and/or space. The remote sensing of river plumes is attractive due to its improved spatial coverage within a short time interval and has been increasingly

useful over the last two decades for water quality monitoring in Lake Michigan. Multiple satellite sensors such as SeaWiFS, AVHRR and MODIS (Lesht et al., 2002; Shuchman et al., 2006; Lohrenz et al., 2004, 2008; Shuchman et al., 2013a) have been used to estimate chlorophyll (chl) concentration and primary production in Lake Michigan. However, there are few studies focusing on the quantitative mapping of river plumes caused by episodic storm events. The ability of satellite imagery in "seeing" river plumes depends particularly on its spatial resolution (Mouw et al., 2015). While instruments such as AVHRR are capable of detecting large suspended plumes in Lake Michigan (Lohrenz et al., 2004), their coarse resolution makes it challenging and inappropriate for the study of small river plumes which extend only several kilometers. In contrast, the spatial resolution of the Hyperion satellite, which is 30 m, is suitable for identifying riverine plumes, as Zhu et al. (2013) have demonstrated. Hyperion also has sufficient spectral resolution to enable mapping of lake water quality from space (Giardino et al., 2007). Therefore, it is likely that Hyperion and future sensors with similar operational characteristics can be used for regular monitoring and the study of the spatial variability of river plumes in Lake Michigan.

One of the main challenges for retrieving water quality parameters in the river plumes of Lake Michigan is that the lake water is assumed to be optically complex Case II water, for which the optical properties are not solely influenced by phytoplankton (Morel and Pieur, 1997). This is particularly true in the near shore areas and river mouths of the Great Lakes since the concentrations of suspended sediments and dissolved organic matter are high enough to optically compete with the phytoplankton (Shuchman et al., 2013b). Current existing band ratio algorithms such as the NASA standard ocean based

algorithms OC3 and OC4 (O'Reilly et al., 1998) assume the water is phytoplankton dominated and are not applicable to the Case II water scenario. In addition, these empirical algorithms are often based on developing best-fit correlational models between chl concentrations and measured remote sensing reflectance, R_{rs}, and therefore are often not transferrable. In order to be used for the Great Lakes, the OC3 and OC4 algorithms were modified and the coefficients were recalculated in the work of Lesht et al. (2013). It is also important to understand that the tuned algorithms for the Great Lakes work well only in certain portions of the Great Lakes and may not be optimal for all types of Great Lakes water (Shuchman et al., 2013b).

The development and application of a truly transferrable and reliable bio-geo-optical model for river plume monitoring is a necessary and important step to enable the use of remote sensing for river plumes study. Bio-geo-optical models focus on the physical properties of each major optically active constituent (OAC) and quantify the relationship between IOPs and apparent optical properties (AOPs), which in this study is the remote sensing reflectance, R_{rs}. Concentrations of each OAC can then be estimated simultaneously from measured R_{rs} by inverting the bio-geo-optical model. The bio-geo-optical algorithm was initially developed by Garver and Siegel (1997) and Maritorena et al. (2002) for oceanic applications and then was reformulated for coastal and lake water observations (Brando and Dekker, 2003; Giardion et al., 2007). The Color Producing Agent Algorithm (CPA-A) was developed specifically for the retrieval of water quality in the Great Lakes using satellite remote sensing (Pozdnyakov et al., 2005). It has been demonstrated that this algorithm can be implemented for all types of Great Lake water, while producing estimates that agree favorably with field measurements and improving

the retrieval accuracy of chl concentration as compared to the band ratio approach (Shuchman et al., 2006, 2013a, 2013b). Unlike other Case II water algorithms, the CPA-A provides estimates of dissolved organic carbon (DOC) but not of colored dissolved organic matter (CDOM) or gelbstoff. CDOM is the portion of DOC in natural waters that absorbs visible light and is directly related to the measured signals leaving out of water surfaces. One underlying assumption of the CPA-A is that good correlations exist between DOC and CDOM. However, this is not always true and the relationship can be complicated by environmental factors and human related activities (Brezonik et al., 2015).

There are multiple techniques that can be used for the inversion of bio-geo-optical models, such as the matrix inversion method (Brando and Dekker, 2003) and the optimization method (Korosov et al., 2009). These methods either require the input of inherent optical properties (IOPs), such as the specific absorption and backscattering coefficients of each OAC at each satellite spectral band or appropriate initial values of unknown parameters including OAC concentrations to be successful. In contrast, another inversion method, the look-up table approach, is very appealing as it requires no prior assumptions for parameterization and is able to simultaneously retrieve multiple parameters (Louchard et al., 2003; Mobley et al., 2005). In the look-up table approach, a database of reflectance spectra is simulated and corresponds to a variety of environmental conditions. By searching the closest match of the field measured spectrum in the database, parameters such as water column properties can then be retrieved.

Characterization of the optical properties of river plumes is important not only as inputs to bio-geo-optical models but also as indicators of the biogeochemical processes. Although multiple investigations on the optical characterization of the Great Lakes have

been conducted (Bukata et al. 1985; Lorenz et al., 2004; Binding et al., 2008; Effler et al., 2010; O'Donnell et al., 2010; Peng, et al., 2010), these measurements are not readily available, and few of these measurements are focused on river plumes. In addition, the heterogeneity of backscattering properties of Great Lake waters can be exacerbated by episodic events (O'Donnell et al., 2010; Effler et al., 2013).

The overall goal of this study is to calibrate a remote sensing inversion algorithm for assessing the spatial variability of water quality parameters including chl, non-algal particles (NAP), and CDOM in river plumes of Lake Michigan that can be used to complement conventional ground-based methods. Our specific objectives are to: (1) collect and disseminate field data including in-situ concentrations of OACs, measurements of IOPs, and spectral signatures of lake water when river plumes occur; (2) calibrate the remote sensing algorithm based on an existing bio-geo-optical model and the look-up table method for adequately retrieving water quality parameters; and (3) evaluate the ability and usefulness of Hyperion imagery for the study of the spatial structure of river plumes in Lake Michigan.

3.3 Study Area

This study was conducted near the mouth of the St Joseph River and its near shore region within Lake Michigan (Figure 3.1). The St Joseph River watershed (Hydrologic Unit Code 04050001) is located in southern Michigan and northern Indiana and drains approximately 12,134 km^2. Land use in the watershed is approximately 60% agriculture, 20% forests, and <10% urban lands. Bank erosion and sedimentation have been found to be associated with agricultural practices in the watershed, while cities located along the mainstem of the St Joseph River also contribute significantly to the degradation of water

quality (Great Lakes Tributary Monitoring Program, http://projects.glc.org/tributary/models/stjoseph.html). Between late spring and late fall, stream discharge associated with storm events usually forms buoyant plumes in the nearshore region of Lake Michigan and contain sediments, nutrient, and pollutants that have significant impacts on the water quality in the receiving lake (Nekouee et al., 2013). The study site was selected after a review of the archive of satellite images confirmed that episodic St Joseph River plumes can be resolved by 30-m Landsat images, which suggested that the Hyperion satellite - which has the same spatial resolution as Landsat - should also be able to detect the St Joseph River plumes.

Figure 3.1 Major study area focuses on the St Joseph River tributary in southern Lake Michigan. River plumes occurred at the river mouth and the near shore region. The Hyperion image was collected on August 7, 2012.

3.4 Data Sources and Methods

3.4.1 Satellite Imagery

Field campaigns were coordinated to capture episodic St Joseph River plumes based on the flyover dates of the EO-1 satellite. After multiple field campaigns, we successfully collected one set of usable EO-1 imagery that coincided with plume field sampling on August 7, 2012 that was associated with a storm event on August 4, 2012. Both EO-1 Advanced Land Imager (ALI) and Hyperion images were acquired and downloaded from the U.S. Geological Survey (USGS) web page (http://eo1.usgs.gov). The ALI and Hyperion footprints are overlapping with a single Hyperion image covering about 1/4 of the ALI footprint. The ALI imagery was used for the georegistration of Hyperion, as described in the following "Image Processing" section.

The Hyperion instrument is on board the EO-1 satellite (http://eo1.gsfc.nasa.org), which was launched by NASA in November 2000 and operates at an altitude of 705 km. Hyperion is a pushbroom-type imaging spectrometer and has a total of 242 spectral bands ranging from 400 nm to 2500 nm. It has a spatial resolution of 30 m and each spectral band is 10 nm wide. This means it can provide more continuous spectral data than the discrete broad bands of more widely used current satellite sensors such as Landsat ETM+, MODIS and SeaWiFS. The swath width and typical swath length of a Hyperion scene is 7.7 km and 42 km, respectively. Hyperion offers a 12-bit dynamic range and the signal-to-noise ratio (SNR) of Hyperion is typically in the range of 50-150. Although the low sensitivity may render Hyperion unsuitable for open ocean water observations, it has been clearly demonstrated that Hyperion imagery can be very useful in mapping water properties of coastal and lake areas (Brando and Dekker, 2003; Giardino et al., 2007).

This has been attributed to the increased water turbidity in these waters, resulting in stronger signals emanating from the water surface.

3.4.2 Field Sampling

In addition to the August 7, 2012 plume event described above, one set of boat-based spectral data was also successfully collected during an EO-1 satellite flyover using a GER1500 spectrometer (http://www.spectravista.com/), which captured another storm-initiated river plume on April 21, 2014. Spectrometer measurements of lake water were taken using the recommended measuring geometry of standing ~135° away from the solar plane and pointing the spectrometer ~40° and ~140° from the zenith angle for the measurements of sky radiance L_s and total upwelling radiance L_u (Mobley, 1999). Foams and floating material as well as boat shadow were avoided during spectrometer measurements (Muller et al., 2003). For both of the two field campaigns on August 7, 2012 and April 21, 2014, boat-based in-situ water sampling was carried out within a 4-hour time window immediately after the EO-1 overpass and image collection. A total of 28 sampling locations (2 at the river mouth and 26 in the near-shore) were measured on August 7, 2012 and 21 locations (all in near-shore region) were sampled on April 21, 2014. All water samples were taken approximately 0.5 m below water surface with a van Dorn sampler.

3.4.3 Lab Analyses

Water samples collected for both plume events were stored in a dark and cold cooler with ice until returned to lab for water quality analysis. Water quality variables quantified were chl, NAP, and CDOM. Standard methods of analysis were applied to estimate the concentrations of chl and total suspended solids (TSS) (Eaton et al., 1998). A

100 ml sub-sample was filtered onto Whatman GF/F glass fiber filters, macerated in 10 ml 90% acetone solutions and analyzed spectrometrically to estimate chl concentration. TSS concentration was determined by filtering a 200 ml sub-sample using Whatman GF/F glass fiber filters and then oven drying the pre-weighted filter at 105 ± 1°C for at least one hour to calculate the weight difference. Since TSS can be divided into phytoplankton and NAP (also referred as tripton), NAP concentration is usually indirectly estimated from concentrations of TSS and chl using the equation $[NAP]=[TSS]-\beta\cdot[chl]$ ([TSS] - concentration of TSS in g m^{-3}, [NAP] - concentration of NAP in g m^{-3}, and [chl] - concentration of chl in mg m^{-3}), with β ranging from 0.02 to 0.1 (Giardino et al., 2007). However, because the chl concentrations in this study are relatively low (< 25 mg m^{-3}), we regard the [TSS] measurements as approximating the NAP concentrations.

All 21 samples collected on April 21, 2014 were also used to measure the absorption spectra of each OAC. These analyses were carried out immediately after the samples arrived in the lab using a Beckman Coulter DU 730 spectrophotometer. CDOM absorption spectra were acquired by comparing the absorbance difference between filtered water samples and a pure water "blank". The total particulate absorption spectra were acquired by scanning pigments and particles retained in filter pads and comparing with the reference filter "blank". The detailed lab procedure followed is described in the NASA's standard operating protocol of satellite ocean color remote sensing (Muller et al., 2003).

3.4.4 Field and Lab Data Processing

Field spectrometer measurements collected on April 21, 2014 were processed to obtain the remote sensing reflectance, R_{rs}, of water targets, which requires unwanted

signals caused by sun and sky glint to be removed. The measured sky radiance, L_s, is used to describe the glinting effect by adopting a correction coefficient, ρ, which represents the Fresnel reflection of the sea surface. In this study, ρ takes a value of about 0.028 (Mobley, 1999). R_{rs} is then calculated using the following equation:

$$R_{rs} = (L_u - \rho \cdot L_s)/E_d \qquad (3.1)$$

with L_u being the total upwelling water radiance, and E_d representing the measured downwelling solar irradiance.

Since absorption coefficients are additive, the total particulate absorption $a_p(\lambda)$ can be expressed using

$$a_p(\lambda) = a_{chl}(\lambda) + a_{nap}(\lambda) \qquad (3.2)$$

where $a_{chl}(\lambda)$ represents the absorption contributed by phytoplankton and $a_{nap}(\lambda)$ is the absorption associated with non-algal particles. The value of $a_{nap}(\lambda)$ can be separated from $a_{chl}(\lambda)$ by extracting the pigments on a filter pad with methanol in lab. However, no separate lab measurements of NAP absorption were performed. Instead, a numerical model was used to partition the total particulate absorption into the absorption of phytoplankton and non-algal particles (Zhang et al., 2009). In the model, the absorption ratios of phytoplankton reported in previous literature were adopted and $a_{nap}(\lambda)$ was described using an exponential model with a background constant.

3.4.5 Image Processing

USGS provides both the Hyperion Level 1 Radiometric product and ALI Level 1 G product. Only the Hyperion image was used for the reflectance model development, as Lee and Carder (2002) suggest that a total of around 15 spectral bands covering 400-800 nm are necessary for most remote sensing of water quality. The ALI image that was

geometrically corrected was used as the base map for the Hyperion image georegistration. The Hyperion image has a total of 242 bands but only 198 bands are radiometricly calibrated due to the detectors' low responsivity. Two noisy bands centered at 427 and 437 nm were discarded as recommended by Jupp et al. (2002). The Hyperion image was then recalibrated, fixed for out-of-range data and outliers, and desmiled according to the procedure described in Datt and Jupp (2004). Along-track stripes are common in push-broom systems and are referred to as "streaks". This "streaking" effect also exists in Hyperion data and needs to be minimized by "destreaking" (Jupp et al., 2002). However, destreaking of the Hyperion image was not done in this study as we found that our specific study area in the images is free from the streaking effect in the visible and near-infrared (VNIR) bands, and destreaking itself can alter the statistics of the images and introduce extra noise (Jupp et al., 2002). Therefore, only the VNIR wavelengths from 478 to 750 nm (27 spectral bands) were selected.

Atmospheric correction of satellite imagery is very important since a considerable part of the signal received at aircraft and satellite sensor platforms is from atmosphere scattering instead of from the ground target, in this case the water (IOCCG, 2010). Atmospheric correction of the Hyperion image was completed using the FLAASH (Fast Line-of-sight Atmospheric Analysis of Spectral Hypercubes) module in ENVI (by Research Systems, Inc). FLAASH supports atmospheric correction for hyperspectral sensors. It incorporates the MODTRAN 4 radiative transfer model with full parameterization of the atmosphere and aerosol types and also corrects for adjacency effects. The output of FLAASH is irradiance reflectance, which is then used to calculate radiance reflectance using a scaling factor of π by assuming the water surface functions

as a Lambertian surface. For this study, we assumed a mid-latitude summer atmospheric model and an urban aerosol model. No water or aerosol retrieval was used. Instead, based on the weather condition on August 7, 2012, initial visibility was set to 40 km in FLAASH to correct the Hyperion image.

3.4.6 Algorithm Description

3.4.6.1 Bio-geo-optical Model

Since lake water in the near-shore region is considered to be optically complex Case II waters, a bio-geo-optical model was used for retrieving water quality variables in this study. The model is based on the radiative transfer properties of water, which quantifies the relationship between the IOPs and apparent optical properties (i.e., remote sensing reflectance measured by spectrometer and satellite in this study) of the water column and in-water constituents, but is simplified for specific assumptions. To validate the robustness of the bio-geo-optical model, we also carried out simulations with Hydrolight 5.2.2 radiative transfer software (Mobley, 1994; Mobley and Sundman, 2013) to see whether the model fits with radiative transfer theory.

A bio-geo-optical model was proposed by Gordon et al. (1988) to fit the radiance reflectance just beneath the water surface, r_{rs}, with a polynomial function of absorption and backscattering coefficients. Austin (1980) suggested using a factor of 0.544 to correct the air-water surface effect and to convert the subsurface radiance to the above-water radiance. Combining these two models together, the above-water radiance reflectance, $R_{rs}(\lambda)$, can be described as:

$$R_{rs}(\lambda) = 0.544 \cdot \{g_0 \cdot u(\lambda) + g_1 \cdot [u(\lambda)]^2\} \qquad (3.3)$$

with

$$u(\lambda)=b_b(\lambda)/(a(\lambda)+b_b(\lambda)) \quad (3.4)$$

Here g_0 and g_1 are constants, $a(\lambda)$ is the total absorption coefficient, $b_b(\lambda)$ is the total backscattering coefficient, and λ is the wavelength. The values of g_0 and g_1 were set to 0.0949 and 0.0794, respectively, according to Gordon et al. (1988).

The total absorption and backscattering coefficients are additive and can be expressed as the sum of absorption and backscattering coefficients of both optically sensitive constituents in the water column and water molecules. Therefore, the total absorption coefficients can be expressed mathematically by introducing absorption terms for water, a_w, and the three optically active components: chl, a_{chl}, CDOM, a_{cdom}, and NAP, a_{nap}:

$$a(\lambda)=a_w(\lambda)+a_{chl}(\lambda)+a_{cdom}(\lambda)+a_{nap}(\lambda) \quad (3.5)$$

In this study, we combined the backscattering coefficients of chl and NAP together by using one single term, $b_{b,p}(\lambda)$, which represents the backscattering coefficients of suspended particles including both chl and NAP. Since CDOM contribution to backscattering is negligible, the total backscattering coefficients can be expressed as:

$$b_b(\lambda)=b_{b,w}(\lambda)+b_{b,p}(\lambda) \quad (3.6)$$

In Equations (3.5) and (3.6), the values of $a_w(\lambda)$ were taken from Pope and Fry (1997) and the backscattering coefficients of pure water, $b_{b,w}(\lambda)$, were taken from Morel (1974). The absorption spectra of CDOM, chl, and NAP can be further expressed as

$$a_{cdom}(\lambda)= a_{cdom}(440)\cdot\exp[-S_{cdom}\cdot(\lambda-440)] \quad (3.7)$$

$$a_{chl}(\lambda)=[chl]\cdot a^*_{chl}(\lambda) \quad (3.8)$$

$$a_{nap}(\lambda)=[NAP]\cdot a^*_{nap}(\lambda) \quad (3.9)$$

where $a_{cdom}(440)$ is the absorption coefficient of CDOM at 440 nm and is used to describe the amount of CDOM; S_{cdom} is the exponential slope for CDOM and was measured in lab with collected water samples; and the specific absorption coefficients (i.e., absorption coefficients per unit of mass) of chl and NAP are denoted as $a^*_{chl}(\lambda)$ and $a^*_{nap}(\lambda)$.

No backscattering coefficients of suspended particles were measured. In this study, $b_{b,p}(\lambda)$ is described using the following equation:

$$b_{b,p}(\lambda)= [p]\cdot b^*_{b,p}(550)\cdot(550/\lambda)^{\gamma} \quad (3.10)$$

where [p] is the concentration of suspended particles, which equals to the lab measured TSS values and is approximated by C_{nap}; γ is the spectral power for particle backscattering coefficient, and $b^*_{b,p}(550)$ is the particle specific backscattering coefficient (i.e., backscattering coefficients per unit of mass) at 550 nm.

3.4.6.2 Look-up Table Method

With the above considerations, there are only five unknowns in this model: $b^*_{b,p}(550)$, γ, [chl], $a_{cdom}(440)$, and [NAP]. Here in this study, a look-up table method was adopted to retrieve the five unknowns (Mobley et al., 2005). A database of R_{rs} spectra was assembled using the bio-geo-optical model described above and using various values of these five unknowns. Values of each unknown were placed at different increments within a pre-defined range. Theoretically, this database should at least contain R_{rs} spectra generated for environmental conditions close to those occurring in nature at the time and

location where the spectral data was acquired. This database also may contain spectra corresponding to environmental conditions much different from our study area.

The ability of the look-up table method to accurately retrieve the concentrations of OACs depends upon the correct selection of the sampling intervals for the five unknowns. Sensitivity analysis of the bio-geo-optical model was carried out to evaluate how sensitive the modeled R_{rs} spectrum responds to the change of these five unknowns. First, initial values of the five unknowns were randomly set; then the change of the R_{rs} spectrum was studied with only one parameter changing at one time. The change of the R_{rs} spectrum is described using mean squared error (MSE). The higher the MSE per change, the more sensitive the model is to the specific parameter.

Values of these five unknowns were retrieved by comparing measured R_{rs} spectrum to each spectrum in the database and finding the closest match. The closest match is defined as minimizing the root mean squared deviation (RMSD) between modeled and measured R_{rs} spectrums, which can be described as

$$\mathrm{RMSD} = \sqrt{\sum_{j=1}^{J} [\breve{R}_{rs}(\lambda_j) - R_{rs}(\lambda_j)]^2 / J} \qquad (3.11)$$

with J representing the number of all the bands used in the model. $\breve{R}_{rs}(\lambda_j)$ is the modeled R_{rs} spectrum at band j and $R_{rs}(\lambda_j)$ is the measured R_{rs} spectrum at band j. Considering the possible uncertainty existing in satellite and field spectral measurements, error analysis was also conducted by statistically analyzing the distribution of estimates for multiple matching spectra, which are defined as matching the satellite/spectrometer measured spectra by showing RMSD within certain level. This is also useful for evaluating the uncertainty of the estimates.

3.5 Results and Discussion

3.5.1 Lab Measurements of IOPs

After normalization using the absorption coefficient at 440 nm $a_{cdom}(440)$, the specific absorption spectra of CDOM were acquired (Figure 3.2). The derived spectral slope, S_{cdom}, ranged from 0.0133 nm^{-1} to 0.0200 nm^{-1}, which is in good agreement with those reported for inland and coastal waters (Binding et al., 2008; Babin et al., 2003; Roesler et al., 1989). The ensemble mean of the specific absorption spectra was used to represent the specific absorption spectra of CDOM in this study and the corresponding S_{cdom} equaled to 0.0176 nm^{-1} (Figure 3.2).

The lab-measured total particulate absorption is shown in Figure 3.3a. It is noticed that the absorption of particles at 750 nm was not zero, which is reasonable for case II waters. The absorption spectra of NAP (a_{nap}) were separated using the numerical modeling method described earlier (Zhang et al., 2009) and the derived spectral slope of NAP, S_{nap}, ranged from 0.004 nm^{-1} to 0.013 nm^{-1}. These values are similar to the reported values for inland and coastal waters in previous literature (Brando and Dekker, 2003; Roesler et al., 1989). After a_{nap} was determined, the absorption spectra of chl were calculated by deducting a_{nap} from the measured total particulate absorption a_p. The specific absorption spectra of chl and NAP, i.e, $a^*_{chl}(\lambda)$ and $a^*_{nap}(\lambda)$, were determined by using the similar method described above for CDOM and are shown in Figure 3.3b.

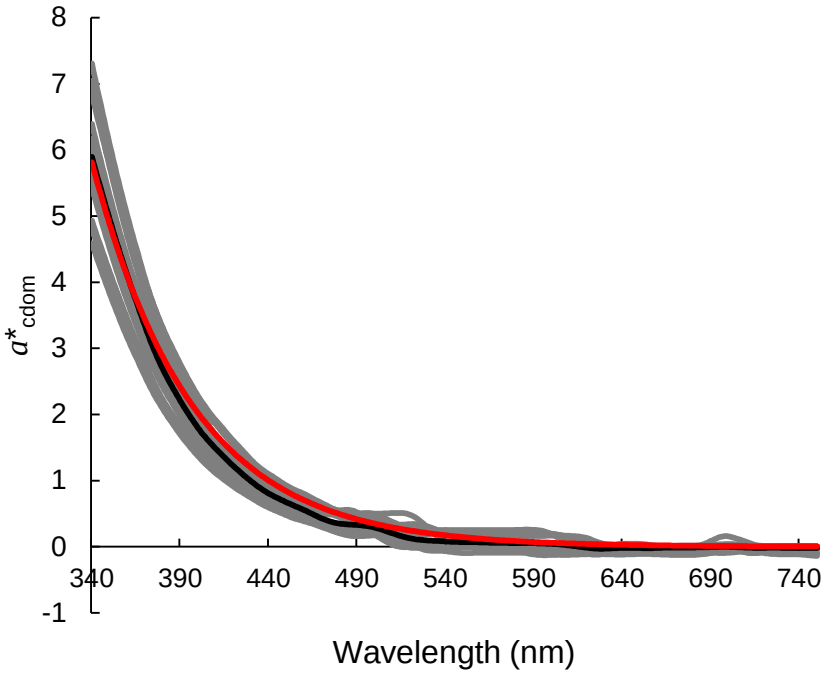

Figure 3.2 Specific absorption coefficients of CDOM – a^*_{cdom} (grey) are measured using 23 water samples collected at the near shore region of St Joseph when the plume occurred on April 21, 2014. The ensemble mean (black) is used to represent the a^*_{cdom} of our study area. The fitted exponential line (red) has a spectral slope S_{cdom} =0.0176 nm^{-1}.

a.

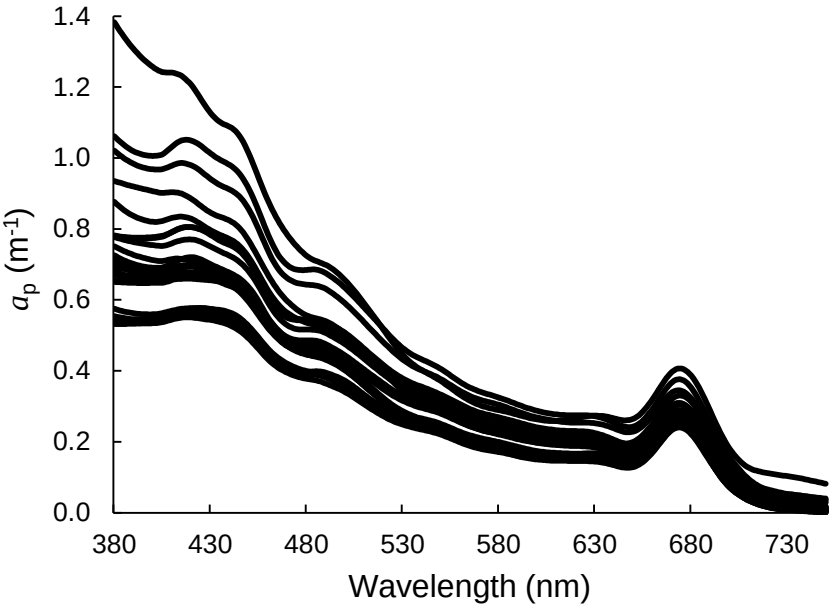

b.

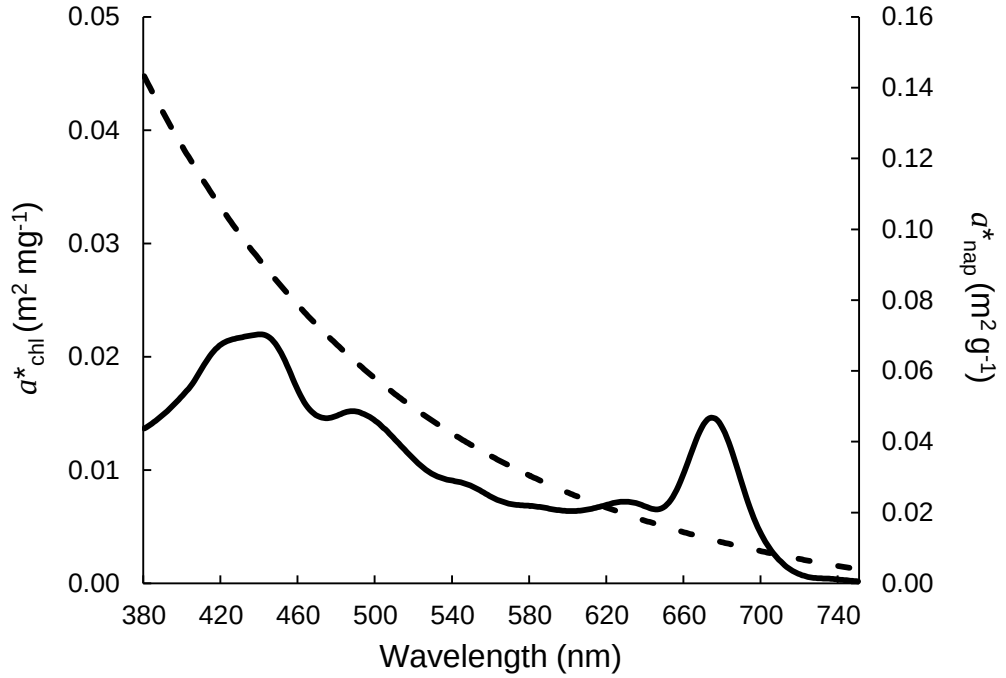

Figure 3.3 (a) Lab measured total particulate absorption; and (b) specific absorption coefficients of chl (solid line) and NAP (dashed line).

3.5.2 Bio-geo-optical Model vs Hydrolight Physical Radiative Transfer Model

Figure 3.4 illustrates the model and Hydrolight results for a representative case of lake water conditions when plumes occurred. The Hydrolight simulation was carried out with [chl] set to 20 mg m^{-3}, [NAP] 5 g m^{-3}, and CDOM absorption at 400 nm equal to 1.5 m^{-1}. The solar zenith angle was set based on the longitude/latitude and the date and time of our sampling event. Wind speed was set to 5 m s^{-1}. The same concentrations and IOPs were used as inputs of the bio-geo-optical model. As shown by Figure 3.4, the R_{rs} spectrum modeled using the bio-opitcal model can be viewed as almost identical to the Hydrolight simulation at the wavelength range 400-650 nm and 700-750 nm. While the reflectance peak around 685 nm was simulated with Hydrolight, it was not captured by the bio-geo-optical model because the bio-geo-optical model does not consider the fluorescence of chl and CDOM. Therefore, only the wavelength range from 400 nm to 650 nm was used for the following analysis to avoid fluorescence (Roesler and Perry, 1995).

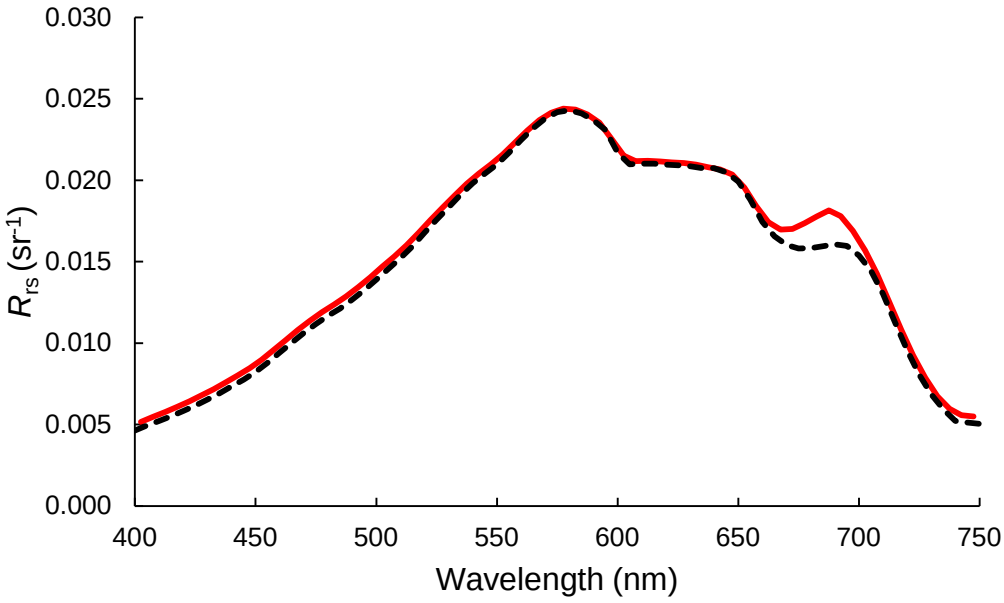

Figure 3.4 Simulated remote sensing reflectance R_{rs} using the bio-optical model used in this study (dashed line) and Hydrolight (solid line).

3.5.3 Sensitivity Analysis

Initial values of the five unknowns were set: [chl]=20 mg m^{-3}, $a_{cdom}(440)$=1.2 m^{-1}, [NAP]=6 g m^{-3}, $b^*_{b,p}(550)$=0.02 m^2 g^{-1}, and γ=1. Figure 3.5a shows the MSE of R_{rs} spectrum corresponding to the percent change of each parameter. As seen from the figure, the model is most sensitive to $b_{b,p}(550)$, followed by [NAP] and insensitive to [chl], $a_{cdom}(440)$, and γ. Figure 3.5b also illustrates how the full R_{rs} spectrum changes with the change of each parameter. An increase of 1 g m^{-3} in NAP concentration can result in up to 0.001 sr^{-1} increase of R_{rs} at 575 nm, while this only happens when the increase of [chl] is larger than 5 mg m^{-3}. A change of 0.1 in γ does not cause a noticeable change in the R_{rs} spectrum; but if $b^*_{b,p}$ (550) increases by 0.001 m^2 g^{-1}, the spectrum changes more significantly than when $a_{cdom}(440)$ increases 0.2 m^{-1}. It is then determined that the sampling intervals of $b^*_{b,p}$ (550) and [NAP] should be small enough to capture the change

in R_{rs} spectrum. The fact that the model is most sensitive to the change of $b^*_{b,p}(550)$ indicates the retrieval will be less reliable if using an empirical value for $b^*_{b,p}(550)$ based on previous literature.

In the work of Effler et al. (2013), $b_{b,p}(532)$ ranges from 0.0 to 0.1 m^{-1} and γ has a distribution from -1.0 to 1.5 for the Great Lakes waters. Therefore, the values of $b^*_{b,p}(550)$ were set to range from 0.0 to 0.1 $m^2\ g^{-1}$ with an interval of 0.0005 $m^2\ g^{-1}$, while γ ranged from -1.0 to 1.5 with an interval of 0.1 in this study. The concentrations of NAP, [NAP], were set to be within 0.0 to 15.0 g m^{-3} with an interval of 0.1 g m^{-3}, chl concentration, [chl], ranged from 0.0 to 30.0 mg m^{-3} with an interval of 1 mg m^{-3}, and $a_{cdom}(440)$ was distributed from 0.0 to 2.0 m^{-1} with an interval of 0.1 m^{-1}. These values contain the typical observations for plume events in southern Lake Michigan so that the generated R_{rs} spectra database is able to capture all possible spectral signatures for retrieval of water quality parameters.

a.

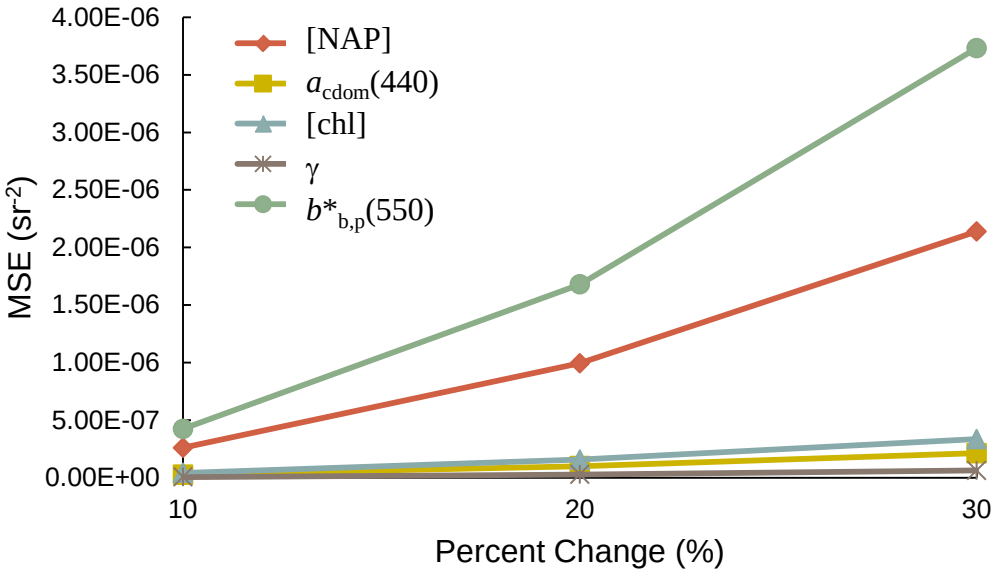

b.

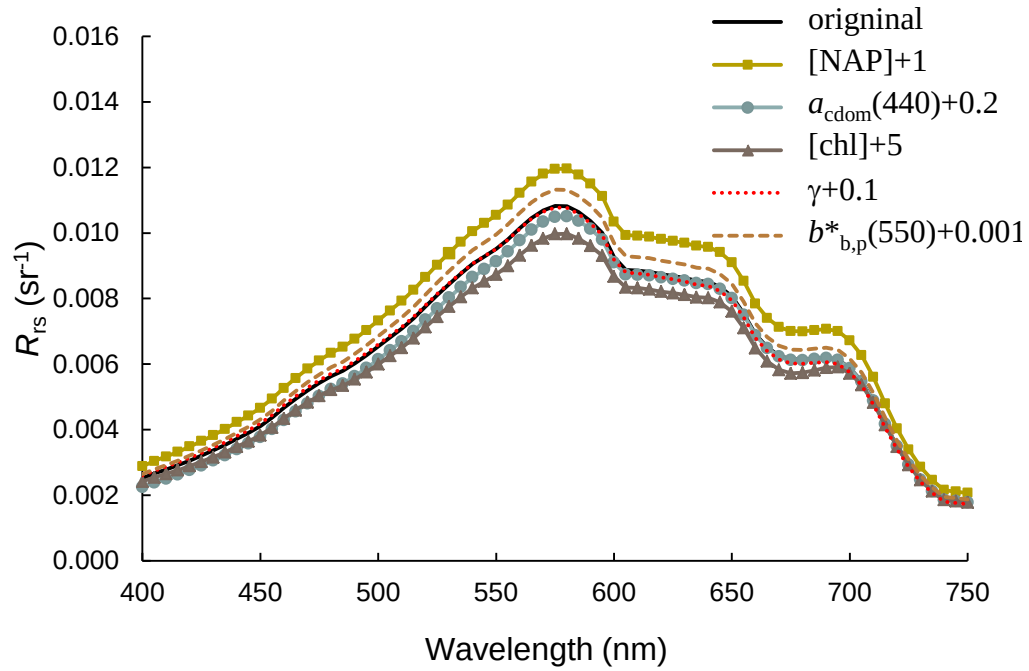

Figure 3.5 (a) MSE of R_{rs} with percent change of one parameter at one time; and (b) R_{rs} change with change of a parameter at one time ([NAP] – increase 1 g m^{-3}, $a_{cdom}(440)$ – increase 0.2 m^{-1}, [chl] – increase 5 mg m^{-3}, γ – increase 0.1, $b^*_{b,p}(550)$ – increase 0.01 m^2 g^{-1}). The initial R_{rs} is simulated using the bio-optical model with inputs: [NAP] =6 g m^{-3}, $a_{cdom}(440)$ =1.2 m^{-1}, [chl] = 20 mg m^{-3}, γ =1, and $b^*_{b,p}(550)$ =0.02 m^2 g^{-1}.

3.5.4 Model Results

Using the iteration intervals described above, about 4.5×10^8 spectra were generated. The algorithm was implemented using C++ and was run on a cluster supercomputer. Field spectrometer measurements were first used to test the robustness of the look-up table method, then the ability of Hyperion image to quantitatively monitor water quality conditions was evaluated and maps showing spatial heterogeneity of water quality parameters were presented and discussed.

3.5.4.1 Spectrometer Measurements

Concentrations of chl, CDOM, and NAP were retrieved using the closest match as well as using the multiple matching spectra with RMSD < 0.00035 sr^{-1}. The retrieved results of $b^*_{b,p}(550)$ and γ are not discussed in this study as no field validation is feasible. Since results for all sampled sites are similar, we only show an example of the retrieved multiple matching spectra as compared to the field measured spectrum (Figure 3.6). Figure 3.7 shows a comparison of [chl], $a_{cdom}(440)$, and [NAP] obtained from field measurements and from model estimates at each sampling site. Points are used to represent the retrieved mean and field measured values, while bars extending up and down from the points represent the mean plus/minus one standard deviation for all three water constituents. It should be noted that the retrieved [chl] at sites 5, 7, and 13 are much lower than the field measurements, and coincide with the lower estimates of NAP as shown by Figure 3.7. Our field records and in-situ measurements of conductivity using a YSI sonde (YSI 6600V2) suggest that these three sites were all located at the plume edge, with measurements of 428 μs cm^{-1}, 412 μs $cm^{-1}$and 471 μs cm^{-1}, respectively, as

compared to about 540 μs cm^{-1} for sites inside the plume. The river plume is highly dynamic, responding to variability in river discharge, lake currents and surface winds, and is expected to have changed shape during the course of boat sampling. This could explain both the low NAP and chl concentrations retrieved from these measured field spectra. Therefore, these three sites are excluded from the following analysis.

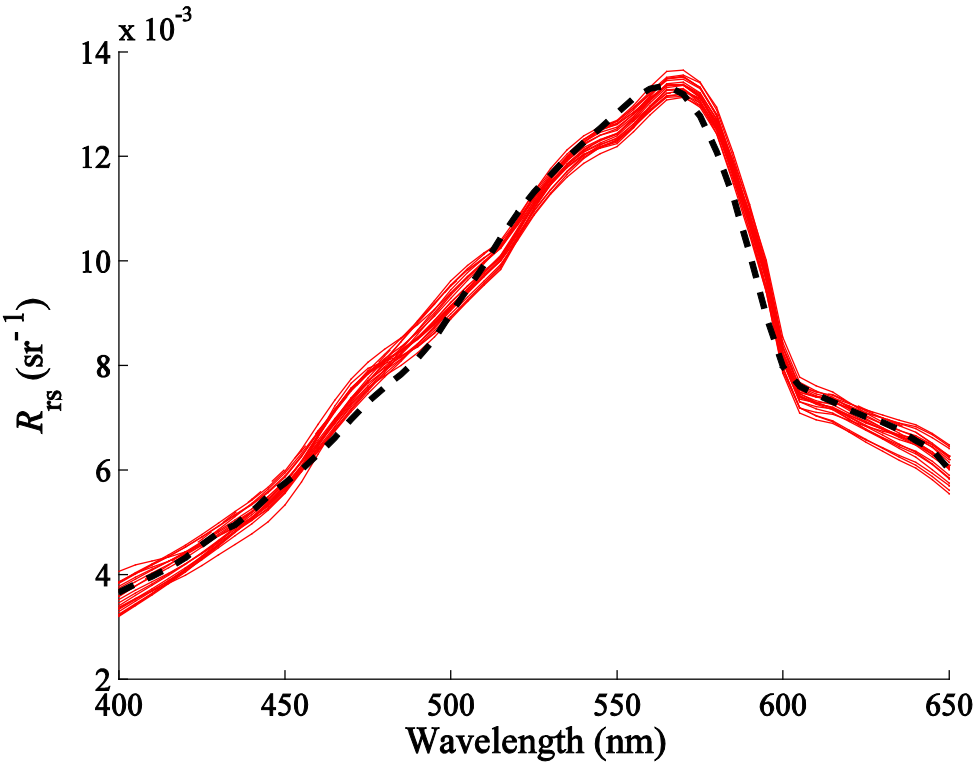

Figure 3.6 Comparison between field measured R_{rs} spectrum (dash line) and 20 randomly selected matching spectra (solid red line) when RMSD <= 0.00035 sr^{-1} for a single sampled site.

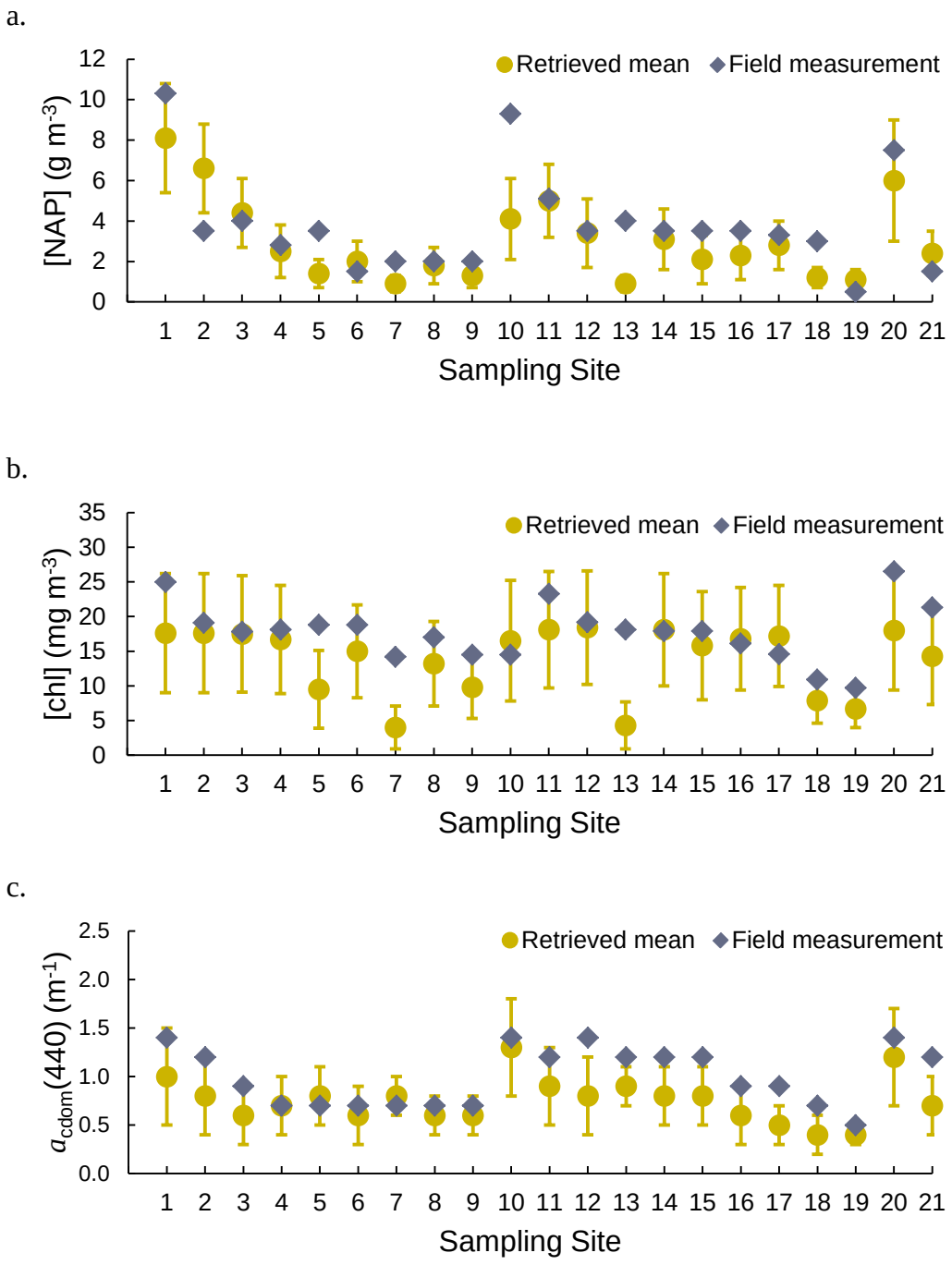

Figure 3.7 Comparison of the (a) NAP, (b) chl, and (c) CDOM concentrations obtained from field measurements and from model retrieval using field spectrometer data for the St Joseph River plume observed on April 21, 2014. Circles and diamonds represent the model retrieved mean and field measured values, respectively, and lines extending from the mean indicate one standard deviation.

As seen from Table 3.1, the closest match does not give the most accurate estimation, which is not surprising considering the possible uncertainty in field and lab measurements. Generally, the mean values from the multiple matching spectra give the best estimates of chl, NAP, and CDOM. An overall underestimation of CDOM is observed. The estimates of chl have the highest variance (up to 8 mg m^{-3}), which is reasonable since the bio-geo-optical model is less sensitive to the concentrations of chl, as determined by the previous sensitivity analysis. A few substantial differences between the in situ and modeled results are believed to be caused by the fact that the specific absorption coefficients of NAP and chl were modeled using the method of Zhang et al. (2009) instead of being directly measured in the laboratory. 67% sampling sites show lab measured concentrations of NAP and CDOM within one standard deviation of the modeled mean. The retrieval of chl concentration is better with lab measurements of 88% sampling sites falling inside one standard deviation of the modeled mean. Therefore, the results should be considered satisfactory. With this in mind, results illustrating the retrieval of spatial distribution of water quality parameters using Hyperion imagery are given and discussed below.

Table 3.1 Retrieved concentrations of NAP, CDOM and chl through finding the closest match of field measured R_{rs} spectra and finding the spectra with RMSD <=0.00035 sr^{-1}. Mean, median and std (standard deviation) of the retrieved values are listed.

Site #	[NAP] (g m^{-3})					$a_{cdom}(440)$ (m^{-1})					[chl] (mg m^{-3})				
	Closest match	median	mean	std	Lab results	Closest match	median	mean	std	Lab results	Closest match	median	mean	std	Lab results
1	8	7.9	8.1	2.7	10.3	0.2	1.1	1.0	0.5	1.4	13.0	19.0	17.6	8.6	25.0
2	7.4	6.5	6.6	2.2	3.5	0.5	0.8	0.8	0.4	1.2	11.0	19.0	17.6	8.6	19.1
3	5.3	4.4	4.4	1.7	4.0	0.1	0.6	0.6	0.3	0.9	8.0	18.0	17.5	8.4	17.8
4	3.9	2.2	2.5	1.3	2.8	0.4	0.7	0.7	0.3	0.7	8.0	17.0	16.7	7.8	18.1
6	2.4	1.8	2.0	1.0	1.5	0.3	0.6	0.6	0.3	0.7	12.0	15.0	15.0	6.7	18.8
8	2.0	1.6	1.8	0.9	2.0	0.3	0.6	0.6	0.2	0.7	12.0	14.0	13.2	6.1	17.0
9	0.6	1.1	1.3	0.6	2.0	0.5	0.6	0.6	0.2	0.7	14.0	10.0	9.8	4.5	14.5
10	6.6	4.0	4.1	2.0	9.3	0.6	1.3	1.3	0.5	1.4	0.0	17.0	16.5	8.7	14.5
11	5.7	4.9	5.0	1.8	5.1	0.3	0.9	0.9	0.4	1.2	13.0	19.0	18.1	8.4	23.3
12	4.3	3.2	3.4	1.7	3.5	0.2	0.8	0.8	0.4	1.4	10.0	20.0	18.4	8.2	19.2
14	3.8	2.8	3.1	1.5	3.5	0.2	0.8	0.8	0.3	1.2	11.0	19.0	18.1	8.1	17.9
15	2.6	1.8	2.1	1.2	3.5	0.3	0.8	0.8	0.3	1.2	11.0	16.0	15.8	7.8	17.9
16	3.1	2.1	2.3	1.2	3.5	0.2	0.6	0.6	0.3	0.9	11.0	18.0	16.8	7.4	16.1
17	3.4	2.6	2.8	1.2	3.3	0.1	0.5	0.5	0.2	0.9	10.0	18.0	17.2	7.3	14.6
18	1.0	1.1	1.2	0.5	3.0	0.3	0.4	0.4	0.2	0.7	9.0	8.0	7.9	3.3	10.9
19	0.9	1.0	1.1	0.5	0.5	0.3	0.4	0.4	0.1	0.5	8.0	7.0	6.7	2.7	9.7
20	6.7	5.7	6.0	3.0	7.5	1.1	1.2	1.2	0.5	1.4	13.0	19.0	18.0	8.6	26.5
21	3.4	2.2	2.4	1.1	1.5	0.2	0.7	0.7	0.3	1.2	8.0	15.0	14.3	7.0	21.3

3.5.4.2 Hyperion Imagery

Accurate atmospheric correction of satellite images for Case II waters has always been a challenge. In this study, atmospheric correction of the Hyperion image that was collected on August 7, 2012 was implemented by using the FLAASH module in ENVI software (Exelis Visual Information Solutions). Only 18 Hyperion bands ranging from 478 nm to 650 nm were used for the retrieval process. It must be noted that FLAASH is designed for land surfaces. For water targets, the atmospherically corrected upwelling water reflectance still includes surface reflected signals that are not needed. Here we assumed the sun and sky glint was uniform for our study area during the Hyperion flyover. Glint was not directly measured but instead estimated using the semi-empirical sky model in Hydrolight. It was found that sun and sky glint contributed about 23%-10% of the total above-water reflectance as the wavelength increases from 478 nm to 650 nm. Considering the noise level (SNR ranging from about 60 to 190 at 478 nm-650 nm) in Hyperion data (Liao et al., 2013) it is assumed that the sun and sky glint was not a significant source of our measured signals, so we did not apply glint correction but used the reflectance spectra obtained from the Hyperion image directly.

A similar look-up table method was used for the retrieval using Hyperion data. Instead of defining the matching spectra as showing RMSD < 0.00035 sr^{-1} with the field measured R_{rs}, the matching spectra of Hyperion data were defined as those with RMSD < 0.0009 sr^{-1}. Figure 3.8 compares in situ measurements to satellite retrieved mean values for all sampled sites. These sites were sampled in the sequence of site number. Unlike the field spectrometer results, some of the Hyperion estimated concentrations match those in

situ measurements, while most, obviously do not (for example, site 6 with modeled chl of 4.5 mg m^{-3}vs measured chl of 18.0 mg m^{-3}). As we mapped the spatial distribution of the retrieved mean concentrations with the Hyperion image in Figure 3.9, it was found that those sites such as site 6, 10, and 23 that experience large discrepancies with field measurements could be visually identified as located outside of the plume or at the plume edge from the image. This is quite possibly due to the fact that the field measurements did not occur simultaneously with Hyperion image acquisition, but instead occurred a few hours after the acquisition. This asynchrony may also explain why the image derived concentrations of chl and NAP at the beginning of the field sampling, which were collected immediately after the satellite flyover, show consistency with field measurements while sites sampled in the later hours such as sites 20-23, clearly outside the plume as seen from the image, show characteristics that are mostly exhibited by plume waters. Therefore, it is likely that the plume migrated toward the shore line as our field sampling continued. This is supported by our observations of southwesterly wind during the field campaign, as well as the historical wind direction data recorded by the NOAA Great Lakes Environmental Research Laboratory (GLERL) weather station at South Haven, MI. Despite all of that, the Hyperion retrieved mean [NAP] range from 0.9 g m^{-3} to 7.0 g $m^{-3}$and mean [chl] vary from 4.3 mg m^{-3} to 19.4 mg m^{-3}; those data ranges are similar to the lab measured results with [NAP] ranging from 0.0 g m^{-3} to 6.6 g m^{-3} and [chl] from 0.4 mg m^{-3} to 25.2 mg m^{-3}). The spatial heterogeneity of chl and NAP concentrations at all sampled sites (Figure 3.9) does reflect the water quality variability during the plume event, which we regard as the true condition observed by the EO-1 satellite.

a.

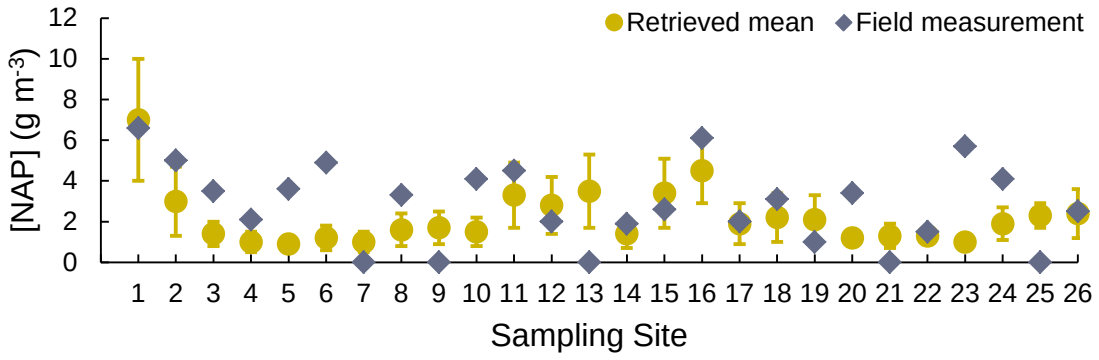

b.

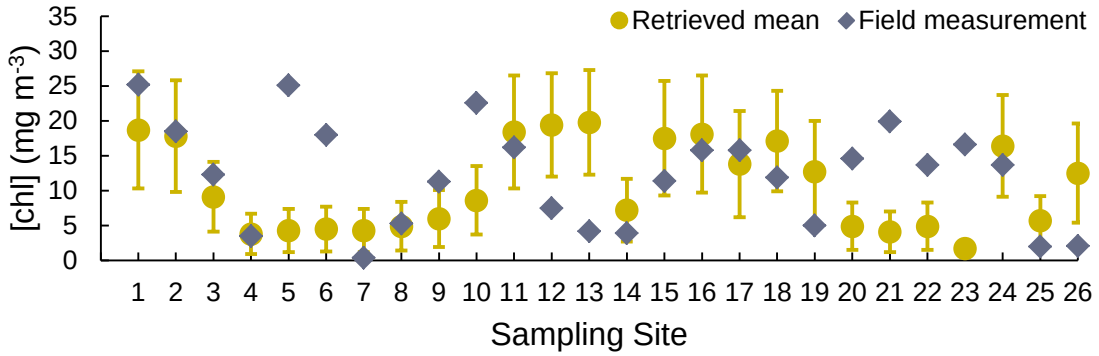

Figure 3.8 Comparison of the (a) NAP and (b) chl concentrations obtained from field measurements and from model retrieval using Hyperion imagery for the St Joseph River plume observed on August 7, 2012. Circles and diamonds represent the model retrieved mean and field measured values, respectively, and lines extending from the mean show standard deviation.

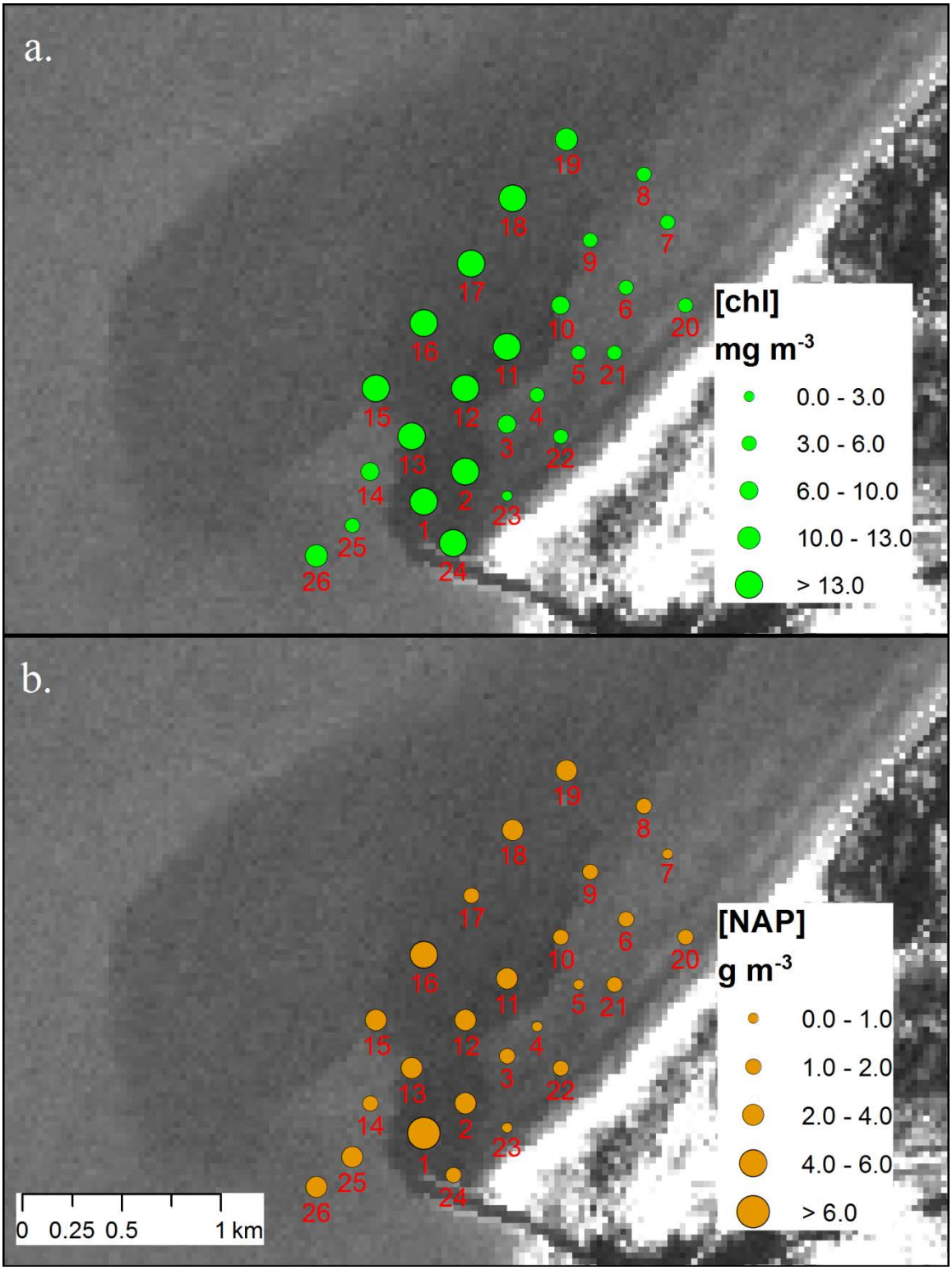

Figure 3.9 Hyperion retrieved concentrations of (a) chl and (b) NAP of all sampled sites on August 7, 2012. Site numbers are placed at the bottom center of each site.

Table 3.2 lists the retrieved NAP and chl concentrations using the Hyperion image for sites that are identified as least likely to be affected by the plume migration. The standard deviations of all retrieved values provide an estimate of overall uncertainty. There is consistency between in situ measurements and satellite retrieval mean values for these sites, with field measured NAP and chl concentrations at 77% of the sampled sites falling within one standard deviation of the mean Hyperion retrieved values. Again, the closest matching spectrum does not provide estimates as accurate as those obtained by inverting multiple matching spectra and adopting the mean values; this implies that the possible variability and inaccuracy of the model inputs needs to be considered. For example, the optical properties of plume water during the Hyperion flyover in August 2012 might be different from that in April 2014. The FLAASH is designed for land surfaces and therefore the atmospherically corrected Hyperion imagery may still contain a certain amount of water surface reflected signals. It also has to be noted that the comparisons shown in Figure 3.8 represent a single in situ sample of the river plume versus the remote sensing data over a 30 m by 30 m lake surface area, and variability can occur on spatial scales smaller than this. Given the results and all these discussed reservations, we conclude that Hyperion imagery, though not specifically designed for water, can still be useful for evaluating the variability of water quality conditions during plume events.

Table 3.2 Hyperion derived concentrations of NAP and chl as compared to field measurements. Both the closest match spectrum and spectra showing RMSD <=0.0009 sr^{-1} are used for retrieval. Median, mean and std (standard deviation) of the retrieved values are listed. Sampled sites are determined as in or out of plume based on the image.

Site #	[NAP] (g m^{-3})					[chl] (mg m^{-3})				
	Closest match	median	mean	std	Lab results	Closest match	median	mean	std	Lab results
1-in plume	6.9	6.6	7.0	3.0	6.6	30.0	20.0	18.7	8.4	25.2
2-in plume	2.1	2.7	3.0	1.7	5.0	30.0	19.0	17.8	8.0	18.5
11-in plume	2.7	3.1	3.3	1.6	4.5	27.0	20.0	18.4	8.1	16.2
12-in plume	1.4	2.5	2.8	1.4	2.0	30.0	20.0	19.4	7.4	7.5
14-out of plume	1.9	1.3	1.4	0.7	1.9	5.0	7.0	7.2	4.5	3.9
15-in plume	3.4	3.1	3.4	1.7	2.6	20.0	18.0	17.5	8.2	11.4
16-in plume	4.9	4.4	4.5	1.6	6.1	18.0	19.0	18.1	8.4	15.8
17-in plume	1.8	1.7	1.9	1.0	2.0	11.0	13.0	13.8	7.6	15.8
18-in plume	1.2	1.9	2.2	1.2	3.1	30.0	17.0	17.1	7.2	11.9
19-in plume	3.6	1.8	2.1	1.2	1.0	6.0	12.0	12.7	7.3	5.0
24-in plume	1.0	1.7	1.9	0.8	4.1	23.0	17.0	16.4	7.3	13.7
25-out of plume	2.7	2.3	2.3	0.6	0.0	4.0	6.0	5.7	3.5	2.0
26-out of plume	3.2	2.2	2.4	1.2	2.5	11.0	13.0	12.5	7.1	2.1

The grayscale image (Figure 3.10a) shows an observable river plume in the near-shore region the west and north of the St Joseph River mouth. Figures 3.10 b-d show the spatial maps of retrieved concentrations of NAP and chl and $a_{cdom}(440)$ by inverting the Hyperion imagery. The concentrations were retrieved through computing the mean of multiple spectra found with RMSD < 0.0009 sr^{-1} as described previously. Since no destreaking of the Hyperion image was conducted in this study (some "streaks" can be seen from Figure 3.10a), pixels with high noise levels often do not meet the criteria of RMSD < 0.0009 sr^{-1}. No successful retrievals exist for those pixels, so they are displayed as black dots across Figure 3.10 b-d. In addition to the 26 sites sampled in the near-shore region, we also sampled two sites in the river mouth. These two sites have chl concentrations of more than 50 mg m^{-3} and NAP concentrations of about 10 mg m^{-3}; both were much higher than those in the near-shore region. This is consistent with the high concentrations of NAP and chl in the river mouth as shown by Figure 3.10b and 3.10c. All three maps (b-d) depict high concentrations in conjunction with river outflow with concentrations decreasing as the plume moves further away from the shore and starts to dissipate. The concentrations of all three parameters were generally higher within the visible plume than outside of it. It is hence concluded that the plume was a significant source of sediments, carbon and chl after storm events, which had more than three times higher concentrations than the ambient water. The noticeably high concentrations of CDOM and chl along the shore line are consistent with what Lohrenz et al. (2004) found in their study, that the stimulation of phytoplankton activity and the enhancement of chl concentrations are associated with river outflow. The spatial variations of these water

quality variables also suggest that traditional water sampling strategies may be challenged to fully characterize the spatial structure and variability of these river plumes.

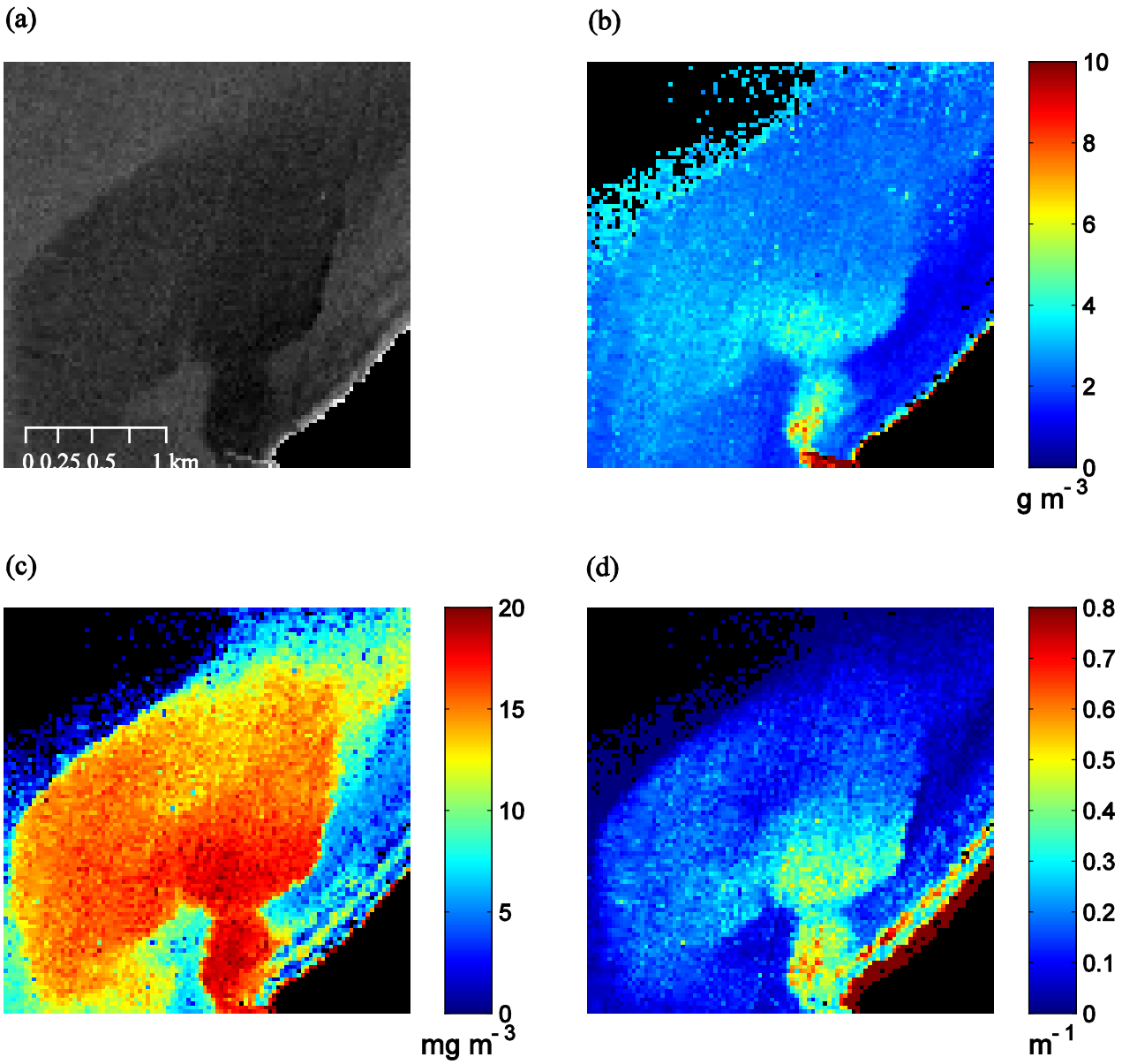

Figure 3.10 Maps show (a) the Hyperion image and the spatial distribution of the modeled mean (b) [NAP] (g m^{-3}), (c) [chl] (mg m^{-3}), and (d) $a_{cdom}(440)$ (m^{-1}) concentrations on August 7, 2012.

3.6 Conclusions

In this study, two field sampling campaigns took place near the mouth of the St Joseph River in southern Lake Michigan based on the timing of EO-1 satellite overpasses and precipitation events. The strategy was designed to capture storm-initiated river plumes in the nearshore region of the St Joseph River. Boat-based field measurements and Hyperion images were collected for two plume events which occurred on August 7, 2012 and April 21, 2014, respectively. The datasets collected during the episodic events allow an initial analysis of water quality parameters as well as the optical properties of river plumes in Southern Lake Michigan.

A remote sensing inversion algorithm based on an existing bio-geo-optical model and the look-up table method was calibrated with the collected datasets for the study of spatial variability of St Joseph River plumes. The bio-geo-optical model is based on the optical properties of the constituents and water molecules and accounts for the complex radiative transfer process within water column; therefore this algorithm is transferrable with accurate and appropriate measurements of IOPs for specific study. However, spatial and temporal variations in IOPs can affect the accuracy for the retrieval of water quality parameters. Therefore, it is important to gain knowledge of the spatial and temporal variability of the IOPs for the future remote sensing of river plumes of the Great Lakes. The measurements of IOPs are not only important as inputs to transferrable optical models that improve the retrieval of OACs (Shuchman et al., 2013 a, b), but also provide a fundamental linkage between the optical properties and the biogeochemical state of water systems (Brown et al., 2001).

Our results demonstrate that the retrieved means from the set of matching spectra within a defined level of uncertainty give the best estimate of the water quality parameters. Modeled concentrations of chl, CDOM and NAP through utilizing the field spectrometer data show correspondence with the field measurements. 67% sampling sites show lab measured concentrations of NAP and CDOM within one standard deviation of the modeled mean and the retrieval of chl concentration at 88% sampling sites falling inside one standard deviation of the modeled mean. Hyperion imagery, which has high resolution both spectrally and spatially, can be used to study the variability of water quality parameters for river plumes although it is not originally designed for water observations. This is consistent with the findings of Brando and Dekker (2003). Hyperion retrieved concentrations for sites located in plumes also show consistency with the field measurements with field measured NAP and chl concentrations at 77% of the sampled sites falling within one standard deviation of the mean Hyperion retrieved values. Finally, maps of the retrieved chl, NAP and CDOM concentrations were generated through inverting the Hyperion imagery and the spatial heterogeneity of all three water quality parameters indicate that it would be difficult to use the traditional sampling strategy for fully characterizing the spatial variability and structure of river plumes. Hyperion imagery also provides much greater detail of the distribution of water quality parameters within the plume area as compared to application of oceanic satellites such as MODIS; therefore it is a valid tool in understanding lake water quality dynamics.

Our study also highlighted some of the limitations of satellite remote sensing for use in the characterization of small river plumes. According to our experience, it is difficult to coordinate coincident field sampling with satellite acquisitions, clear-sky

conditions, and brief storm events. In addition, given the time period required for plume sampling and the dynamic nature of plumes, it is challenging to ensure that the field measurements reflect the instantaneous spatial distribution of water quality corresponding to the satellite imagery. To that end, field spectrometer measurements provide important optical information studying river plumes that aid in the calibration of transferrable bio-geo-optical models. Many of these challenges may be alleviated using airborne systems or unmanned aircraft systems (UAS), which afford high spatial resolution and can be flown on a user-specified schedule. To better understand the water quality dynamics of river plumes in Lake Michigan, investigations of the seasonal and spatial variability of optical properties and spectral signatures of the OACs are recommended in the future.

3.7 Acknowledgements

This project is supported by Illinois-Indiana Sea Grant through the Great Lakes Restoration Initiative administered by U.S. Environment Protection Agency (EPA GL-00E00683). We thank Dr. Tomas Höök and his research group the use of their boat for the field sampling. We are also grateful for Dr Melba Crawford's help in acquiring Hyperion and ALI imagery for our study area.

CHAPTER 4. DEVELOPING A COMPREHENSIVE SPECTRAL-BIOGEOCHEMICAL DATABASE OF MIDWESTERN RIVERS FOR WATER QUALITY RETRIEVAL USING REMOTE SENSING DATA: A CASE STUDY OF THE WABASH RIVER AND ITS TRIBUTARY, INDIANA

4.1 Abstract

A comprehensive spectral-biogeochemical database is developed for the Wabash River and the Tippecanoe River in Indiana, United States. Field sampling of river water was conducted over different hydrologic conditions during the summer of 2014. In addition to the various spectral measurements taken by a handheld field spectrometer, this database includes corresponding in situ measurements of water quality parameters (chlorophyll (chl), non-algal particles (NAP), and colored dissolved organic matter (CDOM)), nutrients (total nitrogen (TN), total phosphorus (TP), dissolved organic carbon (DOC)), water-column inherent optical properties (IOPs), water depths, substrate types and bottom reflectance spectra. First, the temporal variability of water quality parameters and nutrients in the rivers is analyzed and studied. Second, a look-up table (LUT) based spectrum matching methodology is applied to the observations to retrieve water quality parameters. A database of remote sensing reflectance (R_{rs}) spectra is then constructed using the Hydrolight radiative transfer numerical model. Water quality parameters are estimated by finding the closest match of the field measured R_{rs} in the database. Results of this analysis find that the temporal variability of water quality parameters and nutrients in the Wabash River is closely associated with hydrologic conditions. Meanwhile, there

are no significant correlations found between these parameters and streamflow for the Tippecanoe River, probably due to the two upstream reservoirs. The poor relationship between CDOM and DOC indicates that most DOC in the rivers is from human sources such as wastewater. It is also found that the source of water (surface runoff or combined sewer overflow (CSO)) to a river, water temperature, and nutrients are important factors controlling instream concentrations of phytoplankton. The LUT retrieved chl and NAP concentrations are in good agreement with field measurements with slopes close to 1.0. The average estimation errors for NAP and chl concentrations are within 4.1% and 37.7%, respectively, of independently obtained lab measurements. The CDOM levels are not well estimated and the LUT retrievals for CDOM experience large variability, probably due to the small data range collected in this study and the insensitivity of R_{rs} to CDOM change.

4.2 Introduction

Remote sensing provides a practical means for synoptic and multi-temporal monitoring of water quality. The water leaving signals that are captured by remote sensing instruments contain essential information on the constituents in the water column, and if applicable, water column depths and bottom properties. The potential of remote sensing to retrieve water quality parameters, bathymetry, and substrate type/composition has been studied for over two decades and there are four main approaches used: empirical, semi-empirical, analytical and radiative transfer methods. Significant attention has been paid to the empirical approach which focuses on developing best-fit correlational models between remote sensing data (digital numbers, radiance, or reflectance) and measured water quality parameters. A summary of empirical models for water quality assessment

can be found in Ritchie et al. (2003). Instead of screening all wavelengths and finding the band combinations showing the highest correlation, the semi-empirical approach incorporates the spectral characteristics of the interested parameters into the statistical relationship development. For example, many previous studies have shown that the reflectance trough at ~670 nm and the scattering peak at ~700 nm can be used to develop successful models for chlorophyll (chl) estimation and that the scattering peak at ~700 nm is strongly correlated with concentrations of total suspended sediments (TSS) (Olmanson et al., 2013; Tan et al., 2015a). The analytical approach is based on the physical relationship between the inherent optical properties (IOPs) of the water column and measured apparent optical properties (AOPs). The IOPs are the properties of the medium itself and are not affected by the ambient light field. The AOPs are radiometric quantities that display enough stability and can be used for approximately describing the optical properties of the water body, e.g., the remote sensing reflectance. Remote sensing data can be inverted by using the analytical modeling approach to retrieve water column properties and bottom depths (Lee et al., 1999, 2001). In the radiative transfer modeling approach, the software package HydroLight (Mobely and Sundman, 2013) is often required due to the heavy computation required for simulating the complexities of underwater light transfer processes through solving the full set of radiative transfer equations. While analytical models are typically developed by simplifying the full radiative transfer equations based on a set of given assumptions, e.g., level water surface or no internal light sources, the radiative transfer models do not have such constraints. The radiative transfer models can be inverted to extract water column and bottom properties from remote sensing data by using a look-up table based spectrum matching

(LUT) methodology (Louchard et al., 2003; Mobley et al., 2005). Such models have been successfully applied to coral reef mapping in the work of Lesser and Mobely (2007).

The empirical and semi-empirical models developed for water quality assessment are often highly dependent on the data and limited to the locations where data is collected. In contrast, the analytical and radiative transfer models provide physical insight into how environmental conditions (such as water column properties, bottom properties, and sky and water surface conditions) quantitatively affect the water leaving signals. Therefore these physics-based models have several advantages: (1) they are repeatable given appropriate inputs from the sites studied; (2) they are easily transferrable between data collected by a variety of sensors; and (3) sensitivity and uncertainty of the models can be objectively determined (Lee et al., 2010b). The existence of optically complex waters (IOCCG, 2000) and those that are so shallow that water-leaving reflectance includes interference from bottom conditions (Maritorena et al., 1994; Lee et al., 1998) also necessitates these methods. In Chapter 3 we investigated the capabilities of Hyperion imagery for mapping the water quality conditions in river plumes at Lake Michigan. By studying the physical relationship between IOPs and AOPs, the spatial heterogeneity of water quality was adequately captured, which would be challenging for traditional *in-situ* sampling or empirical modeling given the limited sample size and complex optical features.

Despite all the advantages described above, the success of these physics-based approaches depends on two requirements: (1) remote sensing reflectance spectra must be accurately measured and (2) model inputs including the depth, bottom reflectance, and water IOPs must be accurate for the sites of interest (Mobley et al., 2005). While much

attention has been paid to collecting coincident measurements of IOPs and AOPs for oceanic systems (e.g., NASA SeaWiFS Bio-optical Archive and Storage System, http://seabass.gsfc.nasa.gov/), inland waters, especially river systems, have been poorly observed, even though what happens in ocean and coastal waters is highly dependent on these systems (Palmer et al., 2014). It is therefore important and necessary to develop a similar database / archive for bio-optical data of inland waters and make it accessible to the whole scientific community (Mouw et al., 2015). Such a database will provide valuable data for improving satellite algorithm development and product validation. In addition, the observations of IOPs in the database will also provide a fundamental linkage between the optical properties and the biogeochemical state of inland waters. For example, the change in beam attenuation is closely associated with particle size variations and can be used to study particle composition (Boss et al., 2007). Especially for rivers that experience nutrient and sediment loads from terrestrial sources, the measurements of IOPs, when combined with climate and hydrologic flow regime, enable a better understanding of the biogeochemical state of river systems.

Recent years have seen growing interest in the development of hyperspectral imagers and in the application of hyperspectral data for water quality retrieval. Hyperspectral sensors typically collect data in narrow, contiguous spectral bands and are expected to yield advantages in estimation accuracy due to their ability to finely parse the visible spectrum. Lee and Carder (2002) investigated how the number of spectral bands affected the retrieval of water column and bottom properties from remote sensing data and found that hyperspectral data performed much better for optically shallow waters. Although not designed for water targets, the satellite borne Hyperion imager is valid for

adequately estimating water quality in coastal and estuary waters as well as the Great Lakes (Brando and Dekker, 2003; Tan et al., 2015b). The Hyperspectral Imager for the Coastal Ocean (HICO) is the first hyperspectral sensor designed specifically for the coastal ocean and estuarial, riverine, or other shallow-water areas with optimized Signal-to-Noise Ratio (SNR) (Lucke et al., 2011). It has been successfully applied for the study of phytoplankton, colored dissolved organic matter (CDOM), turbidity, and bathymetry in coastal waters (Gitelson et al., 2011; Ryan et al., 2014; Garcia et al., 2014; Keith et al., 2014). Other hyperspectral sensors such as the Hyperspectral Infrared Imager (HyspIRI) (Devred et al., 2013) show great potential for observing water quality of coastal and inland waters. However, the application of such satellite products for inland river monitoring has been hampered since most rivers are not able to be appropriately resolved due to the coarse resolution of current satellite products, of which the finest spatial resolution is 30 m. According to the work of Handcock et al. (2006), the width of the river channel must be at least three pixels for reliable water measurements from remote sensing imagery. Hyperspectral sensors mounted on airborne platforms provide a way to collect data of sufficiently high spatial resolution that rivers can be appropriately resolved and water quality parameters can be retrieved (Shafique et al., 2003; Olmanson et al., 2013). But given the high cost in organization and realization, these airborne platforms are not affordable for agencies with small budgets and therefore regular monitoring of water quality using theses platforms is not realistic. Alternatively, in situ sampling using a handheld spectrometer provides a cost-effective, convenient, and accurate approach for measuring spectral signatures of rivers and streams. Although limited in spatial coverage, it does help fill the gap of missing remote sensing data for rivers and streams. And the

more samples taken, the more useful it will prove in making recommendations for future work on remote sensing of water quality.

The overall goal of this study is to develop a comprehensive spectral-biogeochemical database for the Wabash River and its tributaries and evaluate the ability of the radiative transfer modeling approach by using the database for the retrievals of water quality parameters including concentrations of chl, non-algal particles (NAP), and CDOM. To fulfill the goal, our specific objectives are to: (1) collect extensive field data including *in-situ* concentrations of water quality parameters and nutrients, measurements of IOPs, water depths, bottom albedos, and spectral signatures of river water; (2) analyze the temporal variability of water quality parameters, nutrients, and IOPs, as well as possible factors in affecting the temporal variability, and (3) apply the LUT method to the collected dataset and evaluate its capability for retrieving water quality parameters.

4.3 Background

The Wabash River, which has an average annual flow of approximately 1,000 m^3 s^{-1}, originates from west-central Ohio and is the largest drainage in Indiana. It drains an area of over 85,000 km^2 that covers two-thirds of Indiana's 92 counties. In the basin, land cover is dominated by agricultural row crops (62%) with approximately 20% forest and dispersed urbanization (United States Army Corps of Engineers, 2011). The Wabash River flows a distance of over 650 km from its headwaters to its confluence with the Ohio River and is the second largest tributary of the Ohio River. It is also the longest segment of free flowing river east of the Mississippi River. The Tippecanoe River (average flow of 145 m^3 s^{-1}) is one of over 14 major tributaries contributing flow to the main Wabash River. Lakes and swamps are the major source of the Tippecanoe River

and reduce the amount of sediments carried in the river. The river enters the Wabash River 19 km northeast of Lafayette, Indiana and is one of the nation's most biologically diverse rivers. The drainage basin of the Tippecanoe River is in the north central part of Indiana and drains approximately 4,920 km^2. The land use in the basin is predominately agriculture, which represents approximately 87 percent of the land area. The Wabash River and its tributaries are a vital source for water supply and recreation in Indiana.

Water quality impairment occurs on various segments of the Wabash River and the Tippecanoe River. Issues includes those related to E. Coli, nutrients, pH, dissolved oxygen, and impaired biotic communities, according to the Indiana and Illinois 2010, 2012, and 2014 Clean Water Act (CWA) Section 303(d) listings. Major pollution sources in the watershed include nonpoint sources from agricultural and urban run-off, and point sources from treated and untreated (from combined sewer overflows) municipal wastewater. Both rivers play important roles in transporting pollutants downstream. According to the Ohio River Valley Water Sanitation Commission (ORSANCO, http://www.orsanco.org/wabash-river-project), the Wabash River is one of the largest contributors of nutrient loadings to the Mississippi River and the Gulf of Mexico. Approximately 10.0 gigagrams of total phosphorus and 139.3 gigagrams of total nitrogen are estimated to be contributed by the Wabash River watershed to the Gulf of Mexico each year (United States Environmental Protection Agency, 2011b).

4.4 Materials and Methods

4.4.1 Study Area

The primary study area includes the reach of the Wabash River between French Post Park (about halfway between Delphi, Indiana, and Logansport, Indiana) and Attica,

Indiana, and the reach of the Tippecanoe River between Indiana State Road 18 and it's confluence with the Wabash River (Figure 4.1). Within the study area the Wabash River has a length of about 90 km and ranges in width from 100 m to over 150 m. The Tippecanoe River reach flows approximately 10 km before entering the Wabash River. Two reservoirs, Lake Freeman and Lake Shafer, are located upstream from the confluence 48 km and 29 km, respectively. Throughout the year water depth of the Wabash River (USGS 03335500) ranges from 0.6 m to 6.0 m while the Tippecanoe River (USGS 03333050) is shallower with typical depths of 0.6 m to 2.5 m. The river bed of the Tippecanoe River is often visible through the water during summer when flows are extremely low.

Water quality conditions in these two rivers are quite different. Based on our previous sampling experience, water in the Tippecanoe River carries significantly lower sediment loads than the Wabash River, likely due to the presence of the two upstream reservoirs. The water quality of the Wabash River is complex and dominated by both phytoplankton, usually measured in terms of chl concentrations, and NAP otherwise known as inorganic sediments. The water quality of the Wabash River is closely associated with flow and seasonal dynamics. For example, during spring nitrogen and phosphorus loads in the Wabash River are highest as a consequence of intense agricultural activities and high agricultural runoff. Significant amounts of sediments and nutrients are often found in the river after summer storm events. These nutrients delivered from terrestrial environment, in return, cause algal blooms in the river and turn the water to be visibly green.

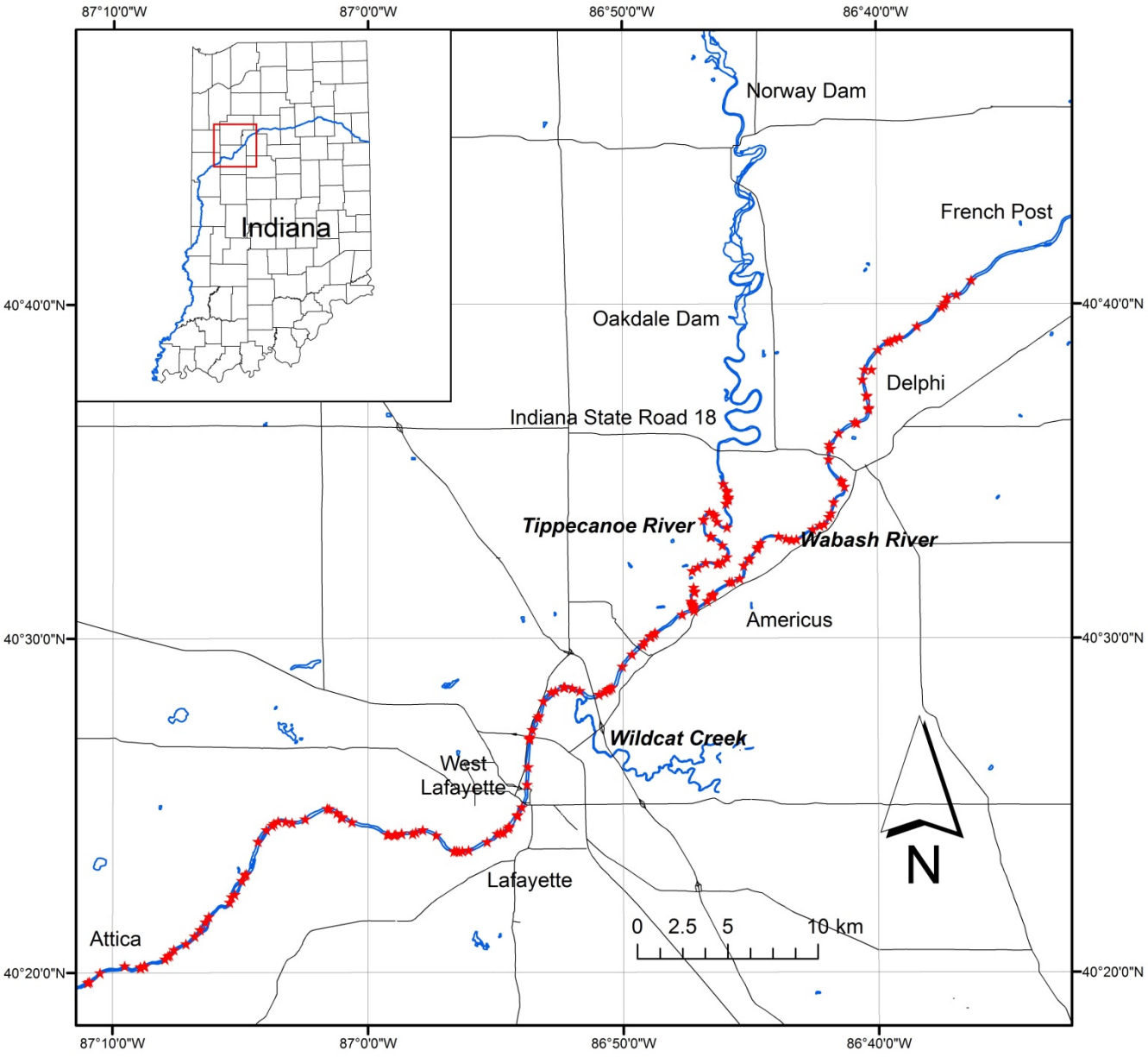

Figure 4.1 Main study area includes two reaches of the Wabash River, including the confluence with the Tippecanoe River. Field spectrometer measurements and water samples (marked as red stars) were collected through the summer of 2014.

4.4.2 Field Work Activities

Regular sampling was conducted using a boat platform on a total of 28 dates during May, June, and July 2014, resulting in a total of 213 samples from the Wabash River and the Tippecanoe River. Surface water samples of each site were collected and stored in brown polyethylene bottles until returned to the laboratory for further analysis. Above-water measurements were taken with a GER 1500 field spectrometer (Spectral Vista Corporation, http://www.spectravista.com/) and a Spectralon panel at each station by following NASA's standard operating protocols of satellite ocean color remote sensing (Mueller et al., 2003). Spectral range of the spectrometer is 350-1050 nm with 1.5 nm sampling interval. To avoid significant changes in illumination conditions, measurements between water target, sky, and the Spectralon panel were done within a very short time period. Sky conditions were also recorded for each station when spectral measurements occurred. For each site, water depths were measured using an ultrasonic device and recorded. A YSI sonde (YSI, https://www.ysi.com) was used to take instantaneous measurements of water temperature, conductivity, salinity, and dissolved oxygen. Water measurements were accompanied also by underwater video which was used to determine the substrate type. During low flow conditions when the streambed emerged, the albedo of various river bottom types were collected and related back to the classification of streambed materials from the video. Locations of all sampled sites were recorded using a handheld GPS device.

4.4.3 Laboratory Analyses

All water samples were stored in the dark and on ice until returned to the laboratory for the determination of the concentrations of water quality parameters and

nutrients (total nitrogen - TN, total phosphorous - TP, and dissolved organic carbon - DOC), as well as spectral absorption properties of chl, NAP and CDOM.

According to the standard methods of the American Public Health Association (APHA) (Eaton et al., 1998), a sub-sample was filtered onto Whatman GF/F filters, then extracted in 90% acetone solution and analyzed spectrophotometrically to determine the concentration of chl (denoted as [chl], where "[X]" indicates a concentration of X). The concentration of TSS ([TSS]) were measured gravimetrically on pre-weighted Whatman GF/F filters after rinsing with pure water. It should be noted that TSS includes both organic and inorganic sediments, i.e., chl and NAP. The organic part of TSS can be converted from [chl] using a ratio of 0.02 which is typical for mesotrophic and eutrophic systems (Likens, 2010). Because the organic sediments took up only a small part of the total mass (<10%), the concentrations of NAP ([NAP]) were assumed to approximate [TSS] in this study. The concentration of DOC ([DOC]) was estimated by chemical analysis of a filtered 250 ml sample using the EPA 415.1 method. The concentrations of TP and TN ([TP] and [TN], respectively) were analyzed using an autoanalyzer after subjecting unfiltered and filtered water samples to alkaline persulfate digestion.

CDOM absorption ($a_{cdom}(\lambda)$) was measured using a laboratory spectrophotometer after filtration through 0.45 μm membrane filters. Total absorption of particulate matter ($a_p(\lambda)$) was acquired using the quantitative filter technique by measuring the particles retained on to Whatman GF/F filters spectrophotometrically. The filters were then bleached with hot methanol so that pigments were extracted. The absorption spectra of NAP ($a_{nap}(\lambda)$) were determined through measurements of particles remaining on these

bleached filters. The difference between $a_{p}(\lambda)$ and $a_{nap}(\lambda)$ gave an estimate of the absorption of phytoplankton $a_{ph}(\lambda)$. All spectral absorption measurements were made at 1 nm increments between 350 nm and 900 nm. The detailed lab procedure can be found in NASA protocols (Mueller et al., 2003).

4.4.4 Data Preprocessing and Analysis

All field spectrometer measurements were processed to remove sky and sun glint by using a constant water surface reflection coefficient (Mobley, 1999). Therefore, remote sensing reflectance, R_{rs}, was calculated using the following equation:

$$R_{rs} = \frac{L_u - \rho \cdot L_s}{E_d} \qquad (4.1)$$

where L_u is the total upwelling radiance, L_s is the sky radiance, ρ is the water surface reflection coefficient which is 0.028, and E_d is the measured downwelling solar irradiance.

Null point corrections were performed to the lab measured absorption to remove residual offsets due to filter manufacturing and scattering artifacts caused by particle loading. For $a_{cdom}(\lambda)$ and $a_{p}(\lambda)$ correction, the average from 750-760 nm was forced to be null. The absorption of non-algal particles $a_{nap}(\lambda)$ was corrected using the average absorption measured between 890 nm and 900 nm and a pathlength amplification factor of 2 (Roesler, 1998). Specific absorption coefficients (absorption per unit of mass concentration) of CDOM, chl and NAP were then estimated after corrections. The averaged values of the specific absorption coefficients were further fitted to exponential functions and used to represent the specific inherent optical properties (SIOPs) of the

study area. The fitting details are presented in the following Results and Discussion section.

The temporal variability of water quality parameters, nutrients, and IOPs in the Wabash River and the Tippecanoe River were analyzed. Pearson's correlation (r) analyses and significance tests were performed to determine possible factors influencing the temporal variability of these parameters. In particular, the daily distribution of [chl] sampled within the Wabash River was also evaluated using box-plots and the Mann-Whitney-Wilcoxon test was performed to determine if significant changes occurred.

4.4.5 Water Quality Retrieval

In this study, the LUT methodology was used for the retrieval of water quality parameters (Mobley et al., 2005). The remote sensing reflectance, R_{rs}, can be computed exactly by solving the radiative transfer equation, as long as the environmental inputs including the water-column IOPs (the water absorption and scattering properties), the sky and water surface conditions, and water depths and bottom boundary conditions are known (Mobley, 1994). Therefore, the LUT methodology includes two major steps: (1) assemble a database of R_{rs} corresponding to different environmental inputs, and (2) compare the field measured R_{rs} to the spectrum in the database and find the closest match. The environmental inputs corresponding to the closest match are then considered to be the real conditions that generate the field measured R_{rs}.

No direct measurements of the backscattering coefficients of particles were available as part of this study. A subset of the samples collected in summer 2014 was selected to calibrate the backscattering properties and the remaining samples were used for model validation. Backscattering coefficients of suspend particles (including both chl

and NAP) were lumped into one variable, $b_{b,p}(\lambda)$, which can be expressed using a power function,

$$b_{b,p}(\lambda) = [\text{TSS}] \cdot b^*_{b,p}(550) \cdot \left(\frac{550}{\lambda}\right)^{\gamma} \qquad (4.2)$$

where $b^*_{b,p}(550)$ is the specific backscattering coefficient at 550 nm, λ is the wavelength, and γ is the spectral shape parameter. The two unknowns $b^*_{b,p}(550)$ and γ of the selected sites were determined by using the LUT methodology. The specific backscattering spectra were then estimated by normalizing the backscattering to the measured [TSS] and the average was used to represent the specific backscattering properties of the Wabash River and the Tippecanoe River.

Together with the lab measured absorption and bottom albedo collected in the field, the retrieved backscattering coefficients were used to construct the R_{rs} database using the HydroLight-EcoLight 5.2.2. radiative transfer model (Mobley and Sundman, 2013). Since the Wabash River and the Tippecanoe River could be optically shallow during low flow conditions, water depth was also considered as a parameter. Therefore, to simulate R_{rs} spectrum, four main parameters are needed: [chl], [TSS], the absorption of CDOM at 440 nm, $a_{cdom}(440)$, and water depth. For the initial LUT, [chl] ranged from 2 mg m^{-3} to 180 mg m^{-3} at increments of 2 mg m^{-3}, [TSS] ranged from 2 g m^{-3} to 180 g m^{-3} at increments of 2 g m^{-3}, and $a_{cdom}(440)$ ranged from 0 to 5 m^{-1} with increments of 0.25 m^{-1}. Water depths were set to start from 0.25 m with increments of 0.25 m according to Mobley et al. (2005). During the iteration of water depths, no further simulations were executed if the R_{rs} spectrum showed no change, which means all light has been absorbed

and/or scattered at this depth. This depth is referred as the maximum depth, D_{max}, and was recorded. If the retrieved depth is less than the maximum depth, it indicates optically shallow water; otherwise, it suggests that the water depth of the specific site is equal to or greater than D_{max}. All simulations were run using the Case 2 IOP model from 400 nm to 750 nm with 5 nm interval and assumed clear sky condition. Fluorescence of chl and CDOM were included. Only one solar zenith angle was used: $\theta_s = 30^o$. And the wind speed was set to be 5 m s^{-1}.

The closest matching spectrum is defined as the one in the database showing minimum difference with field measured R_{rs} spectrum. A term, err, is used to describe the difference

$$err = \sum_{j=1}^{J} [\tilde{R}_{rs}(\lambda_j) - R_{rs}(\lambda_j)]^2 \qquad (4.3)$$

where J represents the total number of wavelengths, $\tilde{R}_{rs}(\lambda_j)$ the database spectrum at band j, and $R_{rs}(\lambda_j)$ is the field measured spectrum at band j. Error analysis was also conducted to evaluate the retrieval accuracy.

4.5 Results and Discussion

4.5.1 Water Quality Observations

Daily discharge data from the Wabash River and the Tippecanoe River were obtained from USGS stations USGS 03335500 and USGS 03333050, respectively. The Mann-Whitney-Wilcoxon test shows that the Wabash River and the Tippecanoe River experience different hydrologic regimes (p<0.05). Since the Wabash River and the Tippecanoe River also experience different optical properties, as shown in section 4.4, they were analyzed separately. A summary of water quality observations from the

Wabash River and the Tippecanoe River during the summer of 2014 is presented in Table 4.1. For the Wabash River, [chl] experienced large variability ranging from 8.9 mg m^{-3} to 175.3 mg m^{-3}, which spans three orders of magnitude. Concentrations of TSS also experienced large variability ranging from 11.0 g m^{-3} to 102.0 g m^{-3}. In contrast, [chl] and [TSS] in the Tippecanoe River were both lower and less variable, which is most likely due to the two upstream reservoirs serving as a settling basin. The CDOM level ($a_{cdom}(440)$) in both rivers was similar and ranged from low to moderate (0.8 m^{-1}-3.1 m^{-1}, and 1.1 m^{-1}- 2.7 m^{-1}, respectively). This is consistent with [DOC] in the two rivers (Table 4.1). Values of [TN] were similar between the Wabash River and the Tippecanoe River, but [TP] in the Wabash River was much higher with the highest value exceeding the Indiana nutrient benchmark of 0.3 g m^{-3}. Both [TSS] and [CDOM] varied independently of phytoplankton (Figure 4.2). Therefore the Wabash River and the Tippecanoe River are optically complex with non-algal particles and organics competing with phytoplankton and belong to the category of Case 2 waters (IOCCG, 2000). The measured water depths for the two rivers indicate that bottom reflectance might be contributing to the water-leaving signals and needs to be considered in the following analysis.

Table 4.1 Summary of water quality observations of the Wabash River and the Tippecanoe Rive in summer 2014

		[chl] mg m^{-3}	[TSS] g m^{-3}	$a_{cdom}(440)$ m^{-1}	[TP] g m^{-3}	[TN] g m^{-3}	[DOC] g m^{-3}	Depth m
Wabash	Mean	56.0	42.2	1.7	0.10	5.9	27.1	2.0
	Min	8.9	11.0	0.8	0.02	1.3	8.9	0.4
	Max	175.3	102.0	3.1	0.47	10.0	41.5	4.4
	Mean	34.2	13.5	1.6	0.05	6.3	25.8	1.3

Tippecanoe	Min	8.3	8.5	1.1	0.01	2.0	8.2	0.3
	Max	53.1	20.4	2.7	0.12	10.6	35.5	2.8

(a)

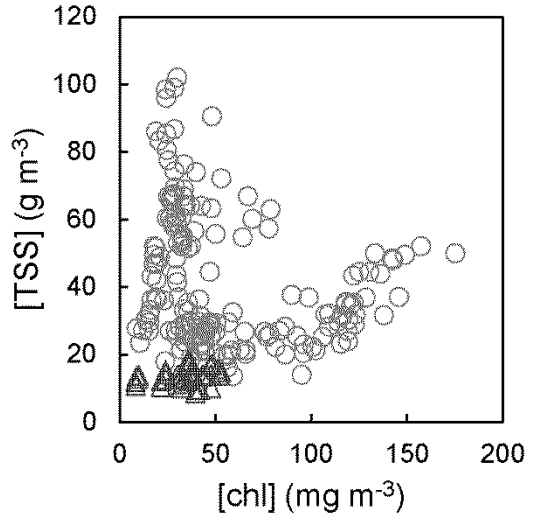

(b)

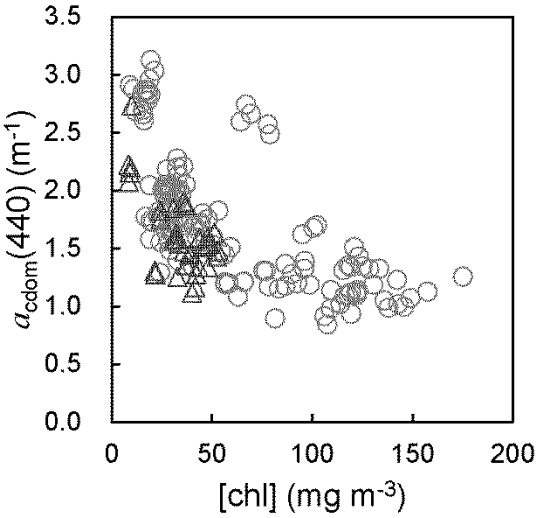

Figure 4.2 Scatterplots of measured (a) [TSS] and (b) $a_{cdom}(440)$ versus [chl] for samples in the Wabash River (circles) and the Tippecanoe River (triangles) in summer 2014.

Figure 4.3 shows time series of the measured water quality parameters and nutrients for summer 2014. It was found that the overall pattern of daily averaged TSS concentrations in the Wabash River followed that of streamflow (Figure 4.3(a)). High concentrations of TSS were typically found in the river when streamflow increased. The bloom of phytoplankton in the Wabash River usually occurred after streamflow peaked (Figure 4.3(c)). In addition, the changes in the level of TN, TP, and carbon in the Wabash River were also associated with those of streamflow. However, such observations were not obviously displayed for the Tippecanoe River. Pearson's correlation coefficients (r) were further calculated between each parameter and streamflow (Table 4.2). Results show that the concentrations of TSS, chl, CDOM, and TN in the Wabash River were significantly correlated with streamflow. The Wabash River watershed is dominated by agricultural land use, which means large amounts of sediments and nutrients were delivered from terrestrial sources to the river during storm events. The increase of [TP] in late July (Julian Day 209, 210, and 212) when streamflow was low coincided with the combined sewer overflow (CSO) events which delivered significant amount of TP into the river (Lafayette Water Pollution Control Department, personal communication). In addition, the relatively low [TP] on May 20 and 22 (Julian Day 140 and 142) was caused by the relatively low amount of TP delivered into the river and the high streamflow up to 680 $m^3 s^{-1}$ on May 16 (Julian Day 136). When these points were removed from the analysis, the correlation between [TP] and streamflow became significant (p=0.025) and increased to 0.50. None of the observed water quality parameters and nutrients showed significant correlation with streamflow for the Tippecanoe River, except for the level of

CDOM (Table 4.2). Such results indicate stream-based instead of runoff-based sources of sediments and nutrients, even though the major land use type in the Tippecanoe River watershed is also agriculture. This is mostly attributed to the two reservoirs located upstream of the Tippecanoe River study reach, which increase the residence time of water increasing the settling of sediment and uptake of nutrients.

There are two major sources of CDOM: (1) allochthonous – derived from the decomposition of woody plants in terrestrial environments, and (2) autochthonous – derived from the decomposition of algae and aquatic vegetation within the rivers. Since CDOM concentrations were significantly correlated with streamflow in both rivers (Table 4.2), it is highly likely that autochthonous is the dominant source in these rivers. It has to be noted that CDOM is only a portion of DOC that absorbs light. Therefore it is not surprising that DOC showed no significant correlation with streamflow in both rivers, which means that most of DOC in the rivers is uncolored and from human sources such as wastewater discharge or from CSO that are prevalent in our study area. For many remote sensing of water quality studies (e.g., Kutser et al., 2005), it is assumed that remote estimates of CDOM can be used to predict [DOC]. However, a weak relationship was observed between CDOM and [DOC] based on our field measurements (Figure 4.4). This is common for water bodies affected by human activities (Brezonik et al., 2015). Therefore, the use of CDOM for estimating [DOC] in inland water bodies should be cautioned and field validation is needed unless more is known about the CDOM-DOC relationship.

As we closely examine the measured [chl] in the Wabash River (Figure 4.5), it is found that variability of [chl] increased between sampled sites when [chl] increased.

Significant increases of [chl] were found around early June (Day 149-160), middle June (Day 169-170), middle July (Day 190-195), and late July (Day 209-210). Specifically, the phytoplankton blooms on Day 149-160, 169-170, and 190-195 followed increases of [TN] and [TP]. Following the algae blooms there were decreases of [TN] and [TP] due to biological uptake and transformations. The increase of [chl] on Day 209-210 is believed to be a result of increased [TP] due to CSO input (Figure 4.3(k)). The magnitude of the [chl] increase was relatively lower in early June as compared to the other bloom events, which might be caused by the relatively lower amount of TP delivered into the river as well as the relatively lower water temperature (ranged approximately 21˚C - 23˚C). The decrease of [chl] on Day 196-197 when [TP] and streamflow were relatively stable is believed to be a result of decreased water temperature, which dropped from 26˚C to 23˚C as shown by our field data. Therefore it is concluded that the source of water (surface runoff or CSO) to a river, water temperature, and nutrients are important factors controlling instream concentrations of phytoplankton.

Table 4.2 Pearson's correlations between concentrations and streamflow of the Wabash River and the Tippecanoe River. The values in bold text represent those correlations that were significant (p<0.05).

	[TSS]	[chl]	$a_{cdom}(440)$	[DOC]	[TP]	[TN]
Wabash	**0.82**	**-0.68**	**0.68**	0.31	0.11	**0.74**
Tippecanoe	0.36	0.02	**0.72**	0.33	0.04	0.66

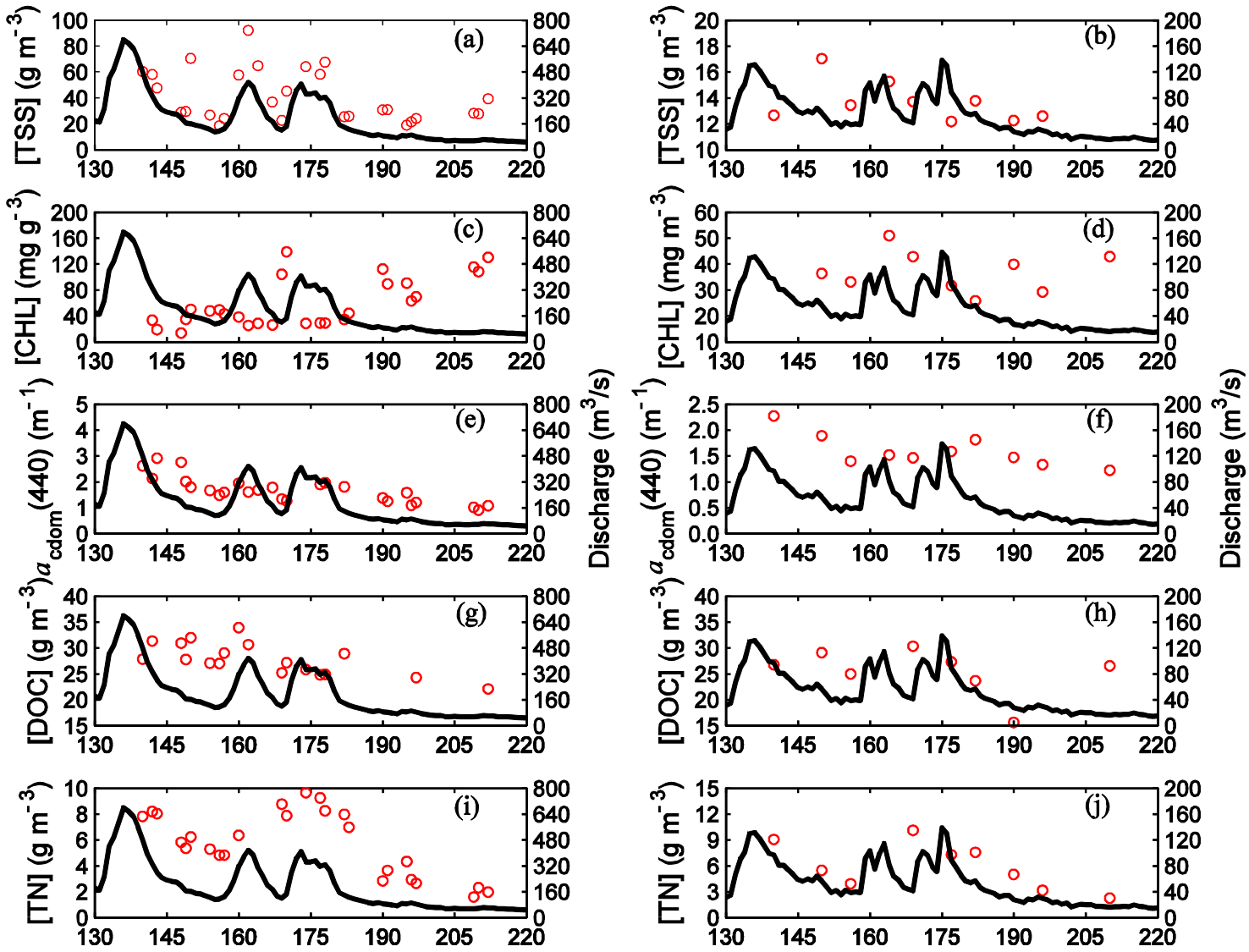
(a)
(b)
(c)
(d)
(e)
(f)
(g)
(h)
(i)
(j)
[TSS] (g m-3)
[CHL] (mg g-3)
[CHL] (mg m-3)
acdom(440) (m-1)
[DOC] (g m-3)
[TN] (g m-3)
Discharge (m3/s)
130
145
160
175
190
205
220

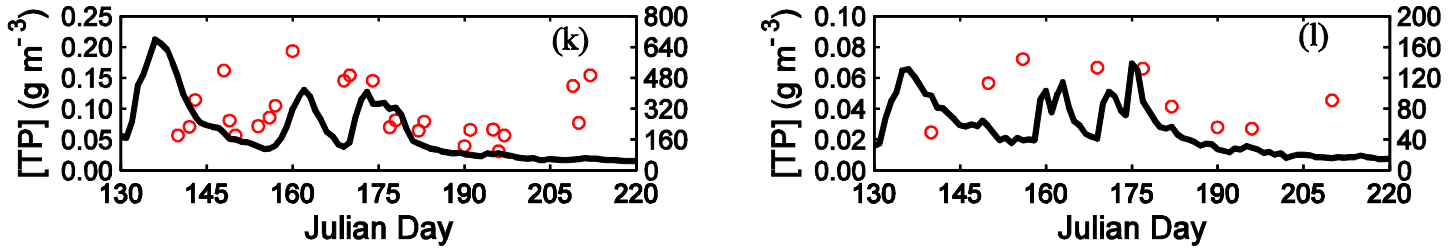

Figure 4.3 Time series of measured concentrations of water quality parameters and nutrients (circles) versus streamflow (solid line) of the Wabash River (left panel) and the Tippecanoe River (right panel). (a) and (b) - [TSS], (c) and (d) - [chl], (e) and (f) - $a_{cdom}(440)$, (g) and (h) - [DOC], (i) and (j) - [TN], and (k) and (l) - [TP].

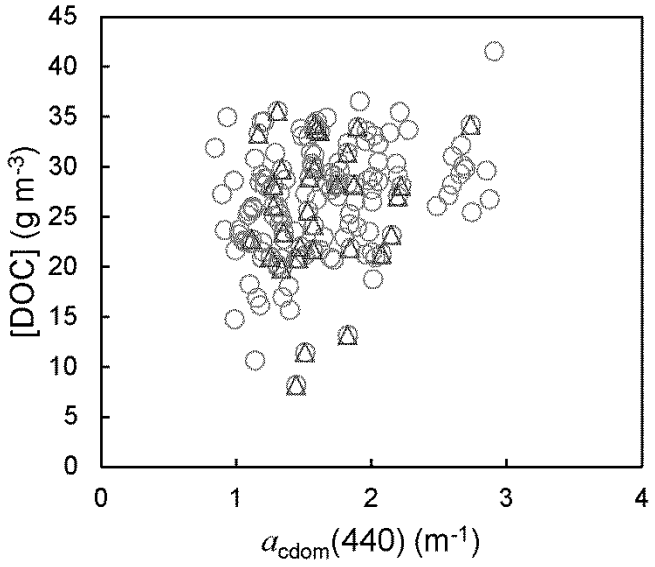

Figure 4.4 Scatterplot showing measured [DOC] versus $a_{cdom}(440)$ for samples collected for the Wabash River (circles) and the Tippecanoe River (triangles) in summer 2014.

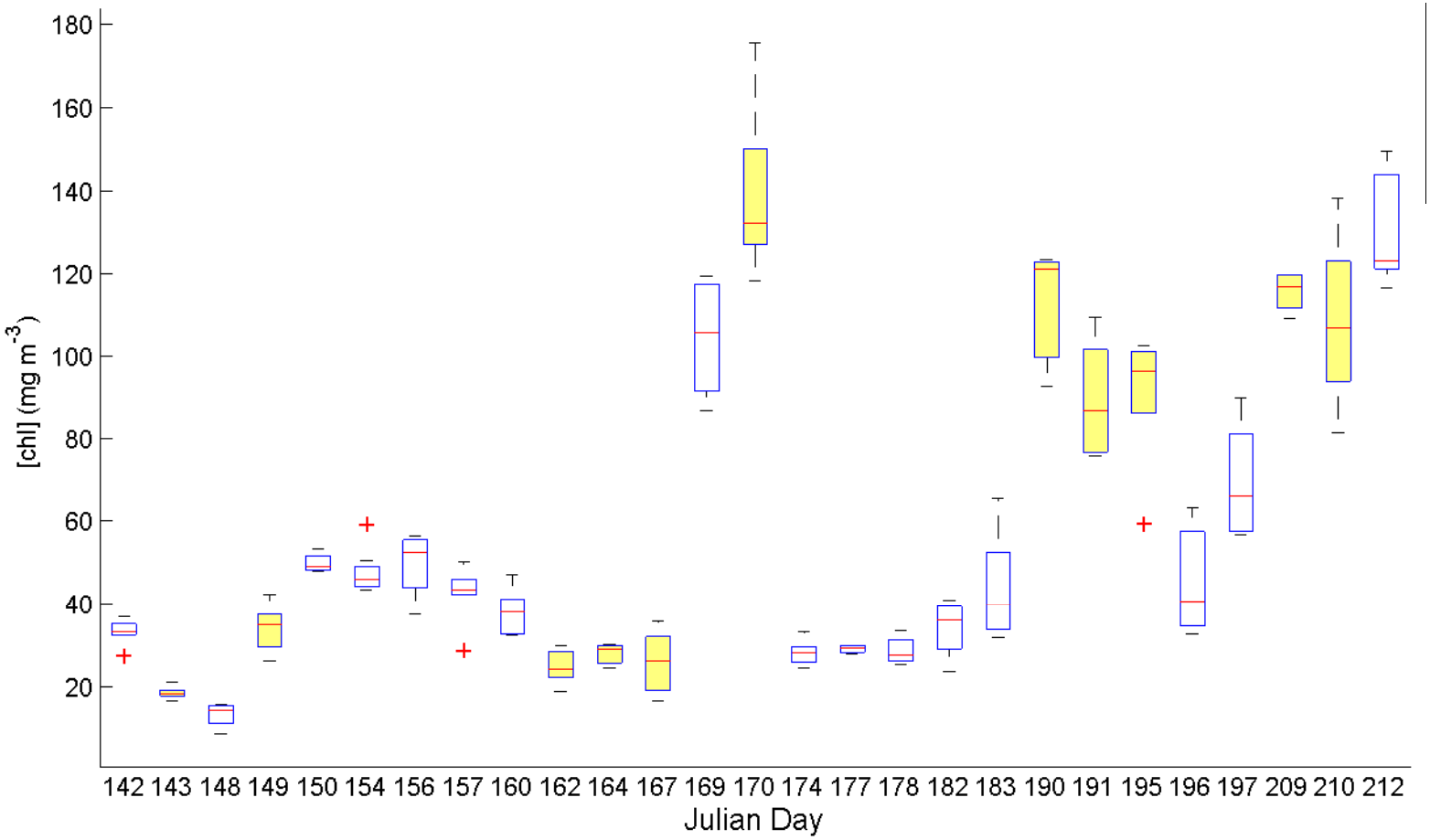

Figure 4.5 Boxplots of measured [chl] for samples collected in the Wabash River during the summer of 2014. Boxes filled with yellow indicate that there is a statistically significant difference (p<0.05) between observations on the highlighted day and the previous day.

4.5.2 Inherent Optical Properties

Absorption by phytoplankton at 676 nm ($a_{ph}(676)$) as estimated from the collected water samples closely paralleled changes in extracted [chl] in the Wabash River with *r* equal to 0.90 (Figure 4.6 (a)). The temporal variability in chl absorption was dominated by algal blooms, which were caused by increased nutrients delivered from terrestrial sources during runoff events. Significant increases in chl absorption were found on days when [chl] increased. Significant correlation between $a_{ph}(676)$ and [chl] were also found in the Tippecanoe River (r=0.93, p<0.05), although absorption by chl was lower and less variable (Figure 4.6(b)).

The observed changes in absorption by NAP at 440 nm ($a_{nap}(440)$) corresponded strongly to the variation in [TSS] in the Wabash River (Figure 4.6(c)). The absorption coefficient of NAP at 440 nm, $a_{nap}(440)$ increased from about 1 m^{-1} to > 3 m^{-1} during summer runoff events. In July (after Julian Day 180) when no rainfall was observed, $a_{nap}(440)$ was low and much less variable since the residence time of water in the river channel was longer and most of the sediment had settled to the bottom of the channel. The Tippecanoe River experiences much lower absorption caused by non-algal particles, ranging from 0.9 m^{-1} to 1.6 m^{-1} (Figure 4.6(d)), primarily because the amount of sediment in the Tippecanoe River is much lower than that in the Wabash River. No significant correlation existed between $a_{nap}(440)$ and [TSS] in the Tippecanoe River and *r* only equaled to 0.35, which indicates that non-algal particles only constituted a part of TSS.

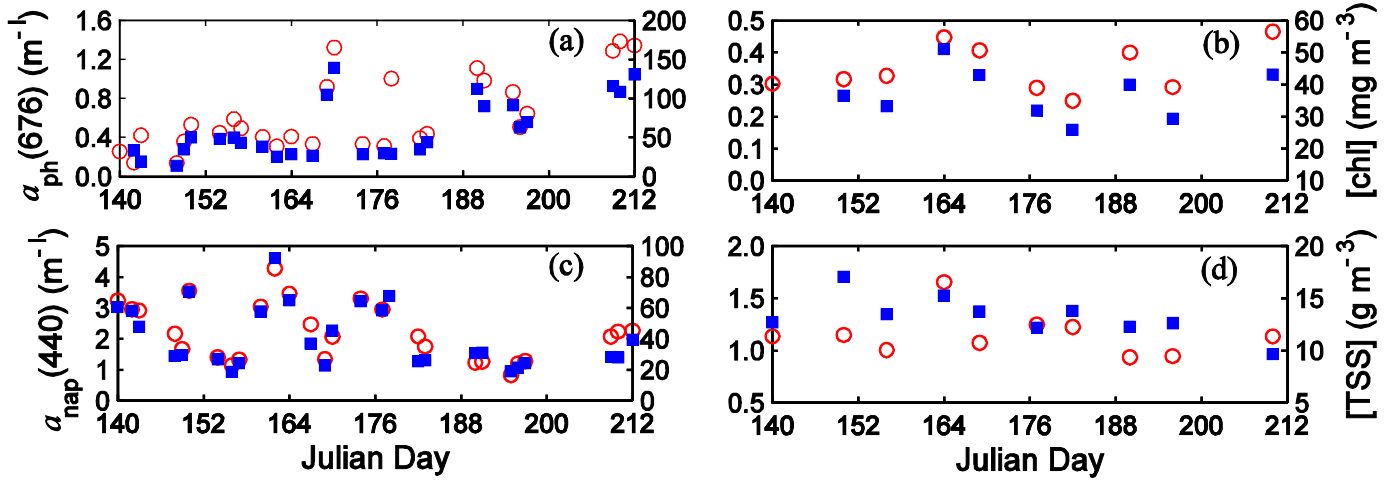

Figure 4.6 Scatterplots of measured IOPs (circles) versus water quality parameters (filled squares) of the Wabash River (left panel) and the Tippecanoe River (right panel). (a) and (b) – $a_{ph}(676)$ vs [chl], (c) and (d) – $a_{nap}(440)$ vs [TSS].

The spectral absorption of CDOM, $a_{cdom}(\lambda)$, can be described using an exponential function,

$$a_{cdom}(\lambda) = a_{cdom}(440) \cdot e^{-Scdom \cdot (\lambda - 440)} \qquad (4.4)$$

with the exponential slope S_{cdom} estimated by non-linear regression. The derived values of S_{cdom} had a narrow range (0.0157-0.0207 nm^{-1}), which is in good agreement with those reported for inland and coastal waters (Rosler et al., 1989; Babin et al., 2003; Binding et al., 2008). The specific absorption of CDOM, $a^*_{cdom}(\lambda)$, was acquired by fitting the ensemble mean of lab estimated specific absorption using Eq. (4.4), with the corresponding S_{cdom} equal to 0.018 nm^{-1} (Figure 4.7(a)).

Similarly, an exponential function was fit to the spectral absorption of non-algal particulate matter, $a_{nap}(\lambda)$,

$$a_{nap}(\lambda) = [TSS] \cdot a^*_{nap}(440) \cdot e^{-Snap \cdot (\lambda - 440)} \qquad (4.5)$$

where $a^*_{nap}(\lambda)$ is the specific absorption coefficient at 440 nm for NAP and [TSS] equals [NAP]. The exponential slopes of NAP, S_{nap}, were estimated by non-linear regression and ranged from 0.0076 nm^{-1} to 0.01 nm^{-1}. These values are also similar to those reported for inland and coastal waters (Rosler et al., 1989; Babin et al., 2003). The $a^*_{nap}(\lambda)$ was retrieved following the same method as for the $a^*_{cdom}(\lambda)$ and the corresponding S_{nap} was 0.089 nm^{-1} (Figure 4.7(a)).

There were no systematic differences between the two rivers in the mean spectral shape of phytoplankton absorption, $a_{ph}(\lambda)$ (data not shown). Coefficients of variations of $a_{ph}(\lambda)$ ranged from 14% to 51% for all wavelengths over the spectral range from 400 nm

to 700 nm, with high variations observed at around 400-420 nm and 600-650 nm. The high variations could be ascribed to the different compositions of chlorophyll *b*, chlorophyll *c*, and other accessory pigments in the Wabash River and the Tippecanoe River. The spectral values of $a_{ph}(\lambda)$ are given in Table 4.3. The small bump around 480 nm and 645 nm is likely to be caused by the comparatively high concentrations of chlorophyll *b* and chlorophyll *c* for some sampled sites (Figure 4.7(a)).

The retrieved average backscattering coefficients are shown in Figure 4.7(b), with $b^*_{b,p}(550)$ equal to 0.0.012 m^2 g^{-1} and γ equal to 1.3. There were no significant differences between the two rivers' backscattering properties. The retrieved $b^*_{b,p}(550)$ values lied between 0.006-0.02 m^2 g^{-1} and the power exponent γ ranged from 0.5 to 2.0, typical for Case 2 waters as reported by previous literature (IOCCG, 2006). The temporal variability of particulate backscattering at 550 nm ($b_{b,p}(550)$) was closely associated with [TSS] and showed weak correlation with [chl] (Figure 4.8), implying the dominance of the backscattering by non-algal particles.

Table 4.3 Spectral values for phytoplankton absorption in summer 2014.

λ	$a_{ph}(\lambda)$
400	0.0095
405	0.0102
410	0.0105
415	0.0110
420	0.0117
425	0.0128
430	0.0141
435	0.0153
440	0.0158
445	0.0157
450	0.0151
455	0.0143
460	0.0135
465	0.0128
470	0.0121
475	0.0116
480	0.0114
485	0.0113
490	0.0113
495	0.0110
500	0.0105
505	0.0097
510	0.0088
515	0.0078
520	0.0070
525	0.0063
530	0.0057
535	0.0053
540	0.0049
545	0.0047
550	0.0045
555	0.0043
560	0.0041
565	0.0040
570	0.0040
575	0.0041
580	0.0042
585	0.0043
590	0.0044
595	0.0045

Table 4.3 Continued

λ	$a_{ph}(\lambda)$
600	0.0046
605	0.0048
610	0.0050
615	0.0053
620	0.0056
625	0.0059
630	0.0061
635	0.0062
640	0.0062
645	0.0060
650	0.0061
655	0.0065
660	0.0075
665	0.0088
670	0.0101
675	0.0110
680	0.0109
685	0.0096
690	0.0075
695	0.0051
700	0.0032

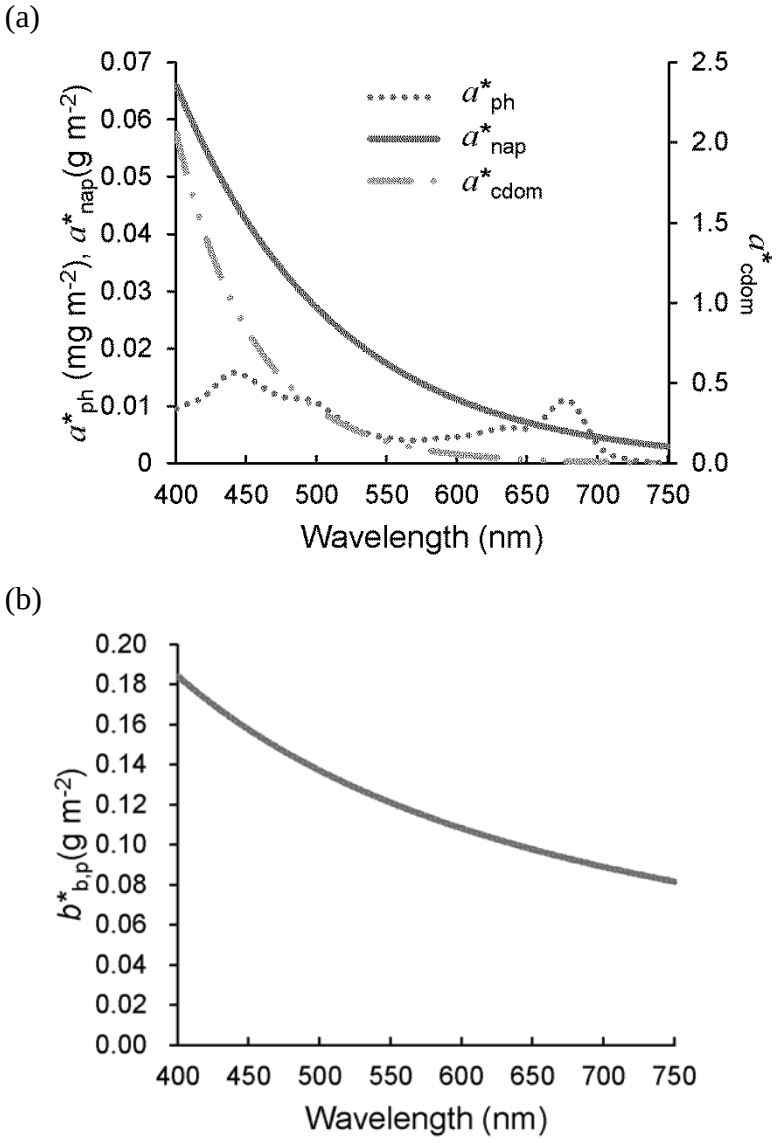

Figure 4.7 Specific inherent optical properties for the Wabash River and the Tippecanoe River: (a) absorptions, and (b) backscattering.

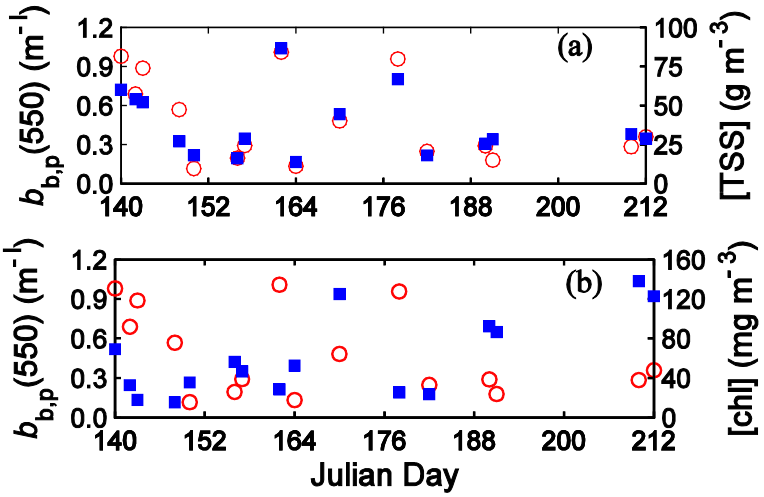

Figure 4.8 Variability of the retrieved $b_{b,p}(550)$ (circles) with measured (a) [TSS] (filled squares) and (b) [chl] (filled squares) in the Wabash River and the Tippecanoe River.

4.5.3 Bottom Properties

The measured bottom depths of sampled sites ranged from 0.3 m to 4.4 m, including both optically deep and shallow water (Table 4.1). Substrate type was categorized into six types based on the sediment size: boulder (>256 mm), cobble (255 mm-64 mm), gravel (63 mm - 2 mm), sand (1 mm -0.25 mm), fines (<0.24 mm), and hardpan (mixture of fines and clay), based on definitions from Wentworth (1992). As observed, major substrate types for our study area consisted of fines, sand, gravel, and cobble with sand predominating (Figure 4.9). Cobbles and gravels were mostly found in the upstream portions of the Wabash River reach from French Post to Delphi and in the Tippecanoe River. The bottom of the Wabash River from Delphi to Attica was dominated by sand with fines occasionally found near the bank.

Figure 4.10 shows the measured albedo for different substrate types. The spectral shapes of the albedos are similar and it is hard to exactly discern each type since the

ranges of measured albedos overlap with each other. Therefore, in this study averaged albedo was used as the bottom reflectance spectrum.

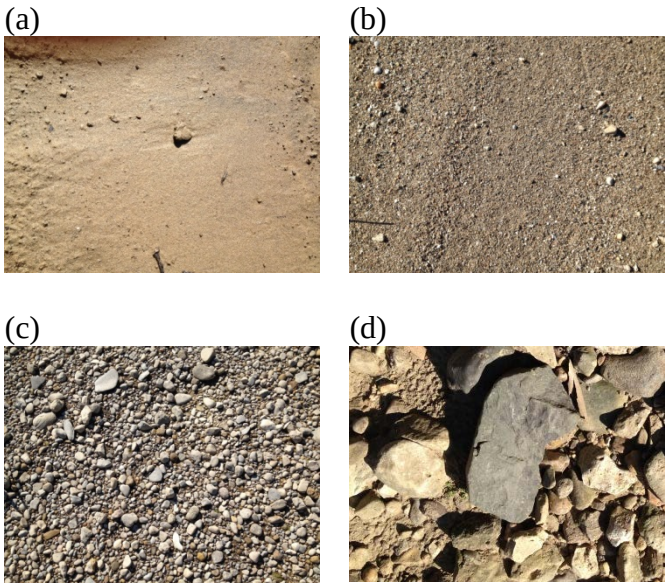

Figure 4.9 Bottom types identified for the Wabash River and the Tippecanoe River. (a) fines, (b) sand, (c) gravel, and (d) cobble.

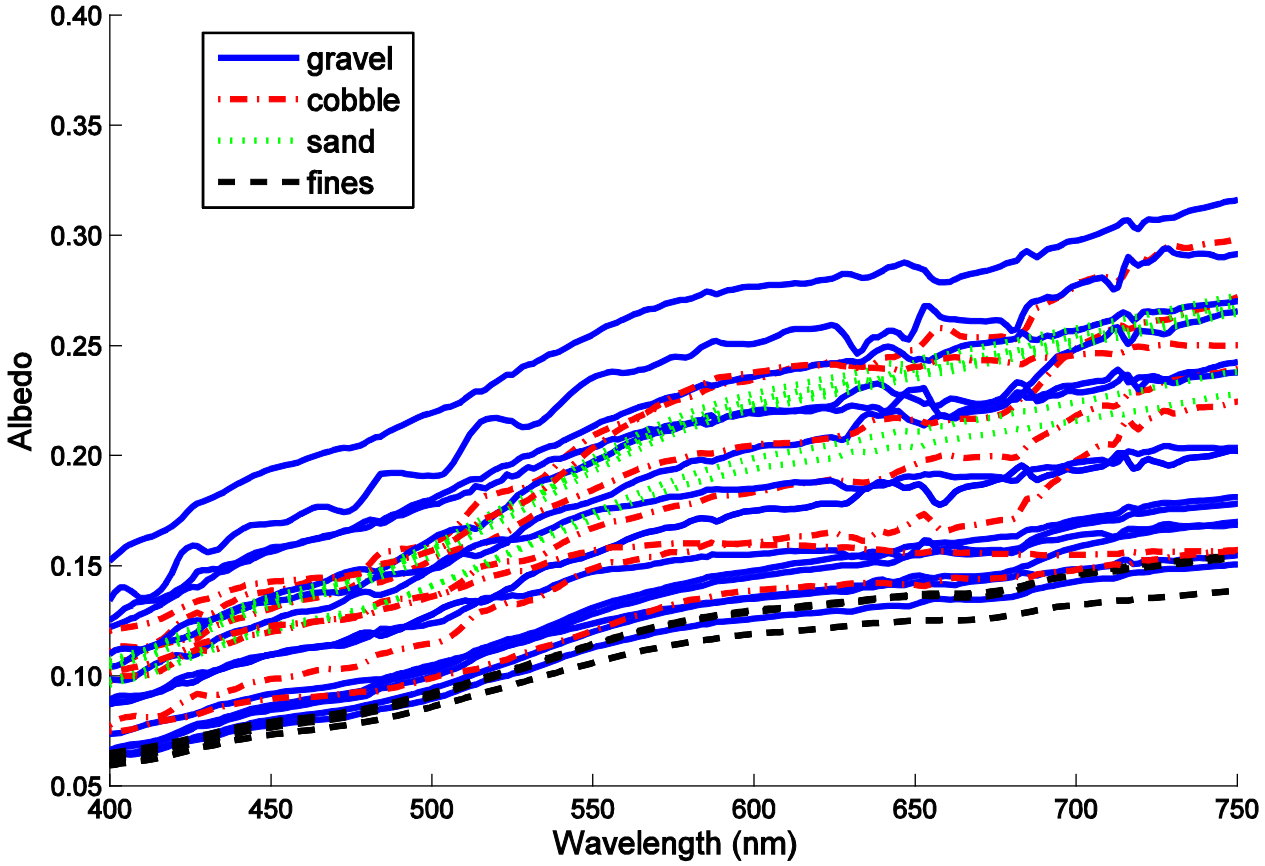

Figure 4.10 Albedo measured for different bottom types of the Wabash River and the Tippecanoe River.

4.5.4 Spectral Characteristics

Figure 4.11(a) shows all the R_{rs} spectra collected for the Wabash River and the Tippecanoe River in the summer of 2014. Based on the spectral characteristics, these spectra can be categorized into two types: (1) phytoplankton dominated and (2) sediment dominated, as shown by Figure 4.11(b). Spectra from phytoplankton dominated water experienced low reflectance in blue (400-500 nm) and red (600-700 nm) wavelengths due to the absorption by chl and other pigments. In particular, the local minimum at 677 nm and peak at 704 nm were caused by the decreasing absorption of chlorophyll and increasing absorption of water as well as the fluorescence of chl (Vasilkov and Kopelevich, 1982). For the sediment dominated spectra, the reflectance values of these waters are relatively high in the green and red wavelengths, especially from 560 to 700 nm, and they lack the reflectance trough and peak in the red region caused by the absorption characteristics of chl.

4.5.5 Water Quality Retrieval

A total of 550,054 spectra were generated using HydroLight. A random selection of the R_{rs} spectra are presented in Figure 4.12 to demonstrate the range of spectra in the database. Before we applied the entire database of R_{rs} spectra to the analysis of the field collected spectrometer data for the Wabash River and the Tippecanoe River as shown in Figure 4.1, we first resampled the field measured R_{rs} spectra with a cubic spline fit to correspond to the LUT wavelengths.

Values for [NAP], [chl], and $a_{cdom}(440)$ were retrieved by finding the closest matching LUT spectra to the field measurements (Figure 4.13). It is clear in Figure 4.13 (a) and 4.13(b) that the resulting points fall close to the 1:1 line for [NAP] and [chl],

which suggests that the LUT estimates are in close agreement with coincident in situ measurements. No statistically significant relationship was found between modeled and measured $a_{cdom}(440)$ (Figure 4.13(c)). Although the points for CDOM comparison visibly cluster near the 1:1 line, the high variability restricts us from making any conclusion. Based on our observations the change in $a_{cdom}(440)$ was within 3 m^{-1} (Table 4.1), while the $a_{cdom}(440)$ value can be as high as 40 m^{-1} for inland water (Brezonik et al., 2015). In Chapter 3 we also found that R_{rs} is not sensitive to the observed changes in $a_{cdom}(440)$, therefore it is highly likely that the small observed changes cannot be adequately captured by the LUT methodology. It is also possible that the LUT retrievals for $a_{cdom}(440)$ display large uncertainties at low CDOM levels (Brezonik et al., 2015), but produce an overall good 1:1 fit with a wider data range than the CDOM levels in the Wabash River and the Tippecanoe River sampled in summer 2014. This needs further investigation with more data collected for the rivers during other seasons of the year, for example, in spring when agricultural activities are intense and streamflow is high.

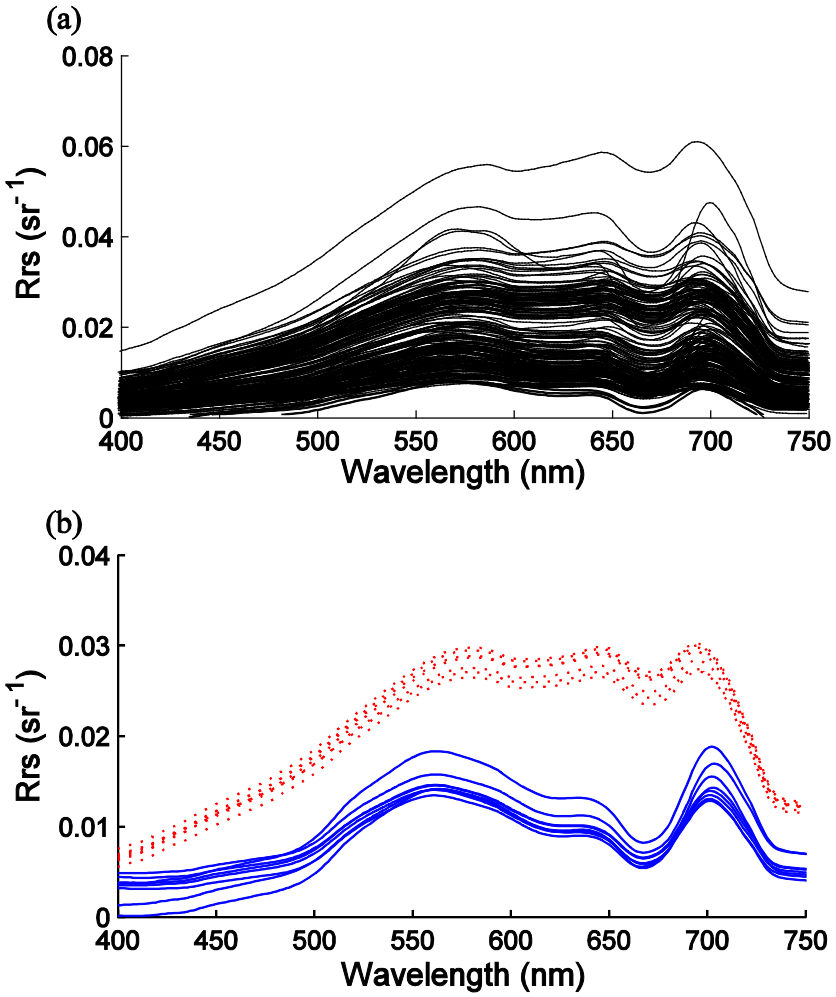

Figure 4.11 (a) All R_{rs} spectra collected in summer 2014 and (b) examples showing phytoplankton dominated (solid lines) and sediment dominated (dotted line) spectra.

To better quantitatively describe the retrieval results for NAP and chl, three metrics were adopted: (1) relative error, (2) percent difference, and (3) concentration difference. Relative error is defined as

$$\text{Relative error} = \frac{C(\text{LUT};i) - C(\text{field};i)}{C(\text{field};i)} \tag{4.6}$$

The average percent difference in the LUT retrieved and field measured concentrations is computed as,

$$\text{Percent difference} = \frac{100}{N} \cdot \sum_{i=1}^{N} \frac{C(\text{LUT};i) - C(\text{field};i)}{C(\text{field};i)} \tag{4.7}$$

And the average concentration difference is computed as,

$$\text{Concentration difference} = \frac{1}{N} \cdot \sum_{i=1}^{N} C(\text{LUT};i) - C(\text{field};i) \tag{4.8}$$

In Eq. (4.6), (4.7) and (4.8), $C(\text{LUT};i)$ is the LUT retrieved concentration for site i, $C(\text{field};i)$ is the field measured concentration at site i, and N is the total number of sampled sites. In each case, a positive (negative) error indicates that the LUT retrieved concentration is too high (low). When the LUT retrieved [NAP] is compared with field measured [NAP], the average percent difference is 4.1% and the concentration difference is -1.0 g m^{-3}. The average error is larger, 37.7% or 18.0 mg m^{-3}, for the estimation of [chl]. This is reasonable since the [chl] has a smaller influence on the R_{rs} spectra, as demonstrated in Chapter 3. It also is possible that the specific absorption spectrum of phytoplankton is perhaps not well represented in the LUT database given the variability introduced by other pigments. The relative error for each site was also examined and the overall estimation of [chl] and [NAP] is not biased.

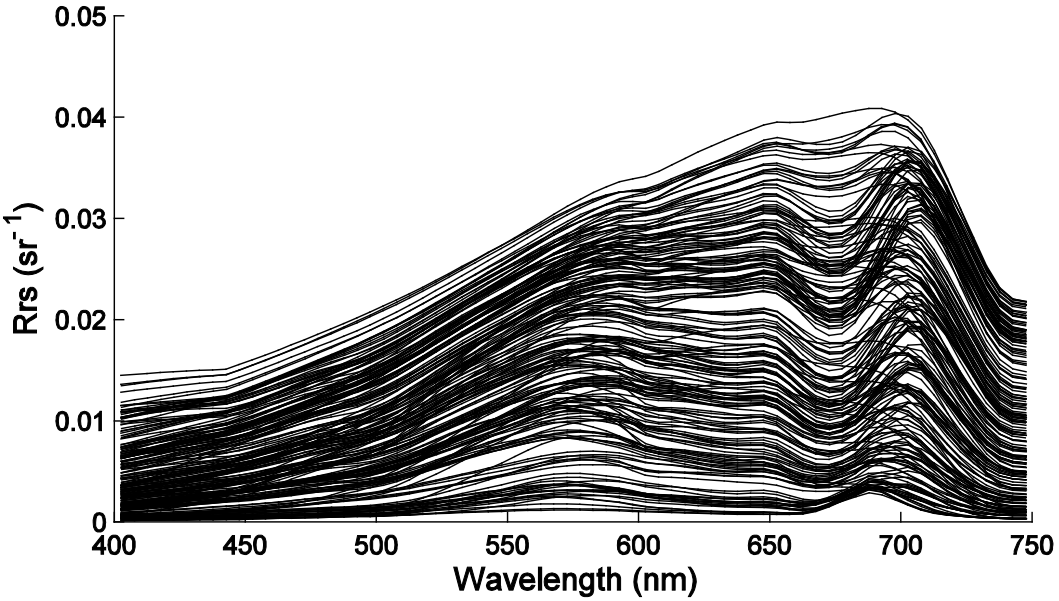

Figure 4.12 Randomly chosen selection of the 550,054 spectra in the LUT database.

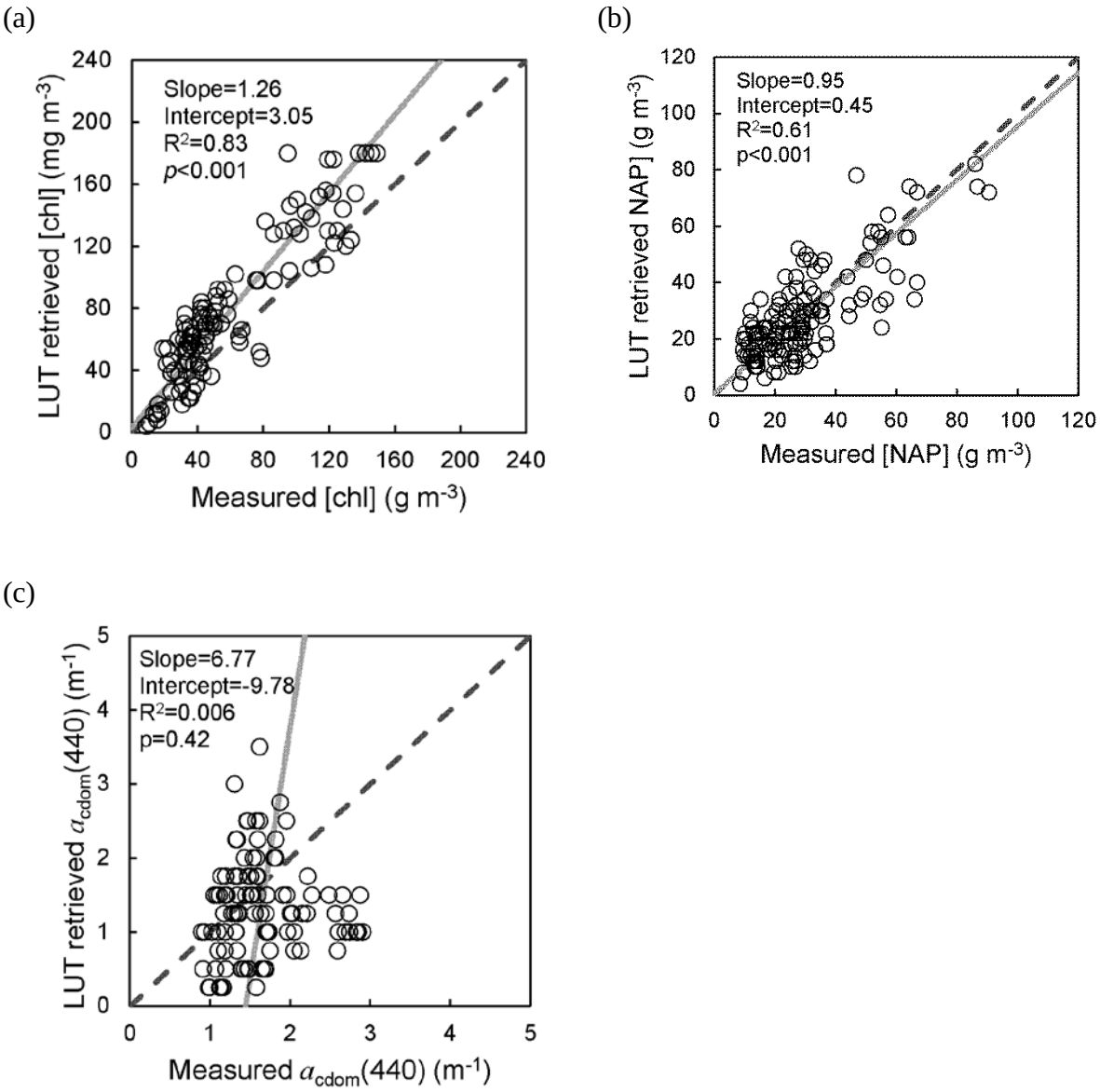

Figure 4.13 Comparison between measured (a) [chl], (b) [TSS], and (c) $a_{cdom}(440)$, and the LUT estimates for the Wabash River and the Tippecanoe River.

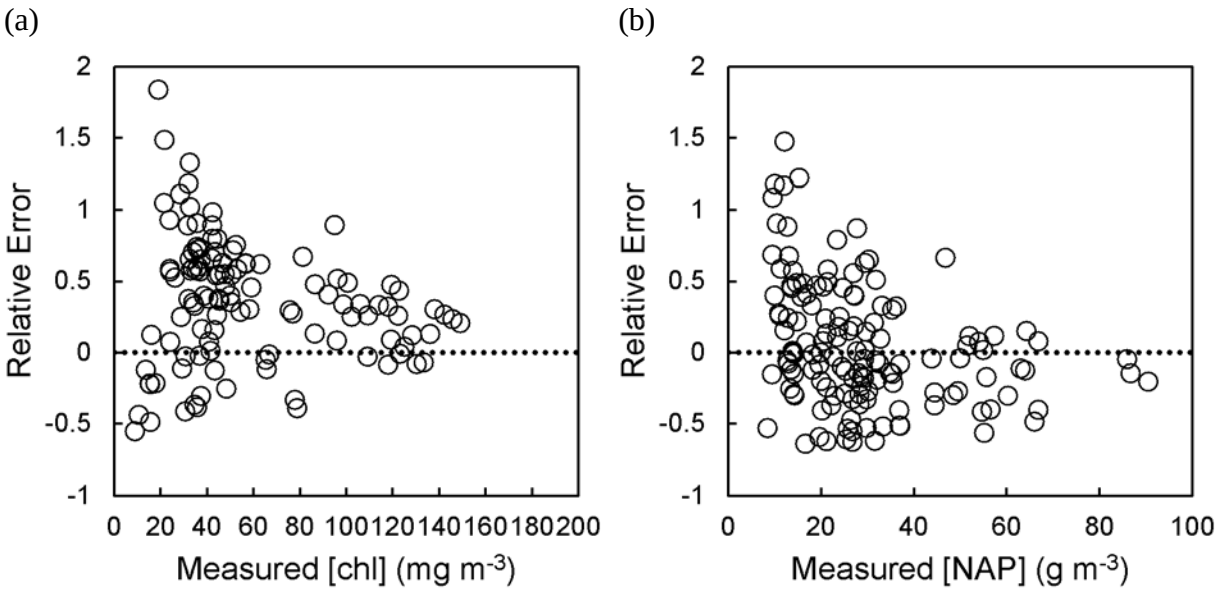

Figure 4.14 Relative error versus (a) [chl] and (b) [NAP] for the Wabash River and the Tippecanoe River.

4.6 Conclusions

In this study, extensive field measurements of the spectral, hydrologic and water quality properties of the Wabash River and the Tippecanoe River, Indiana, were conducted under a range of hydrologic conditions in the summer of 2014. Data collected mainly include remote sensing reflectance spectra of river water taken using a hand-held spectrometer, IOPs, concentrations of water quality parameters (chl, NAP, and CDOM) and nutrients (TP, TN, DOC), water depths, substrate types, and bottom reflectance spectra. These measurements provide valuable data of the optical properties and water quality information for the Wabash River and the Tippecanoe River, which not only enable the development of transferrable physical models for retrieving water quality parameters, but also provide a fundamental linkage between the optical properties and the biogeochemical state of inland river systems.

Our results show that the temporal variability of water quality parameters and nutrients of the Wabash River in the summer of 2014 were closely associated with hydrologic regime. The concentrations of TSS, chl, CDOM, and TN in the Wabash River were significantly correlated with streamflow ($p<0.05$), which indicates that summer runoff events played an important role in delivering nutrients and sediments to the Wabash River. The initial correlation significance test of [TP] with streamflow was not significant and the correlation coefficient r was only 0.11. However, after removing samples during the low flow period in late July when groundwater input of TP became dominant and those around late May when the increase of TP in the river was not able to offset the dilution caused by increased streamflow, the correlation between [TP] and streamflow became significant and r increased to 0.50. None of these parameters showed

significant correlation with streamflow for the Tippecanoe River except for CDOM, most likely due to the two upstream reservoirs which increase the residence time of water. Therefore most of the sediment settled out and nutrient uptaken was more effective resulting in cleaner water in the Tippecanoe River below the reservoirs. While the variation of CDOM was significantly correlated with streamflow in both rivers, [DOC] experienced no such significant correlation. It is highly likely that most of DOC in the rivers is uncolored and from human sources such as wastewater discharged or from combined sewer overflows that are prevalent in our study area. Phytoplankton blooms were typically found in the Wabash River following the increase of nutrient inputs, either due to surface runoff events or groundwater inputs. In addition, water temperature and the intensity of major runoff events are also important factors controlling instream concentrations of phytoplankton.

The LUT methodology was applied to the dataset collected in summer 2014 and was tested successfully with the dataset for the retrieval of water quality parameters. The Hydrolight package fully simulates the complex radiative transfer process within water column and at bottom boundary conditions. It was used to generate a database of R_{rs} spectra, in which the closest match of the specific field measurement was found and the corresponding inputs were thus considered as the real environmental conditions when the field measurement was collected. This method requires no ancillary environmental information and is able to simultaneously retrieve [chl], [NAP], and $a_{cdom}(440)$. The accuracy of this method depends on the accurate and appropriate measurements of IOPs and R_{rs}. Therefore, it is important to have well-characterized field measurements, as was done here, for the specific study area.

Our study demonstrates that the LUT retrieved values from the closest matching spectra give good estimates of the water quality parameters with points cluster near the 1:1 line. The overall estimations of [NAP] and [chl] are not biased based on the analysis of relative errors. Significant linear relationships exist between the LUT retrieved and field measured values of [NAP] with a slope close to 1.0. For [NAP] estimates, the average percent difference is 4.1% and the concentration difference is -1.0 g m^{-3}. The LUT retrieved [chl] values are also in good agreement with the field measurements (slope equal to 1.26). The average error is larger for the estimation of [chl] (37.7% or 18.0 mg m^{-3}). Large variability was found at the LUT retrieved CDOM values, which might be due to the fact of small data ranges and the insensitivity of R_{rs} to the change in CDOM.

All the data collected in this study, including in situ water quality, nutrient level, IOPs, and spectral measurements, as well as all additional associated data (e.g., underwater photos, bottom albedos, water depth, date, time of day) and the LUT, has been integrated into a database using Microsoft Access and will be distributed online through the Purdue University Research Repository (PURR – http://purr.purdue.edu/). Metadata documentation is also included in the database. This dataset will be assigned a Document Object Identifier (DOI) from the Purdue Library and published. Purdue University will maintain the dataset for at least 10 years after the completion of this project. This database, once published, will provide useful ground truth data for remote sensing of water quality in inland waters and valuable sources for further investigation of the relationship between optical and biogeochemical properties.

4.7 Acknowledgements

This work was supported by NASA Headquarters under the NASA Earth and Space Science Fellowship Program – Grant "NNX14AL31H". We thank Purdue Water Community (PWC) and Indiana Water Resource Center (IWRRC) for providing the financial support for the purchase of the Hydrolight software license. We greatly appreciate Dr. Reuben Goforth and his research group in the Department of Forestry and Natural Resources at Purdue University for scheduling our boat sampling trips into their field work timeline. We are also thankful to Amanda Montgomery at the Ecohydrology Laboratory, Purdue University and Megan Heller at the Soil Microbiology Laboratory, Purdue University for their help in nutrient analyses.

CHAPTER 5. SUMMARY AND CONCLUSIONS

Water quality impairment due to excessive concentrations of sediments and nutrients has been a concern in the Midwestern United States. Remote sensing has the potential to provide synoptic water quality information at a short time scale. In this thesis, I applied both in situ spectrometer data and satellite imagery to retrieve water quality parameters in Midwestern rivers and lakes. Different algorithms including empirical and physical models were used to invert remote sensing data. Here I summarize the most significant findings as they relate to the hypotheses presented in Chapter 1.

First I developed a method for removing sun and sky glint from total above-water reflectance for turbid inland waters. Surface reflected glint is a curse for water quality remote sensing from above-water platforms. The glint contribution in the total above-water reflectance is dependent on viewing geometry, sun elevation and azimuth, illumination conditions, and wind speed and direction. All these parameters need to be recorded and taken into account for glint removal. Multiple glint removal procedures have been developed in previous studies. In particular, Kutser et al. (2013) developed a method to represent the surface reflected glint by fitting a power function to the reflectance at 350-380 nm and 890-900 nm. The advantage of this method is that it does not require auxiliary measurements such as wind speed. However, this method does not work well for turbid waters. In this thesis I combined Kutser's correction, Gould's glint

removal algorithm, and Ruddick's similarity spectrum together and tested this new method using the spectrometer measurements collected for the Wabash River and its tributaries in Indiana on August 15, 2013. I found that the reflectance spectra corrected using this new method are fairly close to the corrected results of using Mobley's correction, which is commonly used and accepted for sun and sky glint removal. I also ran 500 Hydrolight simulations using the Case 2 inherent optical property (IOP) model to validate the robustness of this method. Simulated above-water reflectance were corrected and compared to the simulated remote sensing reflectance. The result of this analysis is that I determined that this new method can be used to estimate the surface reflected component in water reflectance spectra for turbid inland waters.

My first hypothesis is that *field spectroscopy provides a potential way to capture spectral characteristics that are indicative of the absorption and backscattering properties of each optically active constituent (OAC). Therefore, key spectral regions can be identified to improve the development of empirical models for inland waters, as well as to provide useful suggestions for future satellite remote sensing missions.* I conducted water sampling concurrent with spectral measurements of the Wabash River and its tributaries in Indiana to estimate concentrations of chlorophyll (chl) and total suspended solids (TSS). In an analysis of the absorbing and backscattering properties of chl, suspended solids, and colored dissolved organic matter (CDOM), wavelengths that experience interference through competing optical features were avoided. Since the concentration of chl is closely associated with the light absorption in the red wavelengths where the influences from CDOM and suspended solids are minimal, the ratio of the reflectance peak at 704 nm to the reflectance trough at 677 nm was used to set up a

statistical relationship with chl concentrations. Result shows that this ratio is a strong predictor of chl concentrations with coefficient of determination (R^2) equal to 0.95. Similarly, the wavelengths that experience interference by the absorption from chl and CDOM were avoided when developing a model for the estimation of TSS concentrations. The reflectance peak at 704 nm generated a robust model with R^2 equal to 0.75. Reflectance values at the near infrared (NIR) wavelengths are closely related to the amount of TSS and also were found to be strongly correlated (0.85-0.91) with TSS concentrations. The success of these empirical models suggests that the hyperspectral information provided by field spectrometer can be used to identify the optimal or key spectral regions for water quality retrieval under complex IOP conditions. The key spectral bands needed for the estimation of water quality parameters may not be effectively captured by some current multi-spectral sensors and should be considered for future satellite remote sensing.

My second hypothesis is that *in situ observations of water quality parameters are spatially limited, but that this spatial limitation can be addressed in part through the use of remote sensing imagery. Physical models which are based on the water column and bottom properties are reliable and transferrable in quantifying water quality parameters from the spectral signatures.* This hypothesis is addressed by both Chapter 3 and Chapter 4. In Chapter 3, field campaigns were conducted near the mouth of the St Joseph River in southern Lake Michigan to capture storm-initiated river plumes. A database of IOP measurements and spectral signatures was generated and used to calibrate a bio-geo-optical model for the estimation of water quality parameters. This bio-geo-optical model is a simplification of full radiative transfer equations and is transferrable with accurate

and appropriate measurements of IOPs for specific study. Results show that modeled concentrations of chl, CDOM and non-algal particles (NAP) through utilizing the field spectrometer data show good correspondence with the field measurements: field measured concentrations of NAP and CDOM at 67% of the sampled sites fall within one standard deviation of the model retrieved value using the spectrometer measurements; the percentage of sites is higher for the estimation of chl concentration, which is 88%. It is also demonstrated that Hyperion imagery, which has high resolution both spectrally and spatially, can be used to study the variability of water quality parameters for river plumes although it is not originally designed for water observations. 77% of the sampled sites show field measured chl and NAP concentrations falling within one standard deviation of the corresponding Hyperion derived values, despite the dynamic nature of the observed plume and the time lag during field sampling. The spatial maps of water quality parameters generated from the Hyperion image provided a synoptic view of water quality conditions. The spatial heterogeneity and great detail of water quality shown by the image indicates that it would be difficult to use the traditional sampling strategy for fully characterizing the spatial variability and structure of river plumes.

Extensive observations of the Wabash River and its tributaries were conducted in Chapter 4, which include measurements of spectral signals, bottom properties, IOPs, and water quality. With this dataset, the full radiative transfer process was simulated and a database of remote sensing reflectance corresponding to various concentrations of water quality parameters was assembled using the radiative transfer software Hydrolight. Water quality parameters were then estimated using the spectrum matching based look-up-table (LUT) method. Results show that the LUT retrieved concentrations of chl and NAP are in

very good agreement with the field measurements with the slope close to 1.0. For the estimation of NAP concentrations, the average percent difference versus field observaions is 4.1% and the concentration difference is -1.0 g m^{-3}. The average error is larger for the estimation of chl concentrations (37.7% or 18.0 mg m^{-3}). However, larger variability was found for the LUT retrieved CDOM values, and I concluded that it might be due to the small data ranges and the insensitivity of R_{rs} to CDOM change that is demonstrated in Chapter 3.

My third hypothesis is that *concentrations of water quality parameters including chl, NAP, and CDOM are indicative of the health of riverine and lake aquatic systems and the spatial and temporal variability of these parameters are closely related to hydrologic conditions and land use patterns.* My findings in Chapter 3 show that concentrations of chl, NAP, and CDOM were more than three times higher in conjunction with river outflow and inside the river plume than in ambient water. I conclude from this that the storm-initiated plume is a significant source of sediments, carbon and chlorophyll to Lake Michigan. The noticeably high concentrations of CDOM and chl along the shore line indicate that the stimulation of phytoplankton activity and the enhancement of chl concentrations are associated with river outflow. These river plumes enhance the amount of nutrients and sediments delivered from terrestrial resources, diminish light that can penetrate through water, and in turn can regulate nutrient cycling and affect the rate and amount of primary production in the lake. The spatial distribution of water quality parameters inside the river plume also changed as the plume migrated inshore and was dependent on wind and wave during the field campaign. The analyses I conducted in Chapter 4 suggest that the temporal variability of water quality parameters

and nutrients in the Wabash River was closely associated with hydrologic conditions, while no significant correlations existed between these parameters and streamflow for the Tippecanoe River probably due to the two upstream reservoirs. The poor relationship between CDOM and DOC indicates that most DOC in the rivers was from human sources such as wastewater. It is also found that the source of water (surface runoff or combined sewer overflow (CSO)) to a river, water temperature, and nutrients are important factors controlling instream concentrations of phytoplankton.

During this project, I also highlighted some of the limitations of satellite/airborne remote sensing for use in the monitoring inland water quality. First, satellite remote sensing for monitoring water quality of rivers and streams are limited by spatial resolutions that are too coarse to appropriately resolve the river headwater streams that contribute most significantly to the overall water quality. Second, according to our experience in remote sensing of small river plumes, it is difficult to coordinate coincident field sampling with satellite acquisitions, clear-sky conditions, and irregular storm events. In addition, given the time period required for plume sampling and the dynamic nature of plumes, it is challenging to ensure that the field measurements reflect the instantaneous spatial distribution of water quality corresponding to the satellite imagery. Airborne platforms can collect highly resolved imagery for river systems and small river plumes, but they are not likely to be operated for regular monitoring due to the high operational cost and requirement of clear atmospheric conditions. To that end, field spectrometer measurements provide important spectral/optical information studying rivers and river plumes. Therefore, field spectroscopy should be used as a potential investigative technique of inland water quality to complement satellite/airborne remote sensing.

The field datasets collected for the St Joseph River plume and the Wabash River and its tributaries were finally distributed online through the Purdue University Research Repository (PURR – http://purr.purdue.edu/). In addition to the retrieval of water quality, these datasets will provide useful ground truth data for remote sensing of water quality in inland waters and valuable sources for further investigation of the relationship between optical and biogeochemical properties. The results of this study suggest future work should: (1) continue to collect coincident water quality and IOP data with spectral measurements in other seasons of the year, especially in spring when stream flow is high and agricultural activities are intense, (2) study the seasonal and interannual variability of water quality parameters and IOPs, and set up empirical/physical relationship between water quality and environmental factors such as hydrologic conditions and land use patterns, (3) collect finely resolved remote sensing imagery that is appropriate for rivers such as Landsat and unmanned aerial vehicle (UAV) imagery for water quality observation and evaluate the application of the LUT developed in this study for water quality retrieval when using these remote sensing images, and (4) continue to develop the data archive of IOPs and AOPs for public sharing and for the calibration/validation of future remote sensing work.

REFERENCES

REFERENCES

Alexander, R. B., R. A. Smith, G. E. Schwarz, E. W. Boyer, J. V. Nolan, and J. W. Brakebill, 2008. Differences in phosphorus and nitrogen deliver to the Gulf of Mexico from the Mississippi River Basin. Environmental Science & Technology 42, 822-830.

Allan, J. D., P. B. McIntyre, S. Smith, B. S. Alpern, G. L. Boyer, A. Buchsbaum, G. A. Burton, Jr., L. M. Campbell, W. L. Chadderton, J. J. H. Ciborowski, P. J. Doran, T. Eder, D. M. Infante, L. B. Johnson, C. A. Joseph, A. L. Marino, A. Prusevich, J. G. Read, J. B. Rose, E. S. Rutheford, S. P. Sowa, and A. D. Steinman, 2013. Joint analysis of stressors and ecosystem services to enhance restoration effectiveness. Proceedings of the National Academy of Science 110, 372-377.

Austin, R. W., 1980. Gulf of Mexico, ocean-colour surface-truth measurements. Boundary-Layer Meteorology 18, 269–285.

Babin, M., A. Morel, V. Fournier-Sicre, F. Fell, and D. Stramski, 2003. Light scattering properties of marine particles in coastal and open ocean waters as related to the particle mass concentration. Limnology and Oceanography 48 (2), 843-859.

Bastviken, D., Tranvik, L.J., Downing, J.A., Crill, P.M., and Enrich-Prast, A., 2011. Freshwater methane emissions offset the continental carbon sink. Science, 331(6013), 50.

Binding, C. E., J. H. Jerome, R. P. Bukata, and W. G. Booty, 2008. Spectral absorption properties of dissolved and particulate matter in Lake Erie. Remote Sensing of Environment 112, 1702-1711.

Blondeau-Patissier, D., J. F. R. Gower, A. G. Dekker, S. R. Phinn, and V. E. Brando, 2014. A review of ocean color remote sensing methods and statistical techniques for the detection, mapping and analysis of phytoplankton blooms in coastal and open oceans. Progress in Oceanography 123, 123–144. doi:10.1016/j.pocean.2013.12.008.

Boss, E. S., R. Collier, G. Larson, K. Fennel, K., and W. S. Pegau, 2007. Measurements of spectral optical properties and their relation to biogeochemical variables and processes in Crater Lake, Crater Lake National Park, OR. Hydrobiologia 574, 149-159.

Brando, V. E., and A. G. Dekker, 2003. Satellite hyperspectral remote sensing for estimating estuarine and coastal water quality. IEEE Transactions on Geoscience and Remote Sensing 41(6), 1378-1387.

Brezonik, P. L., L. G. Olmanson, J. C. Finlay, and M. E. Bauer, 2015. Factors affecting the measurement of CDOM by remote sensing of optically complex inland waters. Remote Sensing of Environment 157, 199-215.

Brönmark, C., and Hansson, L. -A., 2002. Environmental issues in lakes and ponds: Current state and perspectives. Environmental Conservation 29(3), 290-306.

Brown, A.G., S. E. Lohrenz, and G. L. Fahnenstiel, 2001. Optical properties and their relationship to physical processes and biogeochemical constituents during stratified conditions in southeastern Lake Michigan. ASLO Meeting, Albuquerque, NM, 12-16 February 2001.

Brown, T.C., and P. Froemke, 2012. Nationwide assessment of nonpoint source threats to water quality. BioScience 62(2), 136-146.

Bukata, R. P., J. E. Bruton, and J. H. Jerome, 1985. Application of direct measurements of optical parameters to the estimation of lake water quality indicators. Scientific Series, 140. Inland Waters Directorate, National Water Research Institute, Canada Centre for Inland Waters, Burlington, Ontario, Canada.

Bukaveckas, P. A., D. L. Guelda, J. Jack, R. Koch, T. Sellers, and J. Shostell, 2005. Effects of point source loadings, sub-basin inputs and longitudinal variation in material retention on C, N and P delivery from the Ohio River basin. Ecosystems 8 (7), 825-40. doi: 10.1007/s10021-005-0044-3.

Burkart, M. R., and D. E. James, 1999. Agricultural-nitrogen contributions to hypoxia in the Gulf of Mexico. Journal of Environmental Quality 28 (3), 850-859.

Chebud, Y., G. M. Naja, R. G. Rivero, and A. M. Melesse, 2012. Water quality monitoring using remote sensing and an artificial neural network. Water, Air, & Soil Pollution 223, 4875-4887.

Cibin, R., I. Chaubey, and B. Engel, 2011. Watershed scale impacts of corn stover removal for biofuel on hydrology and water quality. Hydrological Processes 26(11), 1629-1641. doi: 10.1002/hyp.8280.

Committee on the Mississippi River, the Clean Water Act, and National Research Council, 2008. Mississippi River Water Quality and the Clean Water Act : Progress, Challenges, and Opportunities. Washington, DC, USA: National Academies Press.

Datt, B., and D. Jupp, 2004. Hyperion data processing workshop: Hands-on processing instruction. CSIRO Earth Observation Centre, Australia.

Devred, E., K. Turpie, W. Moses, V. Klemas, T. Moisan, M. Babin, G. Toro-Farmer, M. Forget, and Y. Jo, 2013. Future retrievals of water column bio-optical properties using the Hyperspectral Infrared Imager (HyspIRI). Remote Sensing 5(12), 6812–6837.

Duker, L., and L. Bore, 2001. Biodiversity conservation of the world's lakes: A preliminary framework for identifying priorities. LakeNet Report Series: Anapolis, Maryland US.

Eaton, Andrew D., Lenore S. Clesceri, Arnold E. Greenberg, M. A. H. Franson, 1998. Standard methods for the examination of water and wastewater. 20th ed. 1 vols. Washington, DC: American Public Health Association.

Effler, S. W., M. Perkins, F. Peng, C. Strait, A. D. Weiderman, and M. T. Auer, 2010. Light-absorbing components in Lake Superior. Journal of Great Lakes Research 356, 656–665.

Effler, S. W., F. Peng, D. M. O'Donnell, and C. Strait, 2013. The backscattering coefficient and its components in the Great Lakes: A review and synthesis. Journal of Great Lakes Research Supplements 39, 108-122.

Fahnenstiel, G. L., T. Nalep, S. Pothoven, H. Carrick, and D. Scavia, 2010a. LakeMichigan lower food web: long-term observations and Dreissena impact. Journal of Great Lakes Research 36 (3), 1-4.

Fahnenstiel, G. L., S. Pothoven, H. Vanderploeg, D. Klarer, T. Nelapa, and D. Scavia, 2010b. Recent changes in primary productivity and phytoplankton in the offshore region of southeastern Lake Michigan. Journal of Great Lakes Research 36 (3), 20-29.

Fu, B., Y. Wang, P. Xu, and K. Yan, 2012. Mapping the flood mitigation services of ecosystems: A case study in the Upper Yangtze River Basin. Ecological Engineering 52, 238-246. doi: 10.1016/j.ecoleng.2012.11.008.

Garcia, R. A., P. R. C. S. Fearns, and L. I. W. Mckinna, 2014. Detecting trend and seasonal changes in bathymetry derived from HICO imagery: A case study of Shark Bay, Western Australia. Remote Sensing of Environment 147, 186-205.

Garver, S. A., and D. A. Siegel, 1997. Inherent optical property inversion of ocean color spectra and its biogeochemical interpretation: I. Time series from the Sargasso Sea. Journal of Geophysical Research 102, 18607-18625.

Giardino, C., V. E. Brando, A. G. Dekker, N. Strombeck, and G. Candiani, 2007. Assessment of water quality in Lake Garda (Italy) using Hyperion. Remote Sensing of Environment 190(2), 183-195.

Gilerson, A. A., J. Zhou, S. Hlaing, I. Ioannou, J. Schalles, B. Gross, F. Moshary, and S. Ahmed, 2007. Fluorescence component in the reflectance spectra from coastal waters. Dependence on water composition. Optics Express 15(24), 15702-16721.

Gilerson, A. A., A. A. Gitelson, J. Zhou, D. Gurlin, W. Moses, I. Ioannou, and S. A., Ahmed, 2010. Algorithms for remote estimation of chlorophyll-a in coastal and inland waters using red and near infrared bands. Optics Express 18 (23), 24109-24125. doi: 10.1364/Oe.18.024109.

Gitelson, A. A., B. Gao, R. Li, S. Berdnikov, and V. Saprygin, 2011. Estimation of chlorophyll-a concentration in productive turbid waters using a Hyperspectral Imager for the Coastal Ocean—the Azov Sea case study. Environmental Research Letters 6, 024023.

Gordon, H. R., O. B. Brown, R. H. Evans, J. W. Brown, R. C. Smith, K. S. Baker, and D. K. Clark, 1988. A semi-analytic radiance model of ocean color. Journal of Geophysical Research 93, 10909-10924.IOCCG, 2010. Atmospheric correction for remotely-sensed ocean-colour products, in: Wang, M. (ed.), IOCCG, Dartmouth, NS, Canada, pp78. Available at: http://www.ioccg.org/reports_ioccg.html

Gould, R. W., R. A. Arnone, and P. M. Martinolich, 1999. Spectral dependence of the scattering coefficient in case 1 and case 2 waters. Applied Optics 38 (12), 2377-2383. doi: 10.1364/Ao.38.002377.

Gould, R. W., R. A. Arnone, and M. Sydor, 2001. Absorption, scattering; and remote-sensing reflectance relationships in coastal waters: Testing a new inversion algorithm. Journal of Coastal Research 17 (2), 328-341.

Hadjimitsis D. G., and Clayton C. R. I., 2011. Field spectroscopy for assisting water quality monitoring and assessment in water treatment reservoirs using atmospheric corrected satellite remotely sensed imagery. Remote Sensing 3(2): 362-377.

Hedley, J. D., A. R. Harborne, and P. J. Mumby, 2005. Simple and robust removal of sun glint for mapping shallow-water benthos. International Journal of Remote Sensing 26 (10), 2107-2112. doi: 10.1080/01431160500034086.

Handcock, R. N., A. R. Gillespie, K. A. Cherkauer, J. E. Kay, S. J. Burges, and S. K. Kampf, 2006. Accuracy and uncertainty of thermal-infrared remote sensing of stream temperatures at multiple spatial scales. Remote Sensing of Environment 100, 427-440.

Horion, S., N. Bergamino, S. Stenuite, J. P. Descy, P. D. Plisnier, S. A. Loiselle, and Y. Cornet, 2010. Optimized extraction of daily bio-optical time series derived from MODIS/Aqua imagery for Lake Tanganyika, Africa. Remote Sensing of Environment 114 (4), 781-791. doi:10.1016/j.rse.2009.11.012.

IOCCG. 2000. Remote sensing of ocean colour in coastal, and other optically-complex waters. Sathyendranath, S. (ed.), Reports of the International Ocean-Colour Coordinating Group No.3, IOCCG, Dartmouth, Canada Available at: http://www.ioccg.org/reports_ioccg.html Accessed 5 May, 2005.

IOCCG. 2006. Remote sensing of inherent optical properties: fundamentals, tests of algorithms, and applications. IOCCG.

Jupp, D. L. B., 2002. Discussion around Hyperion data: Background notes for the Hyperion Data Users Workshop. CSIRO EOC, Canberra, Australia.

Kallio, K., T. Kutser, T. Hannonen, S. Koponen, J. Pulliainen, J. Vepsäläinen, and T. Pyhälahti, 2001. Retrieval of water quality from airborne imaging spectrometry of various lake types in different seasons. Science of The Total Environment 268, 59-77. doi: 10.1016/S0048-9697(00)00685-9.

Kallio, K., S. Koponen, and J. Pulliainen, 2003. Feasibility of airborne imaging spectrometry for lake monitoring - a case study of spatial chlorophyll alpha distribution in two meso-eutrophic lakes. International Journal of Remote Sensing 24 (19), 3771-3790. doi: 10.1080/0143116021000023899.

Keith, D. J., B. A. Schaeffer, R. S. Lunetta, R. J. Gould, K. Rocha, K., and D. J. Cobb, 2014. Remote sensing of selected water-quality indicators with the hyperspectral imager for the coastal ocean (HICO) sensor. International Journal of Remote Sensing 35, 2927-2962.

Kling, G. W., K. Hayhoe, L. B. Johnson, J. J. Magnuson, S. Polasky, S. K. Robinson, B. J. Shuter, M. M. Wander, D. J. Wuebbles, and D. R. Zak, 2003. Confronting climate change in Great Lakes Regions. Ecological Society of America and the Union of Concerned Scientists, Washington D. C.

Koponen, S., J. Attila, J. Pulliainen, K. Kallio, T. Pyhälahti, A. Lindfors, K. Rasmus, and M. Hallikainen, 2007. A case study of airborne and satellite remote sensing of a spring bloom event in the Gulf of Finland. Continental Shelf Research 27 (2), 228-244. doi: 10.1016/j.csr.2006.10.006.

Korosov, A. A., D. V. Pozdnyakov, A. Folkestad, L. H. Pettersson, K. Sørenson, and R. Shuchman, 2009. Semi-empirical algorithm for the retrieval of ecology-relevant water constituents in various aquatic environments. Algorithm 2 (1), 470-497.

Kutser, T., D. C. Pierson, K. Y. Kallio, A. Reinart, A., and S. Sobek, 2005. Mapping lake CDOM by satellite remote sensing. Remote Sensing of Environment 94, 535 – 540.

Kutser, T., E. Vahtmae, and J. Praks, 2009. A sun glint correction method for hyperspectral imagery containing areas with non-negligible water leaving NIR signal. Remote Sensing of Environment 113 (10), 2267-2274. doi: 10.1016/j.rse.2009.06.016.

Kutser, T., E. Vahtmae, B. Paavel, and T. Kauer, 2013. Removing glint effects from field radiometry data measured in optically complex coastal and inland waters. Remote Sensing of Environment 133, 85-89. doi: 10.1016/j.rse.2013.02.011.

Lee, Z., K. Carder, S. Hawes, R. Steward, T. Peacock, and C. Davis, 1994. Model for the interpretation of hyperspectral remote-sensing reflectance. Applied Optics 33, 5721-5732.

Lee, Z., K. L. Carder, C. D. Mobley, R. G. Steward, and J. S. Patch, 1998. Hyperspectral remote sensing for shallow waters. 1. A semi-analytical model. Applied Optics 37, 6329-6338.

Lee, Z., K. L. Carder, C. D. Mobley, R. G. Steward, and J. S. Patch, 1999. Hyperspectral remote sensing for shallow waters: 2. Deriving bottom depths and water properties by optimization. Applied Optics 38(18), 3831-3843.

Lee, Z., L. C. Kendall, R. F. Chen, and T. G. Peacock, 2001. Properties of the water column and bottom derived from Airborne Visible Imaging Spectrometer (AVIRIS) data. Journal of Geophysical Research 106, 11639-11651.

Lee, Z., and K. L. Carder, 2002. Effect of spectral band numbers on the retrieval of water column and bottom properties from ocean color data. Applied Optics 41(12), 2191-2201.

Lee, Z., Y. H. Ahn, C. Mobley, and R. Arnone, 2010a. Removal of surface-reflected light for the measurement of remote-sensing reflectance from an above-surface platform. Optics Express 18 (25), 26313-26324. doi: 10.1364/Oe.18.026313.

Lee, Z., R. Arnone, C. Hu, P. J. Werdell, and B. Lubac, 2010b. Uncertainties of optical parameters and their propagations in an analytical ocean color inversion algorithm. Applied Optics 49(3), 369-381.

Lesht, B. M., J. R. Stroud, M. J. McCormick, G. Fahnenstiel, M. L. Stein, L. J. Welty, and G. A. Leshkevich, 2002. An event-driven phytoplankton bloom in southern Lake Michigan observed by satellite. Geophysical Research Letter 29, 18-22.

Lesht, B. M., R. P. Barbiero, and G. J. Warren, 2013. A band-ratio algorithm for retrieving open-lake chlorophyll values from satellite observations of the Great Lakes. Journal of Great Lakes Research 39, 138-152.

Lesser, M., and C. D. Mobley, 2007. Bathymetry, water optical properties, and benthic classification of coral reefs using hyperspectral remote sensing imagery. Coral Reefs 26, 819-829.

Liao, L., P. Jarecke, D. Gleichauf, and T. Hedman, 2000. Performance characterization of the Hyperion imaging spectrometer instrument. Proceedings of SPIE 4135, Earth Observing Systems V, 264, doi:10.1117/12.494253.

Likens, G. E., 2010. Plankton of Inland Waters. Academic Press. Oxford, UK.

Lohrenz, S. E., G. L. Fahnenstiel, D. F. Millie, O. M. E. Schofield, T. Johengen, and T. Bergmann, 2004. Spring phytoplankton photosynthesis, growth, and primary production andrela tionships to a recurrent coastal sediment plume and river inputs in southeastern Lake Michigan. Journal of Geophysical Research 109, C10S14, doi:10.1029/2004JC002383.

Lohrenz, S., G. Fahnenstiel, O. Schofield, and D. Millie, 2008. Coastal sediment dynamics and river discharge as key factors influencing coastal ecosystem productivity in southeastern Lake Michigan. Oceanography 21, 61–69.

Louchard, E. M., R. P. Reid, F. C. Stephens, C. O. Davis, R. A. Leathers, and T. V. Downes, 2003. Optical remote sensing of benthic habitats and bathymetry in coastal environments at Lee Stocking Island, Bahamas: A comparative spectral classification approach. Limnology and Oceanography 48, 511-521.

Lucke, R. L., M. Corson, N. R. McGlothlin, S. D. Butcher, D. L. Wood, D. R. Korwan, D. R., R. R. Li, W. A. Snyder, C. O. Davis, and D. T. Chen, 2011. Hyperspectral Imager for the Coastal Ocean: Instrument description and first images. Applied Optics 50(11), 1501–1516.

Maritorena, S., A. Morel, and B. Gentili, 1994. Diffuse reflectance of oceanic shallow waters: influence of water depth and bottom albedo. Limnology and Oceanography 39, 1689–1703.

Maritorena S., D. A. Siegel, and A. Peterson, 2002. Optimization of a semi-analytical ocean color model for global scale applications. Applied Optics 41(15), 2705-2714.

Matthews, M., 2011. A current review of empirical procedures of remote sensing in inland and near-coastal transitional waters. International Journal of Remote Sensing 32, 6855-6899.

Mobley, C. D., 1994. Light and Water; Radiative Transfer in Natural Waters.Academic Press. London, U.K..

Mobley, C. D., 1999. Estimation of the remote-sensing reflectance from above-surface measurements. Applied Optics 38 (36), 7442-7455. doi: 10.1364/Ao.38.007442.

Mobley, C.D., and Sundman, L.K., 2013. Hydrolight 5.2 Users'Guide. Bellevue, WA: Sequoia Scientific.

Mobley, C. D., W. P. Bissett, W. P., J. H. Bowles, C. O. Davis, T. V. Downes, A. Gleason, D. D. R. Kohler, R. P. Reid, E. M. Louchard, and A. Gleason, 2005. Interpretation of hyperspectral remote-sensing imagery via spectrum matching and look-up tables. Applied Optics 44(17), 3576-3592.

Moore, G. F., J. Aiken, and S. J. Lavender, 1999. The atmospheric correction of water colour and the quantitative retrieval of suspended particulate matter in Case II waters: application to MERIS. International Journal of Remote Sensing 20 (9), 1713-1733. doi: 10.1080/014311699212434.

Morel, A. 1974. Optical properties of pure water and pure sea water, in: Jerlov, N. G., Steeman-Nielsen, E. (eds.), Optical aspects of oceanography. Academic Press, London, pp. 1-24.

Morel, A., and L. Prieur, 1977. Analysis of Variations in Ocean Color. Limnology and Oceanography 22 (4), 709-722.

Moses, W. J., A. A. Gitelson, S. Berdnikov, and V. Povazhnyy, 2009. Satellite Estimation of Chlorophyll-a Concentration Using the Red and NIR Bands of MERIS-The Azov Sea Case Study. IEEE Geoscience and Remote Sensing Letters 6 (4), 845-849. doi: 10.1109/Lgrs.2009.2026657.

Moses, W. J., A. A. Gitelson, R. L. Perk, D. Gurlin, D. C. Rundquist, B. C. Leavitt, T. M. Barrow, and P. Brakhage, 2012. Estimation of chlorophyll-a concentration in turbid productive waters using airborne hyperspectral data. Water Research 46 (4), 993-1004. doi: 10.1016/j.watres.2011.11.068.

Mouw, C., S. Greb, D. Aurin, P. DiGiacomo, Z. Lee, M. Twardowski, C. Binding, C. Hu, R. Ma, T. Moore, W. Moses, and S. E. Craig, 2015. Aquatic color radiometry remote sensing of coastal and inland waters: Challenges and recommendations for future satellite missions. Remote Sensing of Environment 160, 15-30.

Mueller, J. L., G. S. Fargion, and C. R. Macclain, 2003. Ocean optics protocols for satellite ocean color sensor validation, Revision 4, NASA Tech. Memo 211621. Greenbelt, MD.

Nekouee, N., P. Roberts, D. Schwab, and M. McCormick, 2013. Classification of buoyant river plumes from large aspect ratio channels. Journal of Hydrologic Engineering 139(3), 296-309.

Notaro, M., K. Holman, A. Zarrin, E. Fluck, S. Vavrus, and V. Bennington, 2013. Influence of the Laurentian Great Lakes on Regional Climate. Journal of Climate 26, 789-804. doi: http://dx.doi.org/10.1175/JCLI-D-12-00140.1.

O'Donnell, D.M., S. W. Effler, C. M. Strait, and G. A. Leshkevich, 2010. Optical characteristics and pursuit of optical closure for the western basin of Lake Erie through in situ measurements. Journal of Great Lakes Research 36, 736–746.

Olmanson, L. G., P. L. Brezonik, and M. E. Bauer, 2013. Airborne hyperspectral remote sensing to assess spatial distribution of water quality characteristics in large rivers: The Mississippi River and its tributaries in Minnesota. Remote Sensing of Environment 130, 254-65. doi: 10.1016/j.rse.2012.11.023.

O'Reilly, J. E., S. Maritorena, B. G. Mitchell, D. A. Siegel, K. L. Carder, S. A. Garver, M. Kahru, and C. McClain, 1998. Ocean color chlorophyll algorithms for SeaWiFS. Journal of Geophysical Research-Oceans 103(C11), 24937-53. doi: 10.1029/98jc02160.

Palmer, S. C. J., P. D. Hunter, T. Lankester, S. Hubbard, E. Spyrakos, A. N. Tyler, M. Présinga, H. Horvátha, A. Lamb, H. Balzter, and V. Tóth, 2015. Validation of EnvisatMERIS algorithmfor chlorophyll retrieval in a large, turbid and optically complex shallow lake. Remote Sensing of Environment 157(C), 158–169.

Peng, F., and S. W. Effler, 2010. Characterizations of individual suspended mineral particles in western Lake Erie: Implications for light scattering and water clarity. Journal of Great Lakes Research 36, 686–698.

Pope, R. M., and E. S. Fry, 1997. Absorption spectrum (380-700 nm) of pure water II. Intergrating cavity measurements. Applied Optics 36(33), 8710-8723.

Potter, K. W., 1994. Estimating potential reduction flood benefits of restored wetlands. Water Resource Update, 97, 34-38.

Pozdnyakov, D., R. Shuchman, A. Korosov, and C. Hatt, 2005. Operational algorithm for the retrieval of water quality in the Great Lakes. Remote Sensing of Environment 97, 353-370.

Ritchie, J. C., F. R. Schiebe, C. M. Cooper, and J. A. Harrington, 1994. Chlorophyll measurements in the presence of suspended sediment using broad band spectral sensors aboard satellites. Journal of Freshwater Ecology 9(3), 197-205.

Ritchie, J. C., P. V. Zimba, and J. H. Everitee, J. H., 2003. Remote sensing techniques to assess water quality. Photogrammetric Engineering & Remote Sensing 69(6), 695-704.

Roesler, C. S., M. J. Perry, and K. L. Carder, 1989. Modeling in situ phytoplankton absorption from total absorption spectra in productive inland marine waters. Limnology and Oceanography 34, 1510-1523.

Roesler, C. S., and M. J. Perry, 1995. In situ phytoplankton absorption, fluorescence emission, and particulate backscattering spectra determined from reflectance. Journal of Geophysical Research 100, 13279-13294.

Ruddick, K. G., V. De Cauwer, Y. J. Park, and G. Moore, 2006. Seaborne measurements of near infrared water-leaving reflectance: The similarity spectrum for turbid waters. Limnology and Oceanography 51 (2), 1167-1179.

Ryan, J. P., C. O. Davis, N. B. Tufillaro, R. M. Kudela, and B. Gao, 2014. Application of the Hyperspectral Imager for the Coastal Ocean to Phytoplankton Ecology Studies in Monterey Bay, CA, USA. Remote Sensing 6, 1007-1025.

Segelstein, D., 1981. The complex refractive index of water. Master thesis, University of Missouri.

Shafique, N.A., Fulk, F., Autrey, B.C. and Flotemersch, J., 2003. Hyperspectral remote sensing of water quality parameters for large rivers in the Ohio River basin. Proceedings of First Interagency Conference on Research in the Watersheds. USDA Agricultural Research Service, Washington DC, pp. 216-221.

Shuchman, R., A., Korosov, C. Hatt, D. Pozdnyakov, J. Means, and G. Meadows, 2006. Verification and application of a bio-optical algorithm for Lake Michigan using SeaWiFS: a 7-year inter-annual analysis. Journal of Great Lakes Research 32, 258-279.

Shuchman, R. A., M. Sayers, G. L. Fahnenstiel, and G. Leshkevich, 2013a. A model for determining satellite-derived primary productivity estimates for Lake Michigan. Review of. Journal of Great Lakes Research 39, 46-54. doi: 10.1016/j.jglr.2013.05.001.

Shuchman, R., G. Leshkevich, M. Sayers, T. Johengen, C. Brooks, and D. Pozdnyakov, 2013b. An algorithm to retrieve chlorophyll, dissolved organic carbon, and suspended minerals from Great Lakes satellite data. Journal of Great Lakes Research 39, 14-33.

Smith, R. C., and K. S. Baker, 1981. Optical-Properties of the Clearest Natural-Waters (200-800 Nm). Applied Optics 20 (2), 177-184. doi: 10.1364/Ao.20.000177.

Tan, J., K. A. Cherkauer, and I. Chaubey, 2015a. Using hyperspectral data to quantify water quality parameters in the Wabash River and its tributaries, Indiana. International Journal of Remote Sensing 36(21), 5466-5484.

Tan, J., K. A. Cherkauer, I. Chaubey, C. D. Troy, and R. Essig, 2015b. Water quality estimation of river plumes in southern Lake Michigan using Hyperion. Submitted to Journal of Great Lakes Research.

Thiery, W., E. L. Davin, H. -J. Panitz, M. Demuzere, S. Lhermitte, and N. van Lipzig, 2015. The Impact of the African Great Lakes on the Regional Climate. Journal of Climate 28, 4061-4085. doi: http://dx.doi.org/10.1175/JCLI-D-14-00565.1

United States Environmental Protection Agency, 2011a. Water quality assessment and total maximum daily loads information. USEPA, 20 November 2011.

United States Environmental Protection Agency, 2011b. Wabash River watershed water quality trading feasibility study final report. Accessed May 16 2015. http://water.epa.gov/type/watersheds/trading/upload/Wabash-WQT-Feasibility-Study_091411_final-report.pdf

United States Army Corps of Engineers. 2011. Wabash River Watershed Section 729 Initial Watershed Assessment. Louisville (KY). Available at: http://www.lrl.usace.army.mil/Portals/64/docs/CWProjects/WabashStudy.pdf

Vasilkov, A., and O. Kopelevich, 1982. Reasons for the appearance of the maximum near 700 nm in the radiance spectrum emitted by the ocean layer. Oceanology 22, 697-701.

Wentworth C. K., 1922. A scale of grade and class terms for clastic sediments. Journal of Geology 30, 377-392.

Zhang, Y., M. Liu, M. A. Vandijk, G. Zhu, Z. Gong, Y. Li, and B. Qin, 2009. Measured and numerically partitioned phytoplankton spectral absorption coefficients in inland waters. Journal of Plankton Research 31(3), 311-323.

Zhu, W., Y. Q. Tian, Q. Yu, and B. L. Becker, 2013. Using Hyperion imagery to monitor the spatial and temporal distribution of colored dissolved organic matter in estuarine and coastal regions. Remote Sensing of Environment 134, 342-354.

VITA

VITA

Jing Tan

Research Interests

Jing Tan's research interests lie in the analysis of remote sensing data (in situ, airborne and satellite) and algorithms development for water quality monitoring.

Education

Ph.D., Department of Agricultural and Biological Engineering, Purdue University, May 2016

M.S., Department of Agricultural and Biological Engineering, Purdue University, August 2011

B.S., School of Geography, Beijing Normal University, June 2009

Teaching Experience

Participated in teaching ABE 49500 *Remote Sensing Technology Tools*, Jan 2014 - May 2014

Presentations

Tan, J., Cherkauer, K.A., Chaubey, I., Troy, C.D. and Essig, R. (2013). Monitoring water quality of episodic river inflow plumes in southern Lake Michigan using remote sensing, presented at the 56th Annual Conference of the International Association for Great Lakes Research (IAGLR), West Lafayette, Indiana, USA, 4 June.

Essig, R. R., C. D. Troy, I. Chaubey, K. A. Cherkauer, and J. Tan (2012). Temporal and spatial variations of nutrient loading from southern Lake Michigan, presented at the 55th Annual Conference of the International Association for Great Lakes Research (IAGLR), Cornwall, Ontario, CA, 16 May.

Tan, J., K. A. Cherkauer, and I. Chaubey (2011), Quantification of water quality parameters for the Wabash River using hyperspectral remote sensing, American Geophysical Union (AGU) Fall Meeting, San Francisco, CA. 5-9 Dec. H51I-1325.

Tan, J. and K. A. Cherkauer (2010), Assessing stream temperature variations in the Pacific Northwest using airborne thermal infrared remote sensing, American Geophysical Union (AGU) Fall Meeting, San Francisco, CA. 13-17 Dec. H43G-1333.

Publications

Tan, J., K. A. Cherkauer, and I. Chaubey (2015), Using hypserspectral data to quantify water quality parameters in the Wabash River and its tributaries, Indiana. *International Journal of Remote Sensing*, 36(21), 5466-5484.

Tan, J. and K. A. Cherkauer (2013)**,** Assessing stream temperature variation in the Pacific Northwest using airborne thermal infrared remote sensing, *Journal of Environmental Management*, 115C:206-216, doi: 10.1016/j.jenvman.2012.10.012

Handcock, R. N., C. E. Torgersen, K. A. Cherkauer, A. R. Gillespie, K. Tockner, R. N. Faux, and J. Tan, 2012. CHAPTER 5: Thermal Infrared Remote Sensing of Water Temperature in Riverine Landscapes, in Remote Sensing of Rivers: Management and Applications, editors P. Carbonneau and H. Piegay, John Wiley & Sons Ltd.

Honors and Awards

NASA Earth and Space Science Fellowship, 2014-2016

Incentive grant, Purdue University, 2014

University of Maine/NASA grant for summer class, 2013

Lynn Fellowship, Purdue University, 2009

Professional scholarship, Beijing Normal University, 2006-2009